PORTABLE COLORIMETRIC SENSOR ARRAY TECHNOLOGY

BY

JON ROBERT ASKIM

DISSERTATION

Submitted in partial fulfillment of the requirements
for the degree of Doctor of Philosophy in Chemistry
in the Graduate College of the
University of Illinois at Urbana-Champaign, 2015

Urbana, Illinois

Doctoral Committee:

Professor Kenneth S. Suslick, Chair
Professor Ryan C. Bailey
Professor Andrew A. Gewirth
Professor Gregory S. Girolami

ABSTRACT

Humans as a species are generally audio-visual creatures and do not take full advantage of the olfactory sense. Nonetheless, even humans can recognize and differentiate among thousands of different odorants under challenging conditions. Molecular recognition by the olfactory system derives its specifity from a complex pattern of responses generated by cross-reactive olfactory receptors. These receptors are encoded by approximately one thousand genes, which represents roughly 3% of the entire human genome. As a concept, the use of multiple cross-reactive chemical sensors is broadly applicable to any situation in which the sensors can be simultaneously exposed to each of a set of multiple target analytes; such an "artificial nose" has significant potential in all areas of chemical sensor technology.

The chemical sensor arrays discussed in this work are based upon cross-reactive colorimetric response: each of many sensor elements in an array is a mixture of dyes or other compounds that changes color upon exposure to an analyte. These arrays typically use strong, poorly-reversible chemical reactions involving a diverse set of color-changing dyes or chromogens; such colorimetric sensor arrays have evolved to be fast, sensitive, portable, and inexpensive. Importantly, the analyte scope of the developed arrays has been shown to be capable of tailoring based on their intended applications, and can be made to be either broad or narrow as desired: in previous works, they have proven to be capable of discriminating among a broad range of analytes including both gaseous and aqueous analytes involving many different types of chemical reactivity, including Lewis and Brønsted acidity/basicity, molecular polarity, redox properties, and chelation.

Of particular interest is the study of chemicals which are hazardous to human life, by either directly interacting with the human body or indirectly causing a physical effect. This work discusses development of colorimetric sensor arrays for two such cases: aqueous toxins and explosives materials. Both types of analytes are particularly challenging due to their relative lack of chemical reactivity:

aqueous toxins derive their toxicity from interaction with specific proteins within the human body, while explosives have high potential energy but are kinetically inert. Targeting these analytes while still maintaining high sensitivity, low noise, and the ability to discriminate among them was the primary focus of these two projects.

Further, inexpensive portable technology for the quantitative analysis of these arrays is vitally necessary for their intended use outside of the laboratory. This work discusses development of an automated, truly portable device that fits into a pocket and improves upon previous instrumentation in scan speed, sensitivity, and noise. Since colorimetric sensor arrays are monitored by optical transduction, development of portable scanners involves investigating inexpensive, compact, low-noise optical imagers. Previous works focused on flatbed scanners, which have since shown to have limitations in portability (flatbed scanners will certainly not fit in someone's pocket), scan speed (~15-45 seconds per scan), noise (largely induced by the scanner's moving parts), and processing ability (processed manually). To improve upon this, an optical line imager known as a contact image sensor was used to act as the optical transducer; chemical sensor arrays were printed linearly so as to maintain compatibility with the line imager. The final device included disposable sensor array cartridges, a flow control system, control software, and analysis software for pattern matching.

Aletheia

ACKNOWLEDGMENTS

First and foremost, I would like to acknowledge Ken Suslick for his patience, time, and creativity throughout the period of this entire work. Several other faculty and staff members at the University of Illinois were also invaluable in the development of this work: Michael Harland, Brad Lutz, Rob Brown, and Dave Hire of the SCS Machine Shop for their incredible skill and manifold contributions to developing the equipment used in our sensor projects; Prof. Greg Girolami for insights into sensor reactivity; Prof. Alexander Scheeline for insights into multidimensional data processing; and Nasrin Gahvari, Theresa Struss, Connie Knight, and Beth Myler for keeping everything moving and organized. I would also like to acknowledge Sung Lim of iSense LLC/Metabolomx (also a former postdoctoral researcher for Ken Suslick) for significant contributions toward array development and quality control.

For the handheld array scanner, I would like to acknowledge the critical roles performed by all other members of the development team: Ray Martino and Richard Huang of iSense LLC/Metabolmx for engineering and design; Barry Hand and Boris Metlitsky of Intelligent Product Solutions for engineering and design; Richard Lareau, Alfred Wooten, and Bridget Willoughby of the Transportation Security Laboratory for iterative testing; Trish McDaniel and Erin Tamargo of the U.S. CTTSO for oversight and iterative testing; and Brandon Guitierrez of the U.S. JIEDDO for oversight.

I would also like to acknowledge *many* coworkers and colleagues whose discussions over the years helped shape the direction and quality of the work. These include but are not limited to Brad Zeiger, Chang Cui, Jacqueline Rankin, Jinrui Guo, John Overcash, Jordan Hinman, Kevin Hwang, Laura Huff, Liang Feng, Maria LaGasse, Marshall Brennen, Nick Marshall, Parisa Hosseinzadeh, Qifan Zhang, Rachel Forman, Yinan Zhang, Yuanxi Fu, and Zheng Li.

Additionally, I would like to thank the members of my doctoral committee for their time, effort, and guidance: Ken Suslick, Ryan Bailey, Andrew Gewirth, and Greg Girolami.

TABLE OF CONTENTS

Chapter 1: Optical sensor arrays for chemical sensing

This chapter taken in large part from the following reference:

Askim, J. R.; Mahmoudi, M.; Suslick, K. S. "Optical sensor arrays for chemical sensing: the optoelectronic nose" *Chem. Soc. Rev.* **2013**, *42*, 8649.

1.1 Introduction and classes of chemical sensors

As a species, we are visual creatures and underappreciate the olfactory sense. Nonetheless, even humans can recognize and discriminate more than 10,000 different odorants.[1] Molecular recognition by the primary olfactory system derives its specificity in an entirely different manner than the usual lock-and-key substrate-enzyme specificity. Instead, olfactory specificity originates from pattern recognition of the responses of several hundreds of highly cross-reactive olfactory receptors. Indeed, for land-based animals, there are typically about 1000 active olfactory receptor genes, which represents roughly 3% of our entire genome![2-3]

Development of rapid, sensitive, portable and inexpensive systems for identification of a wide range of toxic gases, vapors, and aqueous solutions has become an urgent societal need and has important applications ranging from the chemical workplace to the general population. New approaches to chemical sensing[4-13] with improved discriminatory powers are essential to eliminate false positives for the monitoring of toxic gases at sub-ppm levels.[14] In 1982, Persaud and Dodd[15] tried to mimic the olfactory system using semiconductor transducers; this was one of the first artificial devices to successfully discriminate among a wide variety of odors without the use of highly specific receptors, i.e., an electronic nose.

The long history of visual indicators in analytical chemistry has led to the development of optical sensor arrays as an alternative to electronic sensors. There has been much recent progress in this "optoelectronic nose" approach,[5,10,14,16-21] and we will present here an overview of the recent progress in

colorimetric and fluorometric sensor arrays, examine the methods of analysis of the high dimensional data so obtained, and review important and diverse applications. We also discuss previous limitations of sensor arrays and prior electronic nose technology and comment on the recent successes in overcoming those failings. Finally, we will examine the emerging trends that are likely to impact the development of new optical sensor arrays.

Optical sensor arrays provide a facile, efficient, and sensitive approach for the rapid detection and identification of wide range of chemical substrates based on colorimetric or fluorescent changes quantified by digital imaging. [7, 22-27] Every optical sensor array must contain both an active center that can interact strongly with desired analytes and an intense chromophore or fluorophore that is strongly coupled to that active center.[14] It is the intermolecular interactions of analytes with the active center, often through strong chemical interactions rather than simple physical adsorption, that results in a colorimetric or fluorometric change (i.e., chemoresponsive). Using a chemically diverse array of such chemo-responsive colorants, one generates a pattern that is an optical fingerprint for any odorant or mixture of odorants. [5,10,16-17,19] The colorants are cross-reactive, but the pattern of the array response is unique: in this manner, olfactory-like responses are converted into an easily monitored optical output, thus acting as an optoelectronic nose.

1.1.1 Chemical sensors

There is an increasing demand to measure the chemical environment both inside our own bodies and in our surrounding environment. The healthy function of the human body is dependent on various chemical processes; thus, *in situ* monitoring is of crucial importance, e.g., the chemical composition of patient blood samples in medical diagnosis. The impact of the environment on living systems similarly is of critical interest, and analysis of types and amounts of a wide range of toxins, pollutants, and even naturally occurring chemical species becomes of increasing importance.

Such analyses and diagnostic methods need suitable sensors. A sensor is a device that converts an input signal from a stimulus into a readable output signal.[13,28] The input signal can be any measurable characteristic such as quantity or physical variation, while the output is ultimately an electrical signal. Small and inexpensive sensors enable mass production and widespread application.[29] Indeed, the development of new sensor technology faces the dilemma of trying to create sensors that are both increasingly sensitive and increasingly robust. Just as position and momentum are canonical variables, one may argue that beyond a certain point, the more sensitive a sensor becomes, inherently the less robust it can be. As we shall see, one path around this dilemma is the development of disposable sensors, thus unlinking the opposing demands.

Chemical sensors respond to the chemical environment (i.e., interactions with molecular species), rather than the physical environment (e.g., temperature or pressure). Chemical sensors can therefore be categorized into two major groups: those that discriminate among analytes based on physical properties (e.g., molecular weight, vapor pressure, etc.) and those that measure chemical properties (e.g., reactivity, redox potential, acid-base interactions, etc.). Chemical sensors can also be grouped by their signal transduction methods into three classes: (1) electrical and electrochemical, (2) thermometric, and (3) optical. We will focus on this last class of sensors as array components, but let us first briefly overview all three sensor transduction classes.

1.1.2 Electrical and electrochemical Sensors

An electrical sensor is a resistive or capacitive measurement device that responds to analyte interactions with receptor layer of sensor. In a sense, the olfactory receptors of the vertebrate olfactory system are a large array of bioelectrical sensors.[30-31] In chemical sensing, electrical and electrochemical sensors are nearly indistinguishable. Both intrinsically involve the interaction of chemical analytes with an electrical circuit and resistance, capacitance, current, or voltage as the monitored response.[13,32,33]

In attempts to mimic the olfactory system, a wide variety of electrical and electrochemical sensors have been explored, including metal oxide semiconductors (e.g. SnO_2)[34], metal oxide semiconductor field effect transistors (FET) (e.g. Ga_2O_3)[35-37] and chemical field-effect transistors (ChemFET),[38-39] conductive polymer sensors[40] of both intrinsically conductive (e.g. polythiophenes)[41] and composite types (e.g. carbon-black polymer composite),[12] and coated quartz vibrators or acoustic wave sensors.[42] In general, electrical sensors rely fundamentally on physical adsorption as the primary interaction between the chemical analytes and the electrically active surface; this reliance on physical adsorption, however, inherently provides for sensitivity to change in humidity, which remains a huge problem for both laboratory and especially field use. [6,8-9,13,28] In addition, aging of the surface of electrical sensors can induce significant baseline drift.[6]

Most recently, tremendous efforts have been developing with low dimensional nanomaterials as highly sensitive sensor transducers: e.g., nanowires, nanotubes, nanofibers, graphene and single (or few) layer two-dimensional materials.[43-44,45,46-51] In large part, the potential for high sensitivity comes from the extreme surface area to mass ratios intrinsic to low dimensional materials, which permit extraordinary sensor exposure to analyte interactions. Selectivity remains key, however, to the future success of such systems for chemical or biomedical sensor applications.

Electrochemical sensors[52-55] are also extremely diverse and can be used for a wide range of applications, but are beyond the scope of this review. The reader is referred to recent reviews on applications in environmental[56-60], clinical[61-63], bio-sensing[39,55,64-67], food[33,68] and biohazard agent[69] analyses.

1.1.3 Thermometric sensors

The mechanism of transduction in thermometric sensors relies on the measurement of the local heat change from specific chemical reactions or adsorption events involving the analyte. Thermometric

sensors are constructed by coating a catalytic sensor layer on the surface of a thermometer. In this case, the interaction of a target analyte with a chemical sensor can generate or consume heat that is then measured by sensitive thermistor (i.e., semiconductors with strongly temperature-dependent conductivity).[70,71] Thermometric sensors most commonly utilize enzymatic reactions with high enthalpy changes[28.72-74] Due to the simplicity of the thermal biosensing approach (e.g., there is no need for labeling reactants), this method can be considered as a suitable replacement for other signal transduction methods that require a sophisticated cascades of reaction steps.

A wide range of applications (e.g. detection of sucrose[75], glucose[76-79], uric acid[80], insulin[81], and lactate[82] by suitable immobilized enzymes) have been reported for thermometric biosensors. Moreover, a multi-analyte determination method has been performed by thermal biosensors using MEMS thermopiles.[78,83-84]

1.1.4 Optical sensors

Optical sensors use visible or ultraviolet light to interrogate sensors for analysis. Optical sensors can be represented in general terms as a wavelength selectable light source, the sensor material itself interacting with analytes, and a light detector (Figure 1.1). What the detector monitors varies by technique (e.g. refractive index, scattering, diffraction, absorbance, reflectance, photoluminescence, chemiluminescence, etc.), can cover different regions of the electromagnetic spectrum, and can allow measurement of multiple properties (e.g. intensity of light, lifetime, polarization, etc.).[28,85] The focus of this review, however, is on optical sensor arrays that use absorbance, reflectance or fluorescence array detectors (i.e., digital cameras or scanners).

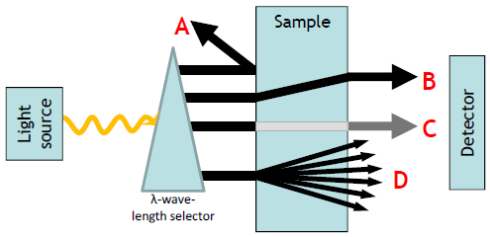

Figure 1.1 General arrangement of spectroscopic measurements: A, light reflection; B, light refraction; C, light absorption; D, fluorescent emission. Reproduced with permission from ref. [85]

Colorimetry (i.e., quantitative measurement of absorbance or reflectance spectra) is, of course, one of the oldest of analytical techniques,[86] and colorimetric sensors stretch back even before the beginnings of chemistry (e.g., squeeze a lemon into tea) with straightforward "naked-eye" quantitation. Colorimetric detection is a fairly simple technique, and the advent of universal digital imaging has given it new and exciting possibilities. We will use the general term colorimetry to include simple three color (i.e., RGB) imaging, hyperspectral imaging (i.e., more color channels), and full spectrophotometry (i.e., hundreds of color channels with nm resolution).

Fluorometry (i.e., the quantitative measurement of fluorescence spectra, cf. Figure 1.2)[87-89] can provide excellent sensitivity and fluorescent sensors often have some advantages (e.g., sensitivity, depending upon the background fluorescence), although at the cost of a more sophisticated experimental apparatus.[90] Fluorescence-based approaches and fluorescence parameters (e.g. Stokes shift, fluorescence intensity and anisotropy, emission and excitation spectra, and fluorescence lifetime) can provide substantial flexibility as an analytical approach.[91-92] Fluorescence techniques can be divided into three main classes: intrinsic fluorescent[93-96], extrinsic fluorescent[91,97-98], and displacement or differential[99-103] probes.

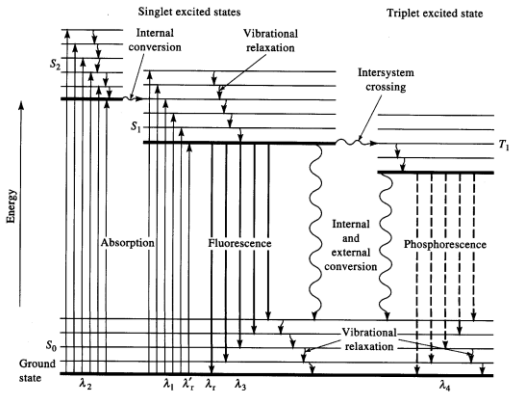

Figure 1.2 Partial Jablonski diagram for absorption, fluorescence, and phosphorescence. Reproduced with permission from ref. [104]

Optical chemical sensors must perform two functions: they must both interact with analytes and subsequently report on such interactions (e.g., by changing color). While many dyes and fluorophores do so intrinsically, there are also many other "artificial receptors" (i.e., compounds capable of supramolecular interactions) that are not spectroscopically active. For example, crown ethers, cryptands, cyclodextrins and calixarenes often have excellent molecular recognition capabilities to selectively bind analytes of interest (especially cations, often anions, and sometimes neutral organics),[100-101,105-106] but they are often spectroscopically inert. Such complexing agents can be covalently modified to incorporate a suitable chromophore or fluorophore, which can then report on analyte binding.

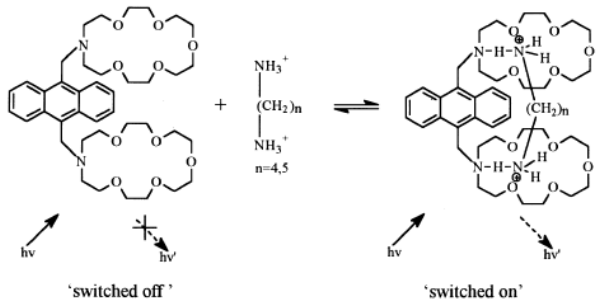

Figure 1.3 Switching on fluorescence of 9,10-bis((1-aza-4,7,10,13,16-pentaoxacylooctadecyl)methyl)anthracene by binding of guest molecules. hv, excitation light; hv', fluorescent emission. Reproduced with permission from ref. [107].

For example, the linkage of an anthracene fluorophore with a crown ether receptor creates a diamine sensor for detecting food spoilage.[107] In the absence of guest molecules (diamines such as putrescine or cadaverine), the fluorescence of anthracene is 'switched-off' by photo-induced electron-transfer; when a diamine is bound, however, fluorescence intensifies substantially (Figure 1.3).

1.2 Optical sensor array concepts

The olfactory system permits differentiation among a huge numbers of chemical compounds and complex mixtures over an enormous range of concentrations. This kind of molecular recognition could not utilize the usual model of biospecificity, i.e., the lock-and-key mechanism of enzyme-substrate interaction. The olfactory receptors represent the exact opposite of that kind of specificity and show highly cross-reactive, non-specific interactions with odorants. Molecular recognition instead occurs through the *pattern of response* from hundreds of different types of olfactory receptor epithelia cells (each of which expresses only a single one of the hundreds of olfactory receptors found in our genome), as analyzed by the olfactory bulb and the brain.

1.2.1 Importance of intermolecular interactions

In applying this concept of cross-reactive pattern recognition to artificial chemical sensing, the importance of intermolecular interactions become predominant. Fundamentally, chemical sensing is molecular recognition, and molecular recognition is the consequence of interactions between molecules.[108-110] The classification and strengths of inter-molecular interactions are well established (Figure 1.4) and form a complete continuum from the weakest of interactions that are manifest only near 0 K to the strongest of covalent or ionic bonds. There is a seamless range from bond formation and ligand coordination, electrostatic ion-ion and proton acid-base interactions, hydrogen-bonding, halogen bonding, charge-transfer and π-π molecular complexation, dipolar and multipolar interactions, and van der Waals interactions (e.g., physical adsorption).

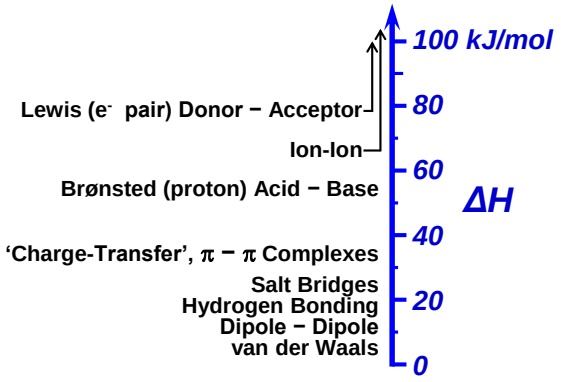

Figure 1.4 The range of intermolecular interactions on a semi-quantitative energy scale. Such interactions are a continuum from the very weakest van der Waals and dispersion forces to the very strongest covalent or ionic bonds.

Remarkably, nearly all prior electronic nose technology relies essentially exclusively on van der Waals and physical adsorption, the weakest and least selective of forces between molecules. As we will

argue here, colorimetric sensor arrays provide a successful method of dealing with the dilemma of sensor sensitivity vs. robustness. In many ways, colorimetric sensor arrays revisit the earlier, pre-electronic era of analytical chemistry,[111-113] updated by the addition of modern digital imaging easily quantified by digital imaging.[7,17,114-116] and pattern recognition techniques (discussed in Section 3).

The advantage of stronger interactions for sensor arrays is both the obvious one of greater inherent sensitivity and the more subtle one of great chemical specificity. Ligation of Lewis base analytes (e.g. amines, thiols, etc.) gives bond enthalpies from ~40 to ~200 kJ/mol. In contrast, the enthalpy of physical adsorption of analytes (e.g., onto metal oxide surfaces) or absorption (e.g., into polymers) is only ~5 to 20 kJ/mol. The effective equilibrium constant for physical adsorption will typically be only about 5×10^{-5} as large as that for ligation to metal ions. Even more importantly, stronger interactions bring a much wider range of chemical interactions than simple physisorption, and consequently one may access a much higher dimensionality and improve one's ability to discriminate among very similar analytes or complex mixtures of analytes.

Based on their recognition elements properties, the sensors used in an array will span a range of molecular specificity. At one end, there are individual sensors that are nearly completely promiscuous, i.e., highly cross-reactive; these include polymers and polymer blends with optical reporters embedded that adsorb analytes primarily based on hydrophobicity.[117-118] Promiscuous sensors can contribute to the sum of an array's response, but are insufficient in and of themselves to provide the differential selectivity most desirable for chemical sensor arrays. At the other extreme, there are highly selective artificial receptors that are specific for one or perhaps one closely related class of analytes. While this class of sensor can produce high specificity for specific analytes, alone they too will not make a sensor array capable of dealing with a wide range of analytes and mixtures;[119] furthermore, the synthesis of such selective artificial receptors can be complex and problematic. The optimal optical sensor array will therefore incorporate a range of colorimetric or fluorometric sensors from the promiscuous to the

monogamous.

One sees exactly this range of receptors and receptor response in the olfactory system. The nose is a sensitive array of sensors able to distinguish many types of volatile analytes, but it is not equally sensitive to all analytes. The limits of detection of human olfaction are well known[120] and span a range of more than 10^9. Consider the human olfactory detection limits for the simplest of analytes, those with one methyl group and one other functionality, as shown in Figure 1.5. Olfactory response to methanethiol is over 1 million times stronger than that of methanol, methylamine is bound more than 100,000 times more strongly than methanol, and the range from ethane to methane thiol is 10^7. Van der Waals forces, hydrogen bonding, and sterics cannot account for such a large range for comparably sized molecules. It has been suggested[121] that the olfactory receptors (ORs) are, in large fraction, metalloproteins, and that metal ion (Cu^+, Zn^{+2}, etc.) ligation of strong Lewis base analytes (e.g., thiols, amines, phosphines, carboxylic acids, etc.) likely contributes substantially to the binding of many analytes by the ORs. In fact, Suslick and coworkers[121] discovered a highly conserved tripodal binding site in roughly 70% of all ORs sequences, and a very recent report from Matsunami and coworkers[122] confirms the crucial role of copper ions in at least one mouse OR.

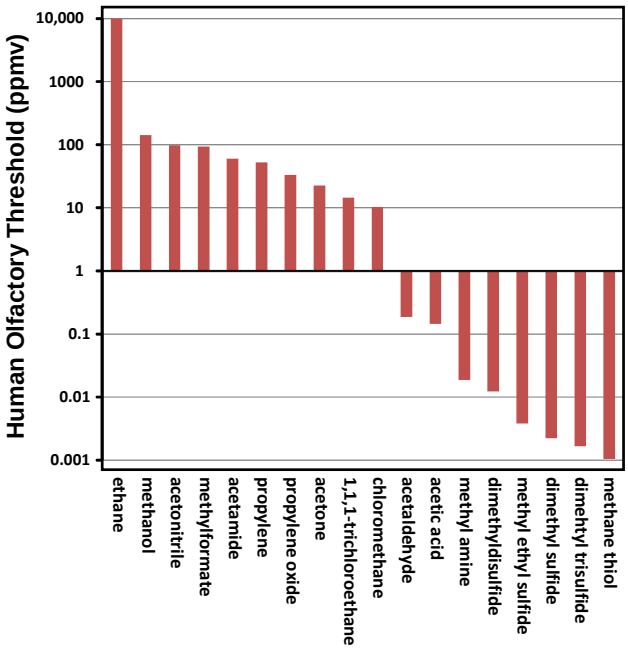

Figure 1.5 Human olfactory thresholds for detection of a series of comparable molecules with the structure HC_3-X.

1.2.2 Design requirements of an optical sensor array

There are two fundamental design requirements for a colorimetric or fluorometric sensor array: (1) the chemo-responsive dye or fluorophore must contain a center to interact with analytes, and (2) this interaction center must be strongly coupled to an intense chromophore or fluorophore. The first requirement implies that it would be highly advantageous for the interaction to be more than simple physical adsorption and involve other, stronger chemical interactions.

Based on the significant intermolecular interactions responsible for optical changes, one may divide chemoresponsive dyes into roughly five separate (albeit slightly overlapping) classes: (1) Lewis acid/base dyes (i.e., metal ion containing dyes), (2) Brønsted acidic or basic dyes (i.e., pH indicators), (3) dyes with large permanent dipoles (i.e., zwitterionic, solvatochromic, or vapochromic dyes) for detection of local polarity and hydrogen bonding, (4) redox responsive dyes, and (5) chromogenic aggregative

colorants (including simple ionic sulfides and plasmonic nanoparticle precursors). In addition, one may also consider environmental modifications to provide shape selectivity, either by modifying the dye peripheral superstructure or by molecularly imprinted polymers. The original colorimetric sensor array[17,123-124] made use of porphyrins and metalloporphyrins as sensors, utilizing primarily aspects of Lewis and Brønsted acid/base dyes; as discussed later, the range of sensors has broadened significantly over the past decade. An example of a 36 spot sensor array for use with gas phase analytes is shown in Figure 1.6.

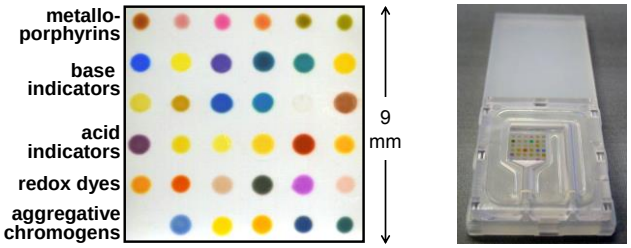

Figure 1.6 An example of a 6x6 colorimetric sensor array and its cartridge packing for use with gas phase analytes.

For gas phase sensing, a colorimetric sensor array is simply digitally imaged before and during exposure to any volatile analyte, odorant, or complex mixture of odorants. The imaging is mostly commonly achieved with an ordinary flatbed scanner, but one may also use digital cameras, portable handheld readers, and even cell phones; constancy of illumination is, of course, important.

From the digital images, a difference map (Figure 1.7) is easily generated by digital subtraction, pixel by pixel, of the image of the array before and after exposure: red value after exposure minus red value before, green minus green, blue minus blue. Averaging of the centers of the spots (typically ~200 pixels) avoids artifacts from non-uniformity of the dye spots, especially at their edges. The other advantage of using the differences in RGB colors is that it tends to cancel out discrepancies in printing because the color differences are only a weak function of variation of the dye concentration or spot intensity from

array to array.[114]

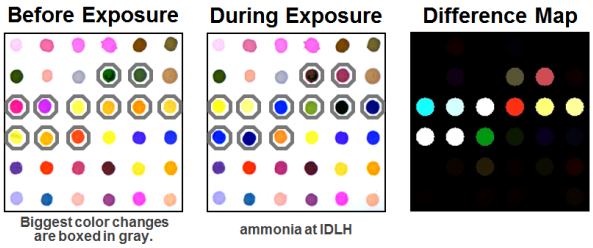

Figure 1.7 Image of the 36-dye colorimetric sensor array (Left) before exposure and (Middle) during exposure to ammonia at its IDLH (immediately dangerous to life or health concentration). (Right) Subtraction of the two images yields a difference vector in 108 dimensions (i.e., 36 changes in red, green, and blue color values); this vector is usefully visualized using a difference map, which shows the absolute values of the color changes. For purposes of display to increase the color palate, the color range of difference maps are usually expanded.

The resulting data is inherently digital (simply a vector of 3N dimensions where N=total number of spots) and all quantitative and statistically analysis is done directly from the digital difference vectors. The color difference maps are useful primarily for convenient visualization of color changes of the dye array; note that the color values are the absolute values of the differences and that expansion of the color space is useful for visualization. Note also that color difference maps shown throughout this review are generally from different arrays and therefore should only be compared within a single figure.

The choice of the individual sensor dyes in an optical sensor array is governed empirically by its intended use. One must consider if this array is meant for a broad range of analyte detection and discrimination or will it have a more specialized application. Keep in mind that the great power of optical sensors is their ability to probe the chemical properties of analytes through intermolecular interactions other than physical adsorption. If one uses only optical probes that measure local polarity (e.g., solvatochromic or vapochromic fluorescent probes doped into various polymers) then one has lost this

opportunity. Potential analytes vary in their chemical properties: hydrophilicity, solubility, redox, hydrogen bonding, Lewis donor/acceptor, and proton acidity and basicity of target analytes need to be considered. In general, an optimal sensor array for general sensing purposes will incorporate as much chemical diversity among the individual sensors as possible. Given the likelihood of metal ion binding sites in the olfactory receptors themselves,[121-122] incorporation of metal ion-containing dyes into optical sensor arrays can make an important contribution to construction of a chemo-responsive sensor array. One must also consider possible interferents presented by ambient, complex environments. Finally, the stability of the dyes used in the array and their quantitative magnitude of response must of course be considered.

1.2.3 Classes of colorimetric and fluorometric sensors

1.2.3.1 Lewis acid/base dyes (i.e., metal ion containing dyes)

Lewis acid dyes

Most strongly odiferous compounds are Lewis bases: thiols, phosphines, amines, carboxylic acids. Not coincidentally, these are also among the most common volatile metabolites of microorganisms; arguably, the primary function of the olfactory system is to keep us (and our digestive system) away from high concentrations of bacteria and other microbes, and hence the location of our nostrils immediately above the mouth! If one desires a sensor for the detection of such Lewis bases, then Lewis acids are the obvious solution, consistent with the likely involvement of metal ions in the olfactory system itself.[121-122]

Among Lewis acid dyes, metalloporphyrins (with different metals and different peripheral substituents) are a natural choice for the detection of metal-ligating vapors because of their open coordination sites for axial ligation, their large spectral shifts upon ligand binding, and their intense coloration. Indeed, the difference in color of scarlet red arterial blood and the purple of venous blood is

an example of the colorimetric detection of dioxygen as it ligates to a metalloporphyrin (i.e., the iron heme of hemoglobin). In addition, it is well recognized that porphyrins show significant solvatochromic effects resulting in distinguishable colorimetric changes before and after interactions with a wide range of both ligating volatile organic compouns (VOCs) (e.g., amines, thiols, phosphines, phosphites, thiols, etc.) and even weakly-interacting vapors (e.g., arenes, halocarbons, or ketones).[17] Metalloporphyrin are therefore nearly ideal for colorimetric[10,14,17,125] or fluorometric[7,126] (for d^{10} metals primarily) detection of metal-ligating vapors. A set of representative structures are shown in Figure 1.8.

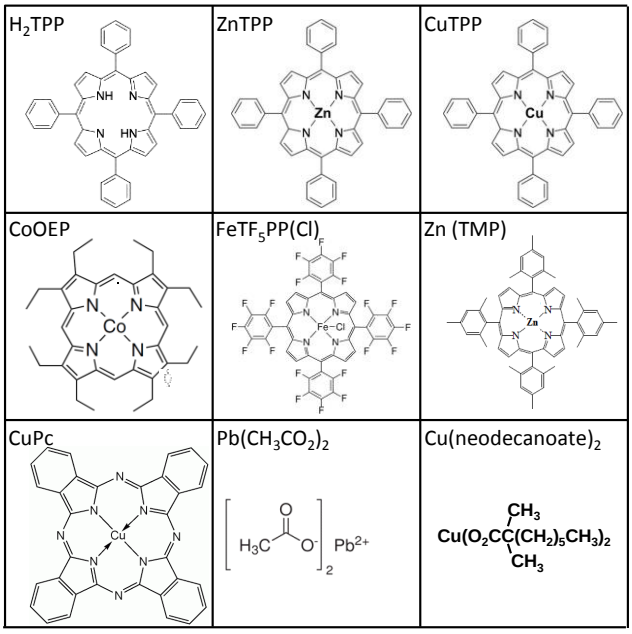

Figure 1.8 Molecular structures of some representative chemoresponsive or chromogenic dyes containing Lewis acid metal ions.

Shape and size selective metalloporphyrins

In addition to color change, another distinguishing feature with metalloporphyrins is one's ability to modify their periphery and provide shaped pockets to restrict access to the metal center. This capability was first developed by Collman and coworkers[127] with the picket-fence porphyrins used for reversible O_2

binding to Fe(II) porphyrins and later expanded by many others. Of special interest was Suslick's development of bis-pocket porphyrins[128-129] for selective hydroxylation of terminal methyl and methylene groups of alkanes and the selective ligation demonstrated on the first dendrimer decorated porphyrins[130-131] by Moore and Suslick. This type of thermodynamic selectivity is desirable for colorimetric sensors, as equilibrium binding to shape-selective metalloporphyrins can distinguish very similar molecules from the same chemical class (e.g., branched vs. linear amines).

A relatively new class of shape-selective metalloporphyrins was developed by Sen and Suslick.[132-133] A family of bis-pocketed porphyrins containing siloxyl groups on the ortho positions of a tetraphenyl porphyrin core has been shown in Figure 1.9. The family contains porphyrins with six, seven, and eight tert-butyldimethylsilyl groups (denoted as Zn(Si_6PP), Zn(Si_7OHPP), and Zn(Si_8PP)), giving a set of metalloporphyrins with very similar electronic characteristics but differing steric encumbrance about the metal binding site. Zn(Si_6PP), for example, has a binding pocket of ~4 Å, greatly restricting the bonding site. These zinc complexes were sensitive to the shape and size of Lewis basic analytes; binding constants for a series of amines were found to be controllable over a range of 10^1 to 10^7 relative to Zn(TPP)[133] and used in a colorimetric array to distinguish among alkyl amines.[134]

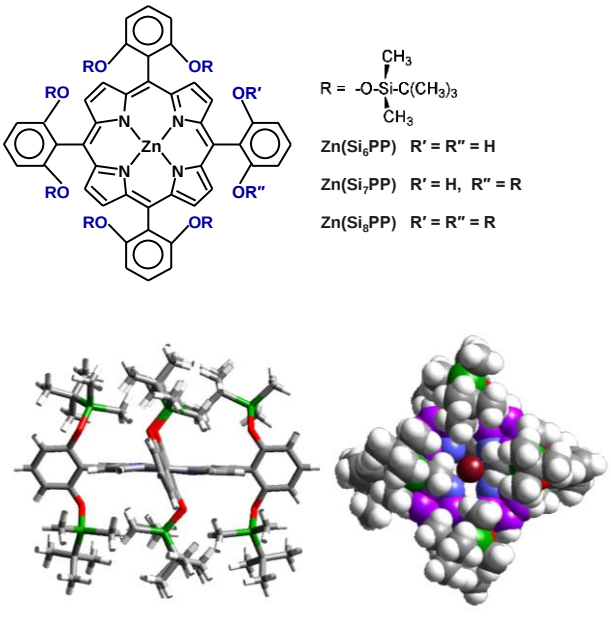

Figure 1.9 Bis-pocketed zinc siloxylporphyrins for shape-selective discrimination of Lewis base analytes. Upper: chemical structures. Lower: molecular models (framework side view and space-filled top-view) of $Zn(Si_8PP)$

Lewis acid sensors for anion detection

The coordination chemistry of anions was a long overlooked area of inorganic chemistry. The biological and medical importance of many anions, from the simple (Cl^-, F^-, HPO_4^{-2}, PO_4^{-3}, etc.) to the complex (ATP, lipid anions, nucleic acids, etc.), has demanded and received much greater attention in recent years.[135] The supramolecular chemistry of anions also plays essential roles in catalysis and environmental sciences.

There has been tremendous recent effort in the design of anion receptors for sensing by colorimetric or fluorometric means. The use of Lewis acid dyes for the detection of anions has been an active area of research and has been extensively reviewed recently.[101,136-145] There are, however, unique challenges to these studies because anion complexation is quite different from that of metal cations, largely because of the relatively large size of anions and the omnipresence of protons in aqueous media. Anion receptors can be neutral or positively charged and in general anion–receptor interactions are

dominated by electrostatics and hydrogen bonding. It is common to link a chromogenic or fluorescent reporter moiety to a specific chelating receptor, but one may also use fluorescent Lewis acids directly.

Displacement assays, dyes with urea, thiourea, or naphthalimide sites, or metal ion containing dyes (especially of lanthanide and labile d^8 and d^{10} transition metal ions) have all been explored especially heavily as anion binding sites for both colorimetric and luminescent detection. Work on colorimetric and fluorometric sensors for specific anions is important, but mostly beyond the scope of this review.

Lewis base sensors for cation detection

Chelating and macrocyclic ligands are, by definition, Lewis bases. Modern supramolecular chemistry finds its origins in the design of crown ethers, cryptands, etc. and their size specific binding of metal ions.[146] However, the use of semi-specific chelating Lewis acid dyes for colorimetric sensors of metal ions, so-called complexometric indicators[147-148] (Figure 1.10), dates back more than 150 years.

Complexometric indicators are used to chelate metal ions while simultaneously inducing a color change. These chromogenic or ionochromic dyes are designed to bring about a specific color change in the interaction with metal cations. Classical complexometric indicators (many of which are natural products also used as histological stains and some of which date back to the early 1800s) may have greater or lesser degrees of specificity: for example, calcein and Eriochrome Black T are used to detect Ca^{+2}, Mg^{+2}, and Al^{+3}; hematoxylin for Fe^{+3} and Al^{+3}; murexide for Ca^{+2}, Cu^{+2}, Ni^{+2}, and rare earth ions; and xylenol orange for Ga^{+3}, In^{+3}, and Sc^{+3}. Traditionally, complexometric titrations were displacement reactions, starting with the metal ions bound to the indicator and then displaced by the addition of EDTA, so that the free dye (rather than the metal ion complex) served as the endpoint indicator. Recent interest in metal ion sensors have taken advantage of the cross-reactivity of complexometric indicators to generate solution based arrays, for example using a microtiter plate or an immersed membrane[149-152] for simple identification of single metal ions in water.

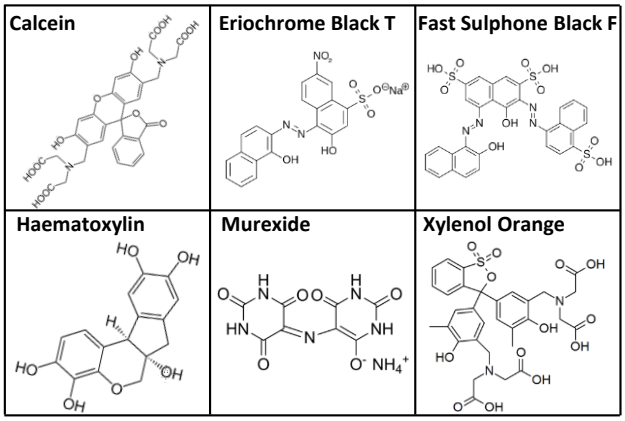

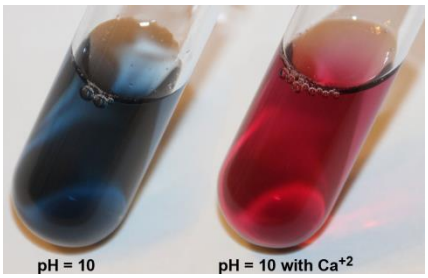

Figure 1.10 Upper: A sampling of traditional complexometric indicators. Lower: Eriochrome Black T in aqueous solution.

1.2.3.2 Brønsted acidic or basic dyes (i.e., pH indicators)

The origins of chemistry as a discipline are closely tied to our fascination with "pretty colors" and the importance of the dye industry to early chemists can hardly be overstated.[153-155] Many dyes, of course, change their colors depending on the pH. Litmus (7-hydroxyphenoxazone) was available even to alchemists in the Medieval times and literally means "colored moss" in Old Norse (litmus is produced by lichens, particularly *Roccella tinctoria*). There are, of course, dozens of pH indicators derived from natural products, especially the anthocyanin oxonium dyes from blueberries to grapes to red cabbage to rhubarb (Figure 1.11).

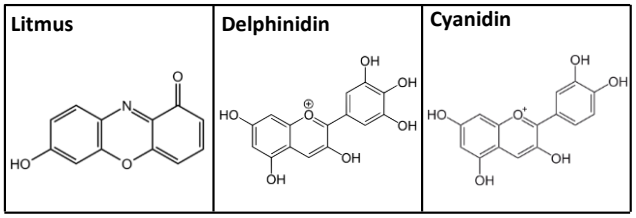

Figure 1.11 Some naturally occurring pH indicators. Litmus is from a lichen, delphinidin from cabernet sauvignon, and cyanidin from blueberries.

Synthetic pH indicators received enormous effort during the first half of the 20th century,[113] but even today substantial interest in new formulations (including sol-gel encapsulated indicators and indicators suitable for intra-cellular use in vivo) continues.[99,156-157] An immense variety of organic chromophores (*e.g.* azo dyes, nitrophenols, phthaleins, sulfophthaleins, aniline-sulfophthaleins, triphenylmethane dyes, etc.) were created largely to measure the pH of aqueous solutions or as histological stains for biomedical applications.[113,158] The pK_a values among various pH indicators for aqueous solutions range, of course, from below 0 to 14. The chemical diversity of some pH indicator dyes that have been used in colorimetric sensor arrays is shown in Figure 1.12.

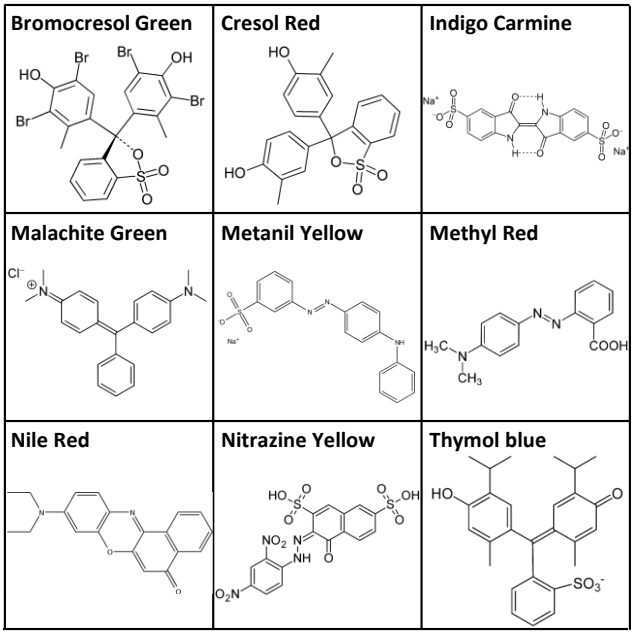

Figure 1.12 A sampling of representative pH indicator dyes.

1.2.3.3 Solvatochromic and vapochromic dyes

Dyes whose dipole moments are significantly different between their ground and excited states will show color changes depending upon the polarity of their environment: i.e., solvatochromism. If the excited state has a larger dipole moment, it will be more stabilized relative to the ground state in a more polar environment and vice versa. Nearly all dyes inherently show some solvatochromism. For "solvatochromic" dyes, these changes in dipole moments are very large, leading to impressive color or fluorescence changes that depend upon the polarity of the solvent in which the dye is dissolved (Figure 1.13).

Common classes of solvatochromic dyes include the merocyanines, azobenzenes, oxazones, thiazines, nitro-amino-substituted polythiophenes, and pyridinium N-phenolate betaine dyes. A common feature of most solvatochromic dyes is that they are "push-pull" systems (Figure 1.11) with a strong zwitterionic component to their electronic structure, i.e., a large conjugated π system with strong electron donor groups at one end and strong electron withdrawing groups at the other.

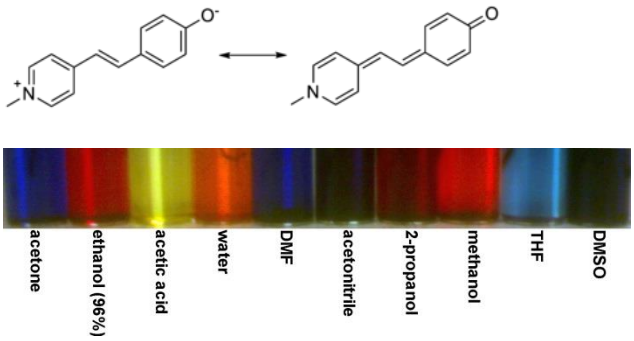

Figure 1.13 Brooker's merocyanine dye, (1-methyl-4-[(oxocyclohexadienylidene)ethylidene]-1,4-dihydropyridine, and its solvatochromic shifts in various solvents.

Several solvent polarity scales[159] have been based on the wavelength shifts of optical transitions of solvatochromic dyes, including Kosower's and Brooker's early studies, Reichardt's ET[159-163] and Taft's π* [164-165] scales. Solvent polarity is very much a multi-parameter property, involving dipolar, quadrupolar, and mult-polar interactions, hydrogen bonding donation and acceptor properties, Lewis acid-base interactions, etc. Thermodynamic and theoretical analysis of the origin and meaning of solvation, solvent polarity, and solvatochromism continue actively;[166-169] especially useful are thorough comparisons among all related multiparameter descriptions of solvent polarity.[159,167,170-171] Of particular interest for optical sensor arrays, the use of polymers doped with a solvatochromic dye (often Nile red) as a reporter on swelling of the polymer by absorbed analytes has been heavily used for optical fiber sensors.[6,172-173]

A separate class of solid-state materials that provide a colorimetric response to solvent vapors are referred to as vapochromic or vapoluminescent solids.[174-175] These are most commonly porous coordination complexes, particularly of square planar Pt(II) d^8 compounds. The vapochromism is triggered by intercalation of solvent molecules into the porous crystals and the color and luminescence changes derive from changes within the solids from weak interactions including coordination of solvent molecules to the metal centers, metallophilic contacts, π-π stacking, hydrogen bonding, and general

non-specific host-guest interactions; these interactions can lead to changes in the ordering of excited states, leading to large luminescent differences. A particularly striking example has been recently reported using triarylboron-functionalized phenylacetylide platinum(II) square planar complexes.[176] Chiral vapochromic materials have also been used for identification of enantiomeric vapors.[177] Because vapochromism requires intercalation into the interstices of crystalline materials, the response time can be somewhat slow (although controllable, perhaps, using nanocrystalline morphologies), and the weak interactions responsible can also lead to limited sensitivity of these materials as sensors.

1.2.3.4 Redox indicator dyes

Oxidation/reduction (redox) indicators are colorimetric reagents which show a distinct color change at a specific electrode potentials. These are all organic compounds exhibiting reversible redox reactions. Examples include anilinic acid, diphenylamine, eriogreen, m-cresol-indophenol, methylene blue, and nile blue.[178-180]

Due to the fact that the majority of redox indicators engage a proton as a participant in their electrochemical reactions, redox indicators are sometimes divided into two groups separating those that are dependent on pH and those that are not. In order to make an optical sensor for sensitive detection of hydrogen peroxide (i.e. in the concentration range of 10^{-8} to 10^{-1} mol/L), a redox indicator (e.g. Meldola blue) was used in a sol-gel layer.[180] In order to have sensitive detection of triacetone triperoxide (TATP) vapor (i.e. in the range of 50 ppb to 10 ppm), a colorimetric sensor array based on redox dyes including Lissamine Green B, o-dianisidine, diphenyl amine, N-phenyl-1,4-phenylenediamine and N,N'-diphenyl-1,4-diphenyldiamine (Figure 1.14) was constructed by Lin and Suslick[181]. Using a method of hydrolyzing TATP vapor to constituent acetone and hydrogen peroxide, the array was capable of detecting concentrations of TATP vapor down to 2 ppb.

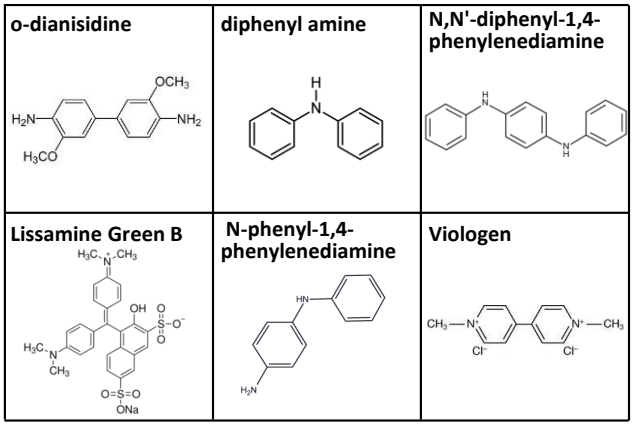

Figure 1.14 Representative structure of some common pH-independent redox dyes.

1.2.3.5 Chromogenic aggregative colorants

Chromogenic colorants whose color is altered by aggregative phenomena has become an area of massive recent development, especially for biosensing.[182-184] Processes that cause aggregation, dispersion, or formation of colloidal materials generate changes in color and fluorescence through various mechanisms, ranging from simple absorbance and scattering by colloidal solids to plasmonic absorbance to quenching of attached or adsorbed fluorophores. The simple precipitation of metal salts or formation of metal nanoclusters on reaction with thiols and sulfides goes back to the earliest qualitative spot tests.[111-112]

The recent cutting edge is represented by control over the nanostructure of optical sensors. For example, gold nanoparticle (NP) agglomerates that efficiently quench adsorbed fluorophores; analyte binding can disperse such nanoparticle agglomerates and create a fluorescence turn-on. Judicious choice of NP functionalization and of fluorophore provides a versatile platform for *solution phase* sensing.

1.2.3.6 Displacement strategies for fluorescent probes

There are three general classes of fluorescent indicators for chemical sensing in solution: (1) intrinsic probes (where the sensor is itself fluorescent), (2) conjugated or extrinsic probes (where a

fluorophore is conjugated to the sensor binding site and its fluorescent properties modulated by analyte binding), and (3); displacement, dissociation, or differential probes (where the analyte competitively binds to an artificial or natural receptor that also binds a fluorophore).[99,102-103,185]

Displacement probe strategies require some sort of reversible interaction between a receptor (natural or artificial) and a reporting fluorophore/chromophore; the binding of the reporter molecule must modify the fluorescence or color the reporter. The receptor can be either specific for one class of analytes or more cross-reactive.

Indicator displacement assays (IDA) use a parallel set of multiple not-too-selective displacement probes, often referred to as differential selectivity, to generate a pattern of response not unlike the colorimetric sensor arrays already discussed. This approach has been particularly well explored by the Anslyn group.[101-103] The potential disadvantage of displacement strategies, of course, is diminished sensitivity because there is an inherent competition between the analyte and the already bound fluorescent or colorimetric reporter.

One normally thinks of sensor arrays as single physical solid devices: a printed array on a polymer membrane or a bundle of fiber optic probes, etc. Displacement strategies, however are generally limited to solution phase sensing and do not lend themselves easily to a solid-state sensor array platform that could be immersed in a solution of analytes. Instead, solution phase array sensing is carried out by a parallel analysis of multiple aliquots of the analyte solution, each with an added, different homogeneous probe, e.g. using microwell plates with a microwell fluorescent scanner.

Kubarych, Adams, and Anslyn used a set of commonly available proteins with a set of fluorophores as non-specific probes for hydrophobic molecules.[186] In this case, non-specific hydrophobic binding interactions were used with an indicator displacement strategy to provide multiple diverse probe sites within a single protein molecule, as shown schematically in Figure 1.15. This led to the ability to differentiate among several different hydrophobic species including fatty acids and food oils.

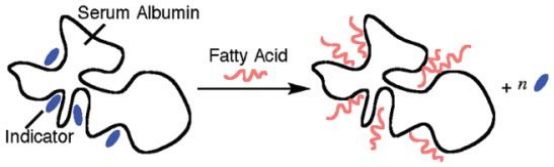

Figure 1.15 Illustration of a displacement strategy using serum albumin as a non-specific receptor and fatty acid as an analyte displacing a fluorescent indicator. Dyes are initially bound in disparate hydrophobic binding sites which lead to differential sensing ability. Reproduced with permission from ref. [186].

1.2.3.7 Molecularly imprinted optical sensors

One way to improve optical sensor resistance to interferents is the application of a molecular imprinting technique.[187] The molecular imprinting is a process which can rapidly synthesize polymers with differential selectivity to targeted analytes, which include both molecular and ionic species as well as enantiomers[188-195] In general terms, one includes a non-polymerizing analyte in the monomer solution during polymerization. The templating analyte is then exhaustively removed from the resulting polymer. This molecularly imprinted polymer (MIP) must be sufficiently crosslinked to retain internal structural integrity, but not so rigid as to prevent template removal. As with displacement assays, MIP sensors face the problems of specificity and are also generally limited to solution phase sensing.

As an example, Shimizu and coworkers[189] constructed a sensitive, selective receptor array with a molecular imprinting procedure which was able to classify different amines (Figure 1.16). They applied a dye-displacement strategy for rapid and versatile measurable colorimetric response. The presence of molecularly imprinted polymers (MIP) with high cross-reactivity as detection elements provided a specific response for each analyte.

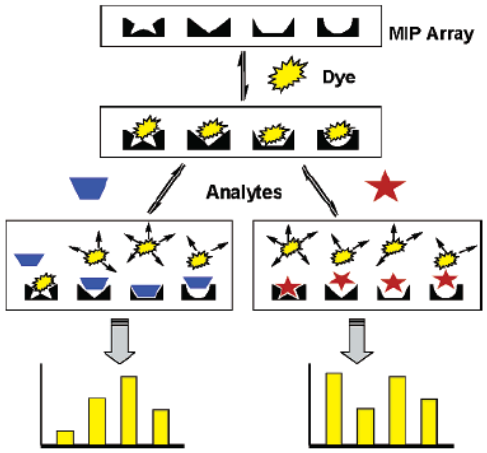

Figure 1.16 A representative Scheme of an molecularly imprinted polymer sensor array that uses a dye-displacement strategy to give an easily visualized and unique colorimetric response pattern for each analyte Used with permission from ref. [189].

1.2.4 Substrate considerations

1.2.4.1 Printed arrays

While the choice of chemoresponsive dye or fluorophore will dominate the effectiveness of any optical sensor array, the functionality of the array will also be influenced by the substrate and morphology of the substrate upon which the colorant is placed. Sensitivity, reliability, accuracy, response time, susceptibility to interferents, and shelf-life of the array can be heavily influenced.

A wide variety of solid supports have been used for colorimetric and fluorometric array construction. The desired properties of such substrates include inertness towards gases and liquids, high surface area (to incorporate sufficient colorant), optical transparency or high reflectivity, and stability over a wide pH range.[16,48,85,89,156] A simple method for array manufacture involves printing dye formulations on the surface of reverse phase silica gel plates, acid-free paper, or porous polymer membranes made out of a material such as cellulose acetate or polyvinylidene difluoride (PVDF). Robotic pin printers serve this function particularly well (Figure 1.17). Ink-jet printing works well for a

limited number of sensors, and spin-coating[196] can also be used, but is difficult for multiple spot arrays.

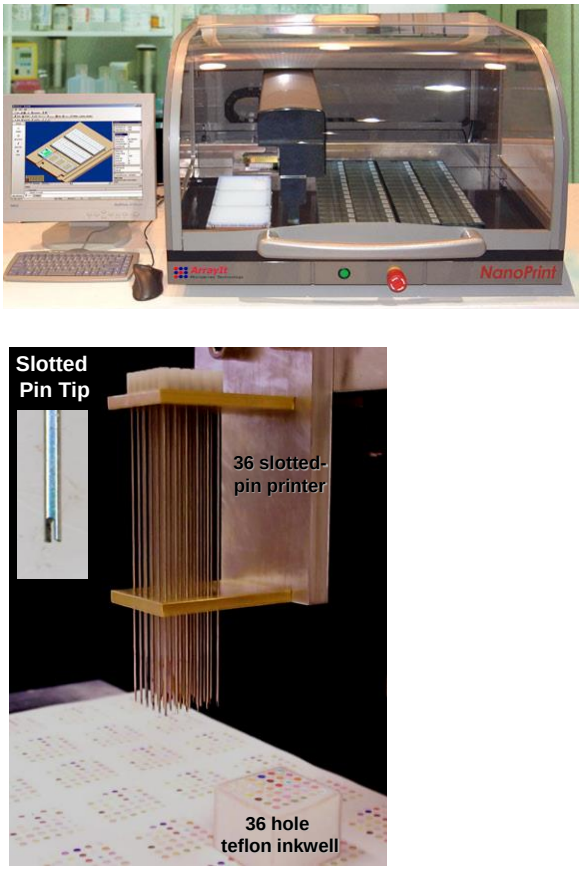

Figure 1.17 A robotic pin printer (upper) with a slotted pin printing array (lower) is capable of printing hundreds of sensor arrays per hour.

A major shortcoming of many chemical sensors is their sensitivity to changes in ambient humidity.[6,8] For any real world application, changes in humidity from day to day or from indoors to outdoors can involve changes of tens of thousands of ppm in water vapor concentration. Any significant response to humidity can prove lethal for detection of ppm concentrations of VOCs. The use of hydrophobic materials (e.g., PVDF membranes) as colorimetric or fluorometric sensor array substrates can be highly advantageous in reducing array response to humidity over a wide range (10 to >95% relative humidity)[14,17,114,197-198] and can even permit the use of such arrays in aqueous solutions.[199]

For sensing applications, soluble, molecularly-based dyes are deposited as a viscous film or on a high surface area membrane or solid, and the analytes can gain access to the colorant with an acceptable response time. In contrast, pigments (which by definition are insoluble colorants) are not generally permeable to analytes and therefore reactive only on their outermost surfaces, which dramatically reduces any colorimetric or fluorometric response to the presence of analytes. Molecular dyes, however, often have limited shelf-life as sensors, particularly when incorporated into viscous films or polymers due to crystallization (and consequent loss of analyte accessibility to the colorant centers).[200]

Porous sol–gel glasses can also provide excellent matrices for chemically responsive colorants.[85,156,201-202] An effective nanoporous pigment sensor can be made by adding chemoresponsive dyes to ormosils prepared from suitable silane precursors in low volatility solvents. [16,197,200,203-204] In addition, the physical and chemical properties of the matrix (e.g., hydrophobicity, porosity) can be easily altered using organically modified sol–gel (i.e., "ormosil") formulations, and different silane precursors are needed depending on the solubility of the dye. The use of these porous pigments significantly improves the stability and shelf-life of the colorimetric sensor arrays and permits direct printing onto non-permeable polymer surfaces.[16,200,203,205] Additionally, we have observed that the matrix may serve as a preconcentrator, improving the overall sensitivity.

Digital image analysis shows that printing of these nanoporous pigments have a uniform color distribution across the center of the spot (Figure 1.18).[200] Reproducibility of the optical densities of printed spots is excellent, and chemical sensing experiments generally use the difference between before-exposure and during-exposure image, which further reduces errors in the pattern analysis. It is also important that image analysis of printed spots utilize the average RGB values of the center portion of the printed spots to eliminate artifacts from the spot edges.[114]

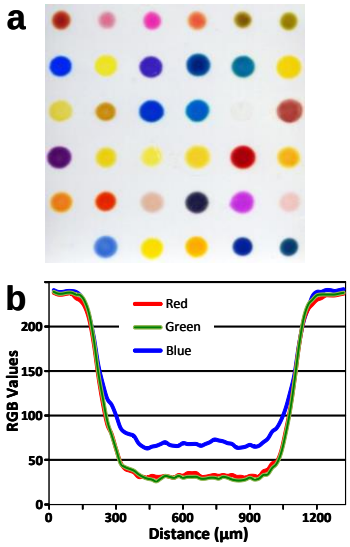

Figure 1.18 (a) Image of a printed array, 1.2.5 x 1.2.5 cm. (b) RGB values of a linescan across the centre of a typical spot. Used with permission from ref. [200].

The development of optically based chemical sensing platforms has increasingly employed substrates manufactured with advanced processing techniques, and the control of over sensor morphology, micro- and nano-structure must be characterized.[21] Scanning electron microscopy has shown that the nanoporous pigment films are typically ~3-4 µm thick with uniform silicon content throughout the spot, and transmission electron micrographs reveal the pore structure of these ormosil films (Figs. 19 and 20), which assist in mass-transport, and are responsible for the fast response times observed during sensing experiments (90% response generally occurs in < 2 minutes).[200]

Another means of generating nanoporous pigments has been reported. Bang *et al.*[205] who prepared silica microspheres using tetramethoxysilane (TMOS) and methyltrimethoxysilane precursors (MTMS) in which chemoresponsive pH and solvatochromic dyes were incorporated with an ultrasonic-spray aerosol-gel synthesis method.[206]

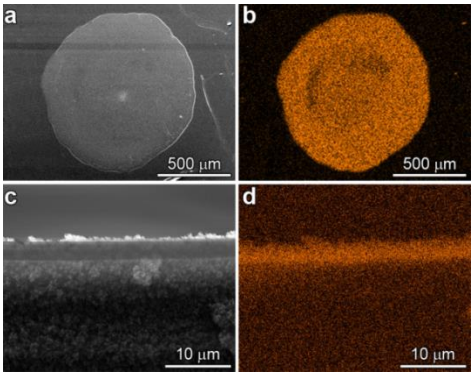

Figure 1.19 SEM micrographs of a 1 mm diameter spot of a porous ormosil pigment printed on PET film: (a) top surface and (b) energy dispersive spectroscopic (EDS) elemental mapping (Si Kα); (c) cross-section and (d) EDS elemental mapping (Si Kα). Used with permission from ref. [200].

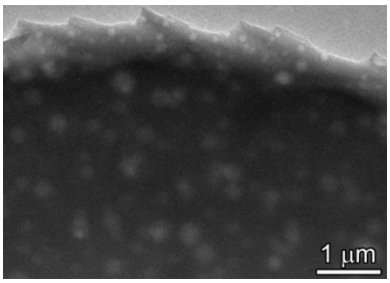

Figure 1.20 TEM micrograph of porous ormosil pigment showing the 50 to 200 nm pore structure created in these ormosil xerogels. Used with permission from ref. [200].

1.2.4.2 Fiber optic arrays

A powerful alternative, especially for fluorescent sensors, is the use of fiber optic arrays. Almost twenty years ago, Walt and co-workers began developing multi-fiber optical bundles as cross-reactive or multi-receptor high-density sensor arrays.[207] In this technique, bundles of very small silica fiber-optic cables are chemically etched to create a 2-dimensional array of microwells, which are used to hold a random distribution of beads containing individual fluorescent probes. In order to ameliorate the loss of physical position as a useful measurable property, these beads are functionalized with optical encoding elements so as to identify themselves during the analysis. A graphical explanation of this process is

shown in Figure 1.21 and SEM images of the final arrays are shown in Figure 1.22.

For achieving simultaneous, multi-analyte, high-density, and high-throughput sensing analysis, the optical fiber-based arrays were developed using optical fiber bundles that comprise thousands of individual single-core fibers which are individually modified with a diverse sensing chemistry using a random assembly method. In general, the fiber arrays (with total size of around 1mm) contain a few thousand up to a hundred thousand individual fibers with size of 2-10 μm prepared by selective etching of the polished array in acid solution[208] (Figure 1.22). This engineered structure enables individual wells to be recognized by the optical fiber defining its base, providing a high-density array of micro-wells that can be simultaneously and independently interrogated by light. Excitation light is introduced into the unfunctionalized end of the fiber; emission signals from individual sensors return through the fiber and are magnified and projected onto a charge-coupled device (CCD) camera, leading to the simultaneous observation of all sensors.[209]

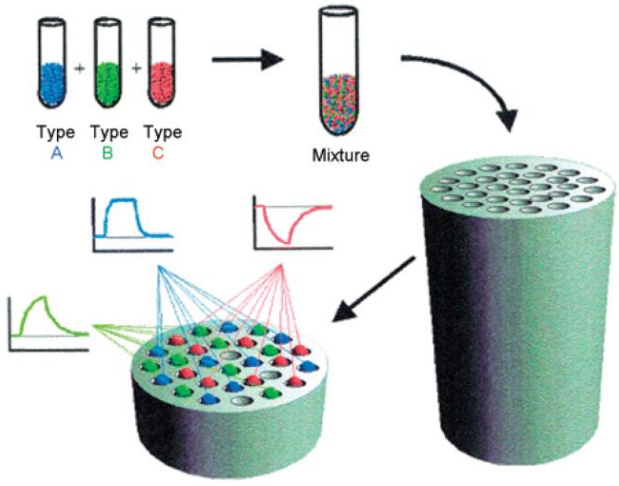

Figure 1.21 General strategy used for creating bead microarrays using etched fiber-optic bundles. Types A, B, and C (blue, green, and red respectively) indicate the types of self-encoded beads, while the insets represent a typical time-based sensor response to an exposed analyte. Reproduced with permission from ref. [210].

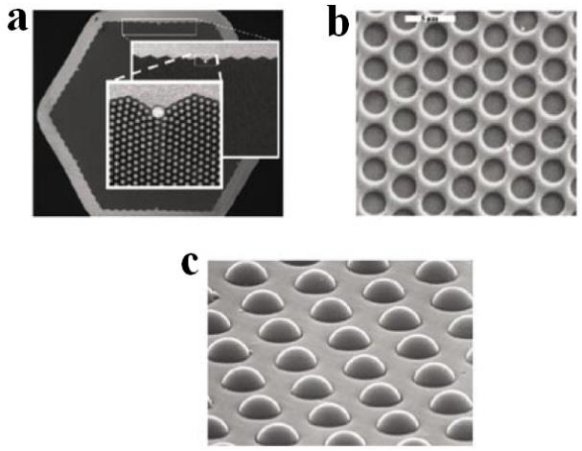

Figure 1.22 SEM images of etched fiber-optic bundles. (a) Optical fiber-based array with hexagonal pits contains 50,000–60,000 fibers; inset shows magnified views of the individual fibers (bright dots); (b) microwells etched into the individual fibers and surrounded by cladding; darker gray circles correspond to the ends of the optical fibers defining the bottom of each well; (c) beads loaded into wells. Reproduced with permission from ref. [173].

These fiber-based fluorescent sensors have found impressive use in biosensing[181, 182] for immobilization of desired bio-molecular sensors[172,211-212], single molecule detection[213-214], and even whole cells[215-216] on the fibers.[217-218] Living cells and beads containing biological recognition elements are loaded into the micro-wells (with the volume of femtoliter).[209,219-220]

1.3. Statistical analysis and modeling

Chemical property space has a very high dimensionality because of the large number of different chemical properties that are largely orthogonal to one another (e.g., Lewis acid/base, Brønsted acid/base, redox, electrophilicity, nucleophilicity, hydrogen bonding, polarity, etc.). To differentiate among all possible volatile compounds and the huge assembly of possible mixtures of those compounds requires highly multidimensional data representing a wide range of chemical properties space. Fundamentally, this is why the olfactory system evolved to incorporate hundreds of highly cross-reactive

receptors: the combinatorials of the responses of those cross-reactive sensors provides the high dimensional data used by the olfactory bulb for pattern recognition of odorants.

If one bases a sensor array on physical properties, however, there is a very limited dimensionality to the resulting data. Physical adsorption/absorption will dominate any interaction of analytes either with simple surfaces (e.g., metal oxide electrical sensors or chemFETs, etc.) or with polymer coatings (e.g., coated quartz microbalances, conductive or composite polymer sensors, etc.). The primary contributions to physisorption (van der Waals, weak hydrogen bonding, polar interactions) are roughly equivalent to what chemists refer to as "hydrophobicity".

As a consequence, one of the dirty little secrets of electronic noses is that *they are only rarely multidimensional arrays in a statistical sense*.[5,8,18] The sensor may be a physical array (e.g., an array of ten or twenty different metal oxides or a dozen different conductive polymer composites), but that does not in and of itself make the sensor a multidimensional array for analytical or statistical purposes. In general, in such physical arrays, there is in fact only one overwhelming dominant dimension that contains >90% of the total variance among analytes: most often,that dimension is essentially hydrophobicity. As a consequence of this intrinsic low dimensionality, most conventional electronic nose technology is not able to distinguish among large libraries of similar complex mixtures.

Low dimensional data does have some advantages. Statistically, analysis is simplified, but often at the cost of more limited discriminatory abilities. The primary advantage of relying on weak analyte-sensor interactions such as physical adsorption is improved reversibility, especially over short periods of time, but even this is a two edged-sword: the reversibility comes directly from the weakness of the interaction, which implies diminished sensor sensitivity!

In contrast, sensor arrays based on chemical properties have intrinsically a much higher dimensionality. Having a high dimensionality has the advantage of much greater ability, at least in principle, of being able to differentiate among analytes with much greater discriminatory power. The

disadvantage of limited reversibility for strong interactions can be overcome by making the sensor array disposable, as we have already discussed, and is counterbalanced by the improvement in sensitivity and improved limits of detection.

The greater dimensionality, however, must also involve a more sophisticated approach to statistics than that which chemists are often comfortable.[221] The inherent problem with high dimensionality is that the analytical volume increases much more rapidly than the available data, so the datasets are often formally "sparse" compared to the total size of the parameter space. In addition, this "curse of dimensionality" creates difficulties for function approximation, model fitting, information extraction, as well as computation.[222] Statistic methods for multidimensional data all share the common goals of displaying multidimensional data effectively, evaluating data sets, and predicting the identity of unidentified samples based on a known library.

There are a variety of statistical methods available to deal with high dimensional data well beyond the scope of this review.[223-224] We will give an overview here only of the three most common approaches: hierarchical cluster analysis (HCA), principal component analysis (PCA), and linear discriminant analysis (LDA).

In general, for chemometric data there are two distinct statistical approaches: clustering vs. classification.[223-225] Cluster analysis essentially tells one what resembles what, e.g., how close the vectors representing data are to one another in a high dimensional space. Classification analysis, on the other hand, attempts to predict to which category (among a fixed number of known categories) any particular (new) datum belongs.

Statistical methods can be either *biased,* in which case the evaluation algorithm is told of the class identities of individual cases, or *unbiased* (or model-free)*,* where all cases are evaluated identically regardless of class identity. Unbiased methods are typically used to evaluate a data set to provide a semi-quantitative idea of the quality of the data set and follow simple, straightforward algorithms.

Biased methods, on the other hand, can provide significantly more power and utility with a concomitant increase in complexity, but at the cost of demanding datasets for which one already knows the answers. Biased methods can be predictive, allowing for class assignment of new experimental cases by using a training set.

1.3.1 Hierarchical Cluster Analysis (HCA)

HCA is an agglomerative clustering technique whereby clusters are determined from the Euclidean distance between experimental data. In its simplest form, nearest-neighbor points are paired into a single cluster which is then paired with other nearest-neighbor points or clusters until all points and clusters are connected to each other, shown schematically in Figure 1.23[224-225] The most common clustering criterion used in HCA is Ward's minimum variance method, which minimizes the total within-cluster variance.

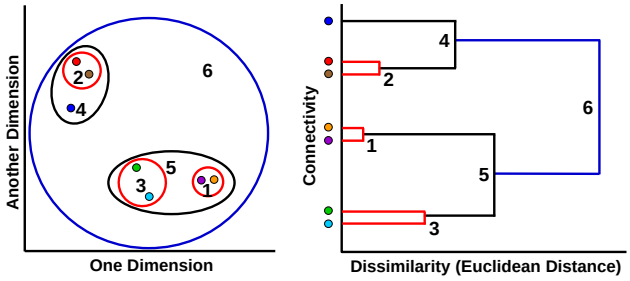

Figure 1.23 Schematic representation of a hierarchical cluster analysis (HCA) of multidimensional data (shown in only two dimensions on the left) that forms a dendrogram based on clustering of those experimental measurements (shown on the right).

The resultant dendrogram shows connectivity and some measure of the distance between each of the pairs. In the context of chemical analyses, these two important pieces of data answer two questions: connectivity explains relationship similarity, i.e. '*what species/samples are similar to each other?*' and

distance explains magnitude, i.e. *'how similar are they?'*.

There are three primary limitations to the HCA technique. The first involves fundamental limitations of all unbiased methods: HCA is not easily capable of predictive analysis. Second, dendrograms created using HCA must be re-created with each addition of a new analyte, so comparing dendrograms (even with a very similar data set) is typically only useful for rough qualitative purposes, i.e. *'what does this new sample look most like?*'. The third limitation is that of interpretation of noisy data. One must be cognizant that the dendrograms are essentially "mobiles" and that rotations around clustering axes do not represent meaningful differences between dendrograms, as shown in Figure 1.24: mis-clustering of noisy data can be easily misinterpreted.

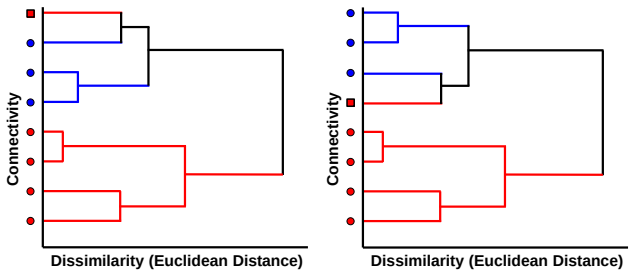

Figure 1.24 The effect of noisy data in dendrograms showing two classes of data, red and blue with one mis-clustering shown as a red square. These two dendrograms are mathematically identical and represent exactly the same data: the order of connectivity is not relevant on the y-axis. At first glance, however, the red square data appears much further out of place in the dendrogram on the left compared to the dendrogram on the right.

Despite these limitations, dendrograms provide a straightforward method of displaying cluster similarity semi-quantitatively. A representative example containing 100 VOCs is shown as Figure 1.25; it is worth noting that similar chemical classes cluster tightly together, which is a consequence of the reactivity of the particular sensor array.

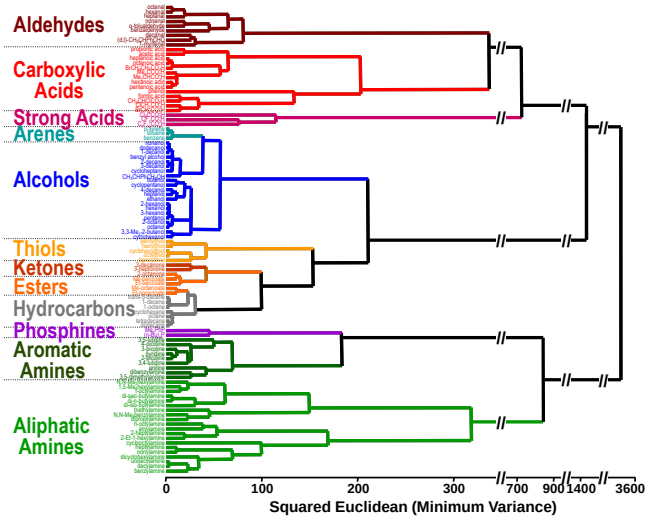

Figure 1.25 Dendrogram from HCA of the colorimetric array responses to 100 common organic compounds at full vapor pressure at 300 K. Reproduced with permission from ref. [10,114].

1.3.2 Principal Component Analysis (PCA)

PCA is a dimensional reduction technique that condenses the variance among several possibly-correlated dimensions by creating a new orthogonal set of dimensions using linear combinations of the initial dimensions. These new dimensions (also called directions, components, etc.) are ranked such that the first dimension explains the largest amount of data variance, the second dimension explains the second largest, and so on. One typically seeks a number of new orthogonal dimensions sufficient to encompass at least 95% of the variance. Plots using the resulting set of principal components are often easier to visualize than the original data set, but *only* if the original dataset is actually low dimensional in a statistical sense. As discussed earlier, electronic nose data often requires only two or perhaps three principal components to express the true variability among the data, regardless of the number of different sensors in the physical array. For low dimensional data, PCA therefore provides a straightforward method of displaying sample set variability, i.e. *'how similar are these species/samples*

to each other?'.

As we shall see in Section 3, when dealing with a large number of analyte classes, a sensor array designed to probe a large reactivity space (i.e., an array with high dimensionality in a statistical sense) is highly desirable. If one is examining a narrow class of analytes, however, then apparent high dimensionality of a sensor array, regardless of the number of actual physical sensors, becomes indicative of large amounts of noise relative to total variance: in such cases, in the absence of noise, the theoretical maximum dimensionality is equal to the lesser of either the number of sample classes or the size of the chemical reactivity space.

As a consequence, the dimensionality of one's data is *not* determined directly by the number of different sensors in one's array. As an example, Lin and Suslick[181] designed a colorimetric array containing 16 redox-sensitive dye formulations to detect specifically strong oxidants and peroxy-based explosives and was not designed with other reactivity properties in mind. This array probes only a small chemical reactivity space, and the PCA reveals that only two dimensions (n.b., *not 16*) were required to reach 95% variance, as shown in Figure 1.26.

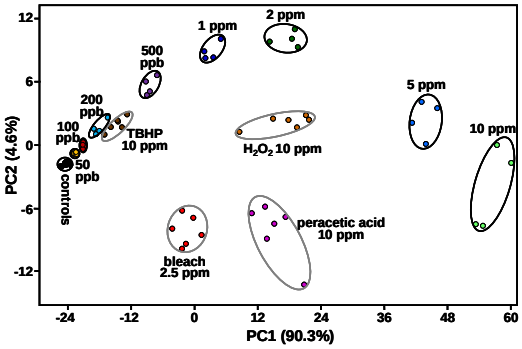

Figure 1.26 PCA score plot showing two-dimensional separation of multiple classes of redox-active analytes generated from triacetone triperoxide vapor (concentration labels only) and other redox-active analytes. Circled areas represent 95% confidence intervals. Note that only two dimensions were required to reach 94.9% variance, implying a small chemical reactivity space probing only one or two

primary reactivity properties; this particular sensor array used several two-electron redox-sensitive dyes encapsulated in a xerogel matrix and was not designed with other reactivity properties in mind. Reproduced with permission from ref. [181].

Since principal components are combinations of individual array component responses, the number of dimensions required for 95% variance provides information about the range of analyte-sensor interactions being probed; an array that probes only pH, for example, may only have one dimension required to reach 95% variance, while an array that probes pH, hydrophobicity, dipole moments, film permeability, and nucleophilicity can be expected to require at least five dimensions. PCA is thus a powerful tool for evaluating sensor arrays, especially those with multiple disparate components, as it allows some insight into the sensor's "chemical reactivity space", i.e. the number and possibly identities of chemical interactions being probed by the sensor array. A scree plot, showing the cumulative contributions of each principal component, provides a quantitative measure of the contributions of different orthogonal reactivities to the variance of the array response (Figure 1.27).

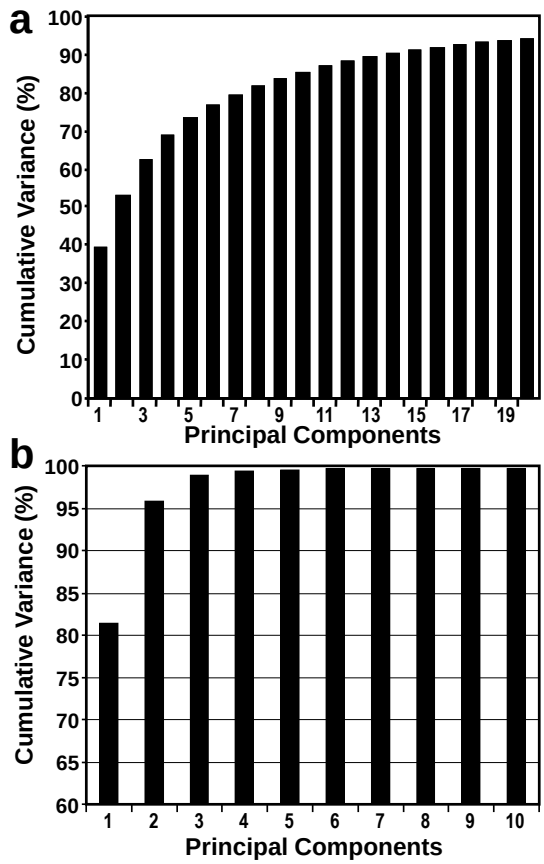

Figure 1.27 (a) a scree plot of data from a colorimetric sensor array tested with 100 VOCs, showing high dimensionality: 22 dimensions required for >95% total variance. (b) a scree plot from a colorimetric sensor array tested with 14 natural and artificial sweeteners, showing low dimensionality: 2 dimensions required for >95% total variance. It can be inferred that the chemical reactivity space of the sensor array interacting with VOCs is large, while that used in the array for artificial sweeteners is small, with pH being a primary component. Reproduced with permission from refs. [114] and [226].

Like HCA, PCA is an unbiased method that is best suited for evaluation of data sets rather than prediction. PCA, however, can make rudimentary prediction methods possible, especially if the data set is low dimensional and has a large separation among sample classes. If the data set does not have a large separation, however, PCA may not adequately be able to predict the identity of an experimental sample. Examples of these are shown as Figure 1.28.

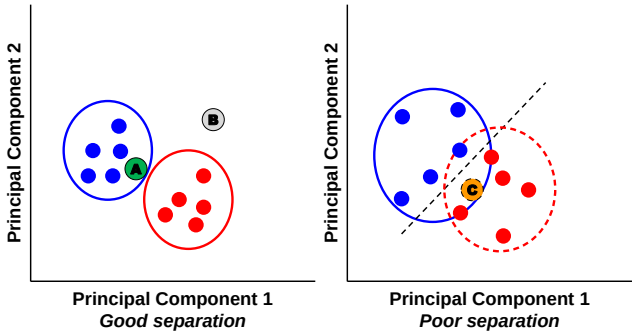

Figure 1.28 PCA score plot showing red and blue classes and three unknown experimental points A, B, and C. Circled areas represent 95% confidence intervals. By using a dataset with good separation (left), it can be inferred that green circle A belongs to the blue class, and grey circle B does not belong to either the blue or red classes. Using a dataset with poor separation (right), orange circle C cannot be unambiguously identified despite appearing to be significantly closer to other members of the red class, with the dashed line representing an obvious (by eye) separation between the two classes.

1.3.3 Linear Discriminant Analysis (LDA)

Like PCA, linear discriminant analysis (LDA) is a dimensional reduction technique that constructs a set of orthogonal dimensions used to describe the data; LDA, however, seeks to find a set of dimensions that best separates data into already known classes, rather than simply describing the total variance. Unlike HCA or PCA, LDA is a biased method; statistical analysis using LDA requires inputting a class label for each sample. Components of each dimension are ranked in order to maximize the ratio of *between-sample variance* to *within-sample variance*; i.e. it ranks components based on their signal to noise ratio as compared among differing sample classes.

LDA can be used to predict the identity of unknown samples by using a training set, similar to PCA. However, because the dimensional components are optimized to maximize differentiability, LDA will show better ability to differentiate among sample classes. A general example of this improvement is

shown as Figure 1.29.

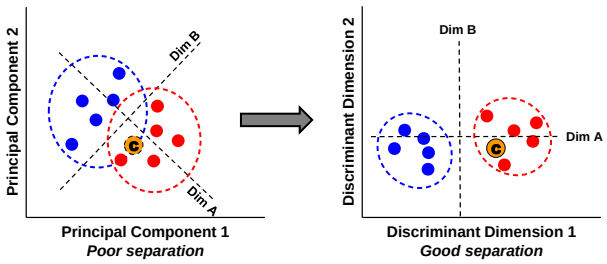

Figure 1.29 Score plots comparing data analyzed with PCA (left) and LDA (right). Circled areas represent 95% confidence intervals. The most obvious separation by eye in the PCA plot is along dimension A, which is orthogonal to dimension B; this is used as the first dimension in LDA analysis and is a visualization of the between-sample variance. Orange circle C is clearly identified as being in the red class using LDA, while identification is ambiguous using PCA.

The primary weakness of LDA is related to sample size. All statistical methods require multiple observations in order to determine any useful data (e.g. mean, variance, etc.); LDA is unique among the three methods presented here, however, as sample class covariances must also be determined in order to allow for comparison among classes. Because of this, the covariance matrix tends to be unstable when sample size is not significantly larger than the number of sample classes being analyzed, and this is more problematic for high dimensional data;[222] consequently, LDA can give drastically fluctuating results with small sample sizes (compare to PCA or LDA, which can be unreliable with small sample size, but not unstable). A representative example of a two-component LDA plot is shown as Figure 1.30.

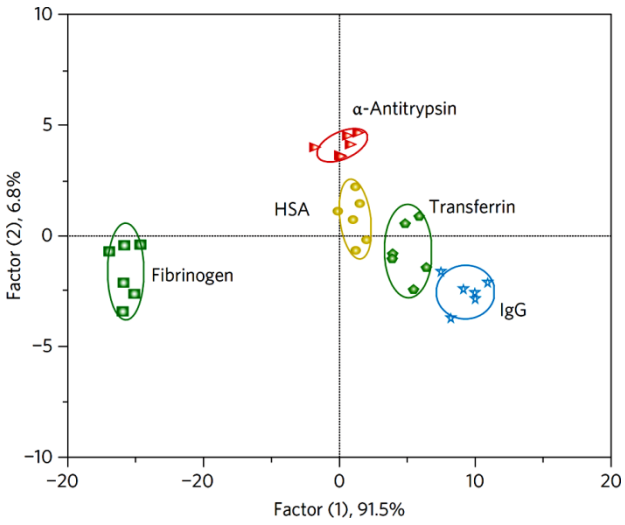

Figure 1.30 LDA score plot showing separation among five serum proteins at 25 nM concentration. Circled areas represent 95% confidence intervals. Reproduced with permission from ref. [227].

As an improvement on LDA, tensor discriminant analysis[228-230] (TDA) is an array generalization of LDA better able to take advantage of high dimensionality. More precisely, tensor discriminant analysis is used to classify multi-way array measurements (i.e., "tensor measurements"), rather than one-way vector measurements.[228-229] For example, the data collected using colorimetric sensor arrays can be viewed as a 3-way tensor with the first way corresponding to choice of the dye, the second way corresponding to the effects of the color changes (i.e., ΔR, ΔG, ΔB, which are not fully independent for any one dye), and the third way corresponding to time progression (for kinetic responses).[230] The general strategy of tensor discriminant analysis is to find orthogonal linear classifiers, which are essentially linear combinations of the three-way interactions of the effects of the dye spot choice, the three color changes of each spot (i.e., ΔR, ΔG, ΔB), and the temporal evolution, to maximize the ratio of between-class variation to within-class variation. Tensor discriminant analysis can greatly improve the sensitivity, specificity, and computational efficiency of discriminant analysis method because of the dimensionality reduction. For example, if there are 36 dyes, then LDA would have to deal with 36*3=108 dimensions, whereas TDA would reduce that to 36+3=39 dimensions, thus eliminating 69

dimensions (i.e., 108-39) that contain primarily noise.

1.4 Applications of optical sensor arrays

1.4.1 Discrimination of volatile organic compounds

The colorimetric sensor array first developed by Rakow and Suslick used an array of different metalloporphyrins exclusively for the visual identification of different families of organic vapors.[17] Ligation of analytes to metalloporphyrins induced large color changes that were used for their identification. The sensor array was able to respond to a wide range of organic compounds such as alcohols, amines, ethers, phosphines, phosphites, thioethers, thiols, arenes, halocarbons and ketones, often with sensitivities below 1 ppm and importantly, without response to change in humidity. Using different metalloporphyrins with a wide range of chemical hardness and ligand-binding affinities as well as solvatochromic effects allowed differentiation among a wide range of volatile analytes.

By broadening the types of sensors in the colorimetric array to include shape selective bis-pocketed porphyrins, pH indicators, and solvatochromic dyes to a total of 24 sensors, Rakow *et al.*[134] were able to demonstrate highly selective discrimination among very closely related amines, with sub-ppm sensitivities. Discrimination among linear alkyl amines, and even isomeric amines was possible, as shown in Figure 1.31. Similar arrays were tested by Tang *et al.*[231] and by Luo *et al.*[232] who were able to demonstrate limits of detection for trimethyl amine and ammonia, respectively, below 50 ppb.

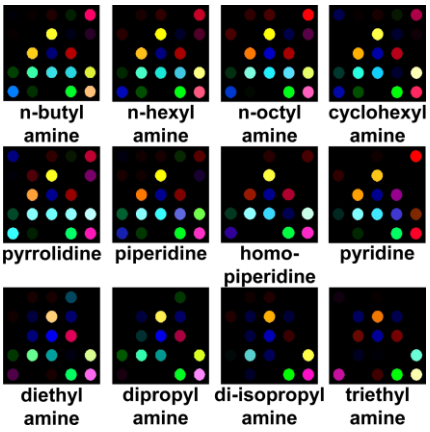

Figure 1.31 Color-difference maps for a family of 12 amines using a 24 spot colorimetric sensor array containing shape selective bis-pocket metalloporphyrins. Reproduced with permission from ref. [134].

With further expansion of the array to 36 colorimetric sensors, Suslick and coworkers[114] were able to demonstrate error-free discrimination among 100 different VOCs with common organic functionalities including primary, secondary, tertiary, and aromatic substituents of amines, arenes, alcohols, aldehydes, carboxylic acids, esters, hydrocarbons, ketones, phosphines, and thiols. The array discriminates among VOCs by probing a wide range of intermolecular interactions, including Lewis acid-base, Brønsted acid-base, metal ion coordination, hydrogen bonding, and dipolar interactions. LODs are analyte dependent and were not determined in this study, but were generally in the low ppbv range for amines, carboxylic acids, thiols, and phosphines. The sensitivity of the array to bases and acids is a result of the strong metal-analyte interactions, either by metal ligation (i.e., coordination or dative bonding) or by Brønsted acid-base interactions. Weakly coordinating vapors such as esters, ketones, alcohols, arenes, and hydrocarbons show a lower response, just as the mammalian olfactory system.

Importantly, by proper choice of dyes and substrate, the array is essentially non-responsive to changes in humidity. A selection of the difference maps of a representative subset of 24 VOCs are presented in Figure 1.32

The PCA of the dataset representing the full 100 VOCs shows an extraordinarily high level of

dispersion by the colorimetric sensor array: 14 dimensions are required to define 90% of the total variance, 22 dimensions for 95% of the total variance, and 40 dimensions for 99% (Figure 1.27).

Most remarkably, because the colorimetric sensor array is based on analyte-array chemical reactivity, chemical class information becomes readily available from the data analysis.[114] Figure 1.32 shows the familial similarities of the color difference maps of alkyl amines vs. aromatic amines vs. carboxylic acids vs. aldehydes vs. phosphines, simply by inspection. The more detailed analysis afforded by HCA shows how well that chemical class information can be revealed (Figure 1.25).

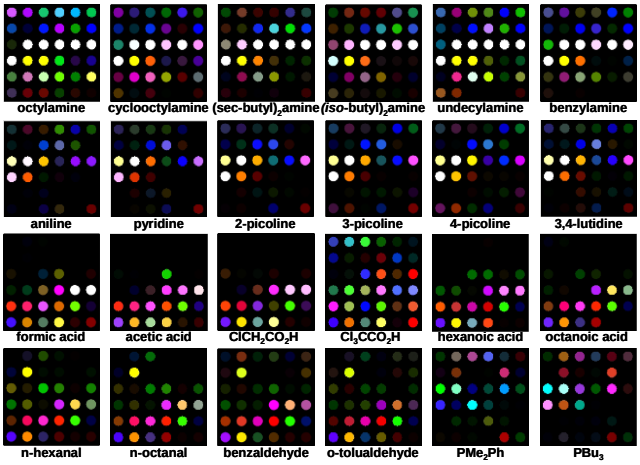

Figure 1.32 Colorimetric array response to VOCs visualized as color difference maps. Shown are 24 representative VOCs after equilibration at their vapor pressure at 295 K. Reproduced with permission from ref. [114].

While these colorimetric sensor arrays work exceedingly well for *reactive* volatiles, they have *not* had especially high sensitivity to less reactive vapors. For example, common VOC indoor air pollutants (e.g., aromatic hydrocarbons, chlorocarbons, other organic solvents) are generally not especially reactive and are not detected at low concentrations. Lin, Jang, and Suslick recently reported[19] a dramatic improvement in the sensitivity of colorimetric sensors for the detection and identification of such less-reactive VOCs by the use of a disposable pre-oxidation technique in which the analyte-stream

was passed through an oxidation tube (of chromic acid on silica) before reaching the array (Figure 1.33). Preoxidation of VOCs produces reactive species such as carboxylic acids, phenols, and aldehydes which have a stronger interaction with the colorimetric sensor array. This results in a ~300-fold enhancement of sensitivity with a concomitant increase in discrimination ability.

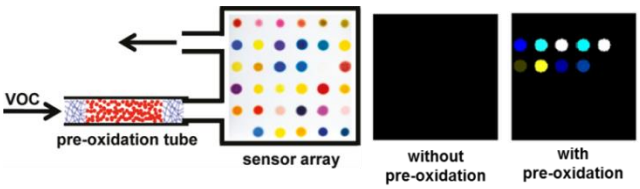

Figure 1.33 Left: Schematic illustration of the preoxidation technique. A Teflon tube is packed with chromic acid to pretreat the gas flow containing a VOC before it is passed over the colorimetric sensor array. Center and Right: Responses to p-Xylene at IDLH concentrations without (center) and with (right) pre-oxidation tube. Reproduced with permission from ref. 19.

Since each VOC produces a different mixture of oxidized derivatives, the array response to these more reactive volatile by-products provides a unique, but much more sensitive, signature for the initial VOC. 20 commonly found VOC pollutants in indoor air were examined as representative analytes and all were discriminable by HCA, as shown in Figure 1.34, both at their immediately dangerous to life or health (IDLH) and at their permissible exposure limit (PEL).

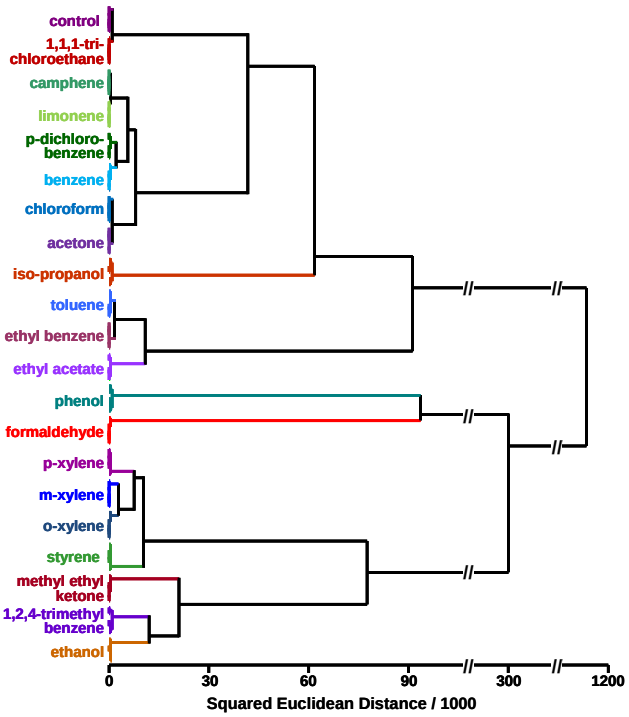

Figure 1.34 HCA dendrogram for 20 commonly found indoor pollutant VOCs at their IDLH concentrations and a control. All experiments were run in quintuplicate with 30 mg chromic acid on silica as the pre-oxidation reagent; no confusions or errors in classification were observed in 105 trials. Reproduced with permission from ref. [19].

1.4.2 Toxic Industrial Chemicals (TICs)

Toxic industrial chemicals (TICs), by their very nature, are chemically reactive. The toxicities inherent in toxic industrial chemicals derive from a very wide range of specific chemical reactivities that affect multiple systems within living organisms. Some acute toxins target specific, critical metabolic enzymes (e.g., HCN inhibits cytochrome c oxidase while phosgene inhibits pulmonary function); some cause cell lysis in the lungs creating pulmonary edema (e.g., HCl, HF) and others are potent oxidants or reductants that can target various biosystems. There is an obvious need for rapid, sensitive identification, and determination of TICs,[233] yet we have no small and inexpensive technology for personal dosimetry of TICs in the chemical workplace or by first responders to industrial fires or chemical spills.

Prior electronic nose technology, which utilizes weak analyte-sensor interactions, have had a limited ability to detect compounds at low concentrations relative to analyte saturation vapor pressure and therefore are often unable to detect TICs at their IDLH (immediately dangerous to life or health), PEL (permissible exposure limit) concentrations. In addition, interference from large environmental changes in humidity or temperature remains highly problematic.

Colorimetric sensor arrays, however, are exceptionally well designed for the detection, identification and quantification of TICs due to their reliance on analyte chemical reactivity. Suslick and coworkers in a series of papers[16,197,203-204] developed the use of nanoporous sol-gel pigments for the chemoresponsive elements of an extremely sensitive colorimetric sensor array. They selected high hazard TICs from the reports of the NATO International Task Force 25 and 40[234] and examined the ability of their array to discriminate among the 20 TICs shown in Table 1.1.

Table 1.1 List of toxic industrial chemicals at their IDLH (Immediately Dangerous to Life or Health) and PEL (Permissible Exposure Limit) concentrations compared to limits of detection extrapolated using data collected at 20% PEL concentration.[197]

TIC	IDLH (ppm)	PEL (ppm)	Extrapolated LOD (ppm)
ammonia	300	50	0.08
arsine	3	0.05	0.01
chlorine	10	1	0.01
diborane	15	0.1	0.01
dimethylamine	500	10	0.01
fluorine	25	0.1	0.01
formaldehyde	20	0.75	0.12
hydrogen chloride	50	5	0.02
hydrogen cyanide	50	10	0.02
hydrogen fluoride	30	3	0.02
hydrogen sulfide	100	20	0.08
hydrazine	50	1	0.01
methylamine	100	10	0.01
methyl hydrazine	20	0.2	0.01
nitric acid	25	2	0.02
nitrogen dioxide	20	5	0.03
phosgene	2	0.1	0.01
phosphine	50	0.3	0.01
sulfur dioxide	100	5	0.06
trimethylamine	200	10	0.03

The sensor array was able to discriminate without error among these 20 TICs at both their IDLH concentration within two minutes of exposure and at PEL concentration within five minutes of exposure; HCA showed no mis-clustering errors and jackknifed LDA gave an error rate below 0.7% out of 147 trials (Figs. 35 and 36). Limits of detection limits (listed in Table 1) were generally well below the PEL (in most cases below 5% of PEL) and are typically in the low ppb range. The colorimetric sensor array was not responsive to changes in humidity or temperature over a substantial range. The array performed well in the presence of various common potential interferents and has shown excellent stability and reproducibility.

While LODs are defined absolutely with respect to S/N, that only defines when one can determine that some analyte is present. Limits of recognition are much more important, but they are also library dependent. Figure 1.37 demonstrates a limit of recognition for a subset of TICs is well below 5% of their

PEL, which becomes of interest for epidemiological studies. Consistent with the array's ability to discriminate among many possible TICs over many possible concentrations, PCA and LDA confirmed the high dimensionality of the colorimetric sensor array with 17 PCA dimensions required to capture 95% of the variance.[197]

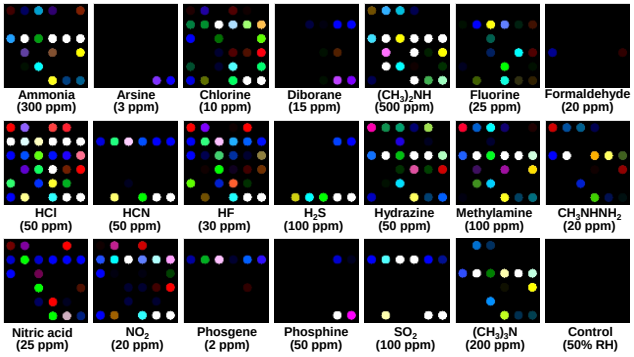

Figure 1.35 Color difference maps of 20 representative TICs at their IDLH. Reproduced with permission from ref. [204].

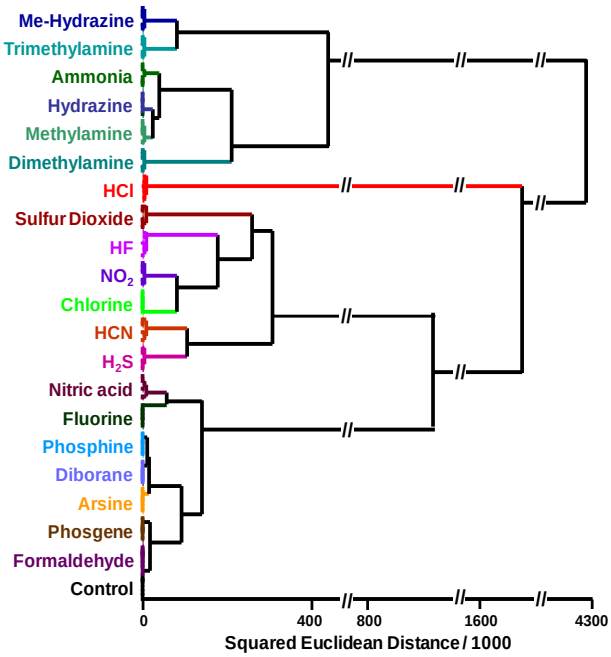

Figure 1.36 HCA dendrogram for 20 TICs at IDLH concentrations and a control. All experiments were performed in septuplicate; no confusions or errors in clustering were observed in 147 trials. Reproduced with permission from ref. [197]

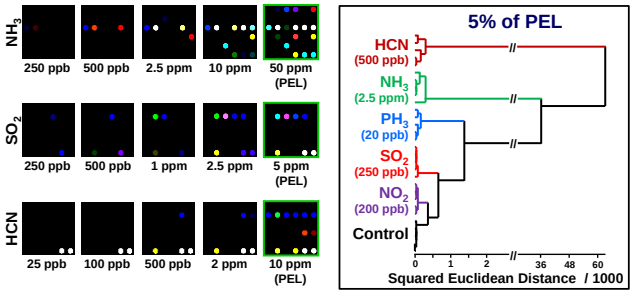

Figure 1.37 Limits of recognition for TIC identification. Left: the effect of concentration on array response to NH_3, SO_2, and HCN. Right: HCA of a subset of TICs demonstrates a limit of recognition well below 5% of the PEL. Reproduced with permission from ref. [204].

Several reports of more specialized arrays for specific subsets of TICs have also been published. For example, Sen *et al.*[235] developed a disposable colorimetric sensor array which can detect H_2S concentrations in the range of 50 ppb to 50 ppm at ambient temperature. Bang *et al.*[205] prepared

nanoporous silica microspheres incorporating chemoresponsive dyes and used an array of these to detect and quantify ammonia gas at its IDLH (immediately dangerous to life or health), PEL (permissible exposure limits), and 0.1 PEL concentrations with a reported LOD of 100 ppb. Sen, Kim and coworkers[236] expanded their work to a sensor array for ammonia, chlorine, hydrogen chloride and sulfur dioxide. This sensor is able to rapidly measure IDLH concentrations (100 ppm) of SO_2 with a response time of about 30 s. Hou *et al.*[237] also report a very similar portable device for toxic gas detection. The reported sensor includes a transparent and hermetic gas of chlorine, sulfur dioxide, ammonia, benzene and isoprene with LODs for some analytes in the ppb regime.

1.4.3 Explosives detection

Triacetone triperoxide (TATP), one of the most dangerous primary explosives, has emerged as an explosive of choice for terrorists in recent years. TATP is easily produced by an acid catalyzed reaction of acetone with hydrogen peroxide.[238] Owing to lack of UV absorbance, fluorescence or facile ionization, TATP is difficult to detect directly.[239] Techniques that are able to detect generally require expensive instrumentation, need extensive sample preparation, or cannot detect TATP in the gas phase. Lin and Suslick[181] reported a new method for determination of TATP vapor using a colorimetric sensor array. In this method, the gas stream containing TATP vapor is decomposed by a solid acid catalyst (Amberlyst 15) and the resulting H_2O_2 vapor, being kinetically much more reactive, is easily detected by redox indicators (Figure 1.38).

TATP was detectable even at very low concentrations using this technique, with an LOD below 2 ppb (i.e., <0.02% of its saturation vapor pressure). Common potential interferences (e.g., humidity, personal hygiene products, perfume, laundry supplies, volatile organic compounds, etc.) did not generate an array response, and the array could also differentiate TATP from other chemical oxidants (e.g., hydrogen peroxide, bleach, t-butylhydroperoxide, peracetic acid) (Figure 1.26).

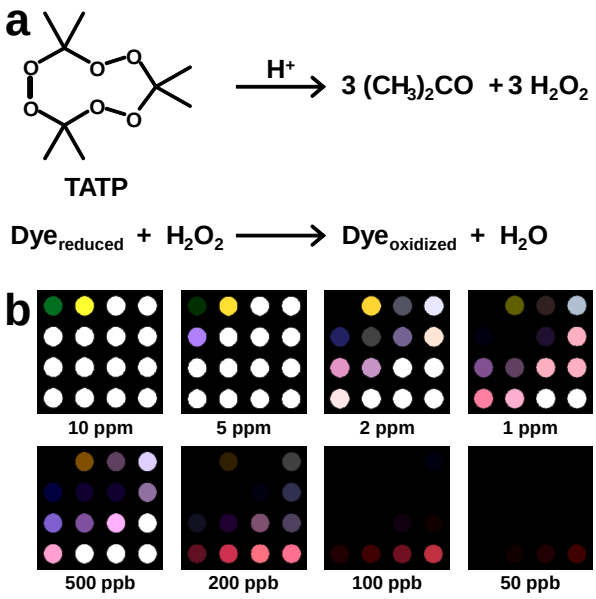

Figure 1.38 (a) Acid catalyzed decomposition of TATP. (b) Color difference maps of TATP vapor at concentrations specified after 5 min (top row) and10 min (bottom row) of exposure. Reproduced with permission from ref. [181]

Kostesha, Alstrøm *et al.* [240-241] have reported very briefly on a colorimetric sensor array capable of detection of explosives' vapors, but no details were given on dyes used in their array. In this work, classification ability of K–nearest neighbor (KNN), artificial neural networks (ANN) and sparse logistic regression (SLR) methods were compared.

1.4.4 Aqueous analytes

If a colorimetric sensor array is printed on a hydrophobic membrane and the dye formulations sufficiently hydrophobic, then upon immersion into an aqueous solution containing organic compounds, the sensor array will respond to the volatile vapors of solutes. Zhang and Suslick[199] prepared a simple colorimetric sensor array that was able to probe different organic compounds at very low concentrations (below 1 μM) in water. As shown in Figure 1.39, unique fingerprints were observed for a wide range of dissolved organic compounds.

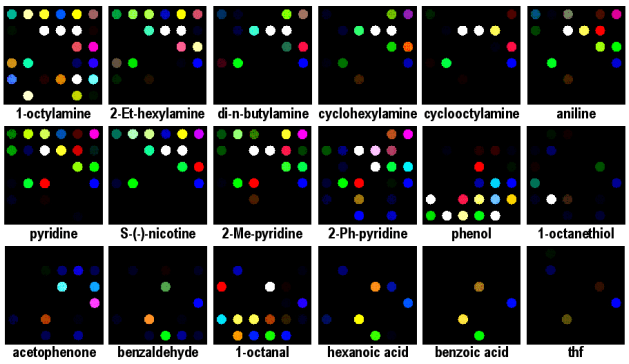

Figure 1.39 Color change profiles with the base-sensitive sensor array for representative aqueous solutions of organic compounds (all amines 10 mM, all others 50 mM, in pH 7 phosphate buffer). Reproduced with permission from ref. [199].

Monitoring toxic metal ions in water has also been accomplished using a nanoporous pigment array. Feng *et al.*[151] reported a CSA for identification trace heavy metal ions (including Hg, Pb, Cd, Zn, Ag, As, Ni and Cu) at waste water-discharge standard concentrations. Suitable chemoresponsive dyes were immobilized using ormosil formulations; in this case, five separate probes were analyzed asynchronously through a filtration method and organized into an array. Discrimination of heavy metal ions was performed without interference of Na^+, K^+, Ca^{2+}, Mg^{2+} ions and good repeatability and high stability was obtained for this sensor.

Recognition of amino acids in aqueous solutions has also been accomplished using a colorimetric sensor array. Dan-Qun *et al.*[242] used a 6×6 array to distinguish among amino acids based on differences between their chemical properties and specific residue structures. Ten natural amino acids including glycine (Gly), valine (Val), methionine (Met), proline (Pro),serine (Ser), tyrosine (Tyr), glutamine (Gln), glutamate (Glu), lysine (Lys), and histidine (His) were identified within 5 min of exposure at concentrations of 375 μM (Figure 1.40).

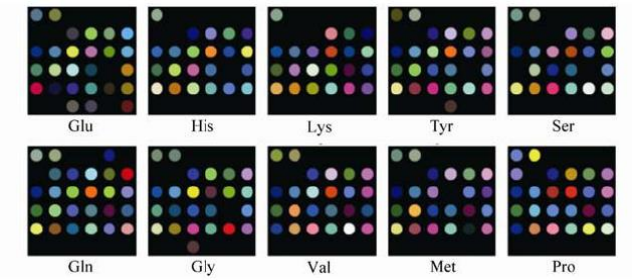

Figure 1.40 Average color change profiles of 10 amino acids visualized as color difference maps. Reproduced with permission from ref. [242].

Fluorescent displacement assays have also been used for identification of amino acids in solution. For example, dansyl-modified β-cyclodextrins bearing a metal binding site, with pendant L-amino acids, were employed for selective identification of unmodified amino acids in aqueous buffer at neutral pH[243-244] and as enantioselective fluorescence sensors for the discrimination of enantiomers of the amino acids valine and proline. The best conditions to perform enantiomeric analyses l used fluorescence quenching by the copper(II)/amino acid complexes in a fluorescence microplate reader.

Fluorometric displacement assays using complexometric solution sensor arrays have been used for identification of metal ions. In 2003, Mayr *et al.*[152] developed an eight-component fluorometric array for discrimination among five separate metal cations using cross-reactive complexometric fluorophores in solutions held in a microtiter plate. The wells were monitored simultaneously using a CCD camera and a set of fiber-optic cables to reduce the imaged area (Figure 1.41). The fluorescence decay profile of the indicator is referenced against the phosphorescence of an added inert reference dye at a different wavelength. The source of illumination were blue LEDs, one for each well. The assembly allows the detection of dye concentrations in the nanomoles-per-liter range without amplification and the acquisition of 96 wells simultaneously. Some discriminatory ability was shown by this straightforward liquid-phase array, but limited statistical analysis was performed; classification accuracy of 82 to 93% was reported. A gray-scale image showing the raw fluorescence response to several analyte sets are

shown as Figure 1.42.

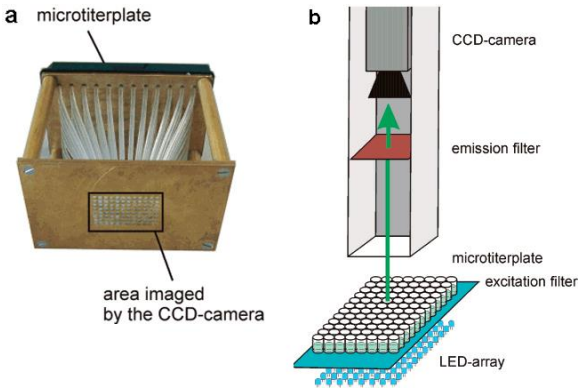

Figure 1.41 (a) Fiber-optic adapter for fluorescent imaging of 96 well microtiterplates; (b) schematic of the apparatus showing LED array illumination and CCD camera detection. Reproduced with permission from ref. [152].

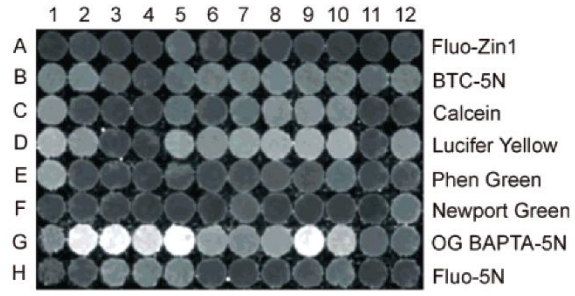

Figure 1.42 Greyscale output of eight-component array after exposure to various concentrations of metal ions. Analytes vary by column, and included some multi-ion solutions; specific concentrations are given in ref. [152]. Of note, columns 5-9 are set at 1 □M Ca^{2+}, Cu^{2+}, Ni^{2+}, Zn^{2+}, and Cd^{2+} respectively. Reproduced with permission from ref. [152].

1.4.5 Applications to complex mixtures

1.4.5.1 Foods and beverages

Colorimetric Sensor Arrays

The analysis of complex mixtures presents a difficult challenge even for the most sophisticated analytical techniques, and the ability to discriminate among closely similar such mixtures often remains problematic. Foods and beverages are characteristic in the complexity of their compositions. A component by component analysis is generally unwanted and often impractically difficult, given the hundreds of different compounds found in edible materials. Instead, one is more interested in questions of authenticity, contamination, and food processing quality control. For these goals, the sort of fingerprinting that sensor arrays provides can prove extremely valuable.

Coffee provides a readily available archetype of such highly multicomponent systems. While unroasted, green coffee contains more than 300 volatile compounds, while more than 1000 volatile compounds have been identified for roasted coffee including carboxylic acids, alcohols, aldehydes, alkanes, alkenes, aromatics, esters, furans, ketones, lactones, oxazoles, phenols, pyridines, pyrazines, pyrroles, thiazoles, and thiophenes.[245-247] Furthermore, the roasting of coffee beans is highly dynamic, and the processes that develop the flavor and aroma of coffee are strongly time and temperature dependent.

Suslick, Feng and Suslick[248] made use of the same sensor array developed for TIC identification to the analysis of coffee aromas. The color changes of the sensor array were used as a digital representation of the array response and analyzed with standard statistical methods. PCA revealed that the sensor array has exceptionally high dimensionality with 18 dimensions required to define 90% of the total variance and 25 dimensions for 95%. In quintuplicate runs of ten commercial coffees and controls, no confusions or errors in classification by HCA were observed in 55 trials (Figure 1.43). In addition, the effects of temperature and time in the roasting of green coffee beans were readily observed and

distinguishable with a resolution better than 10 °C and 5 min, respectively.

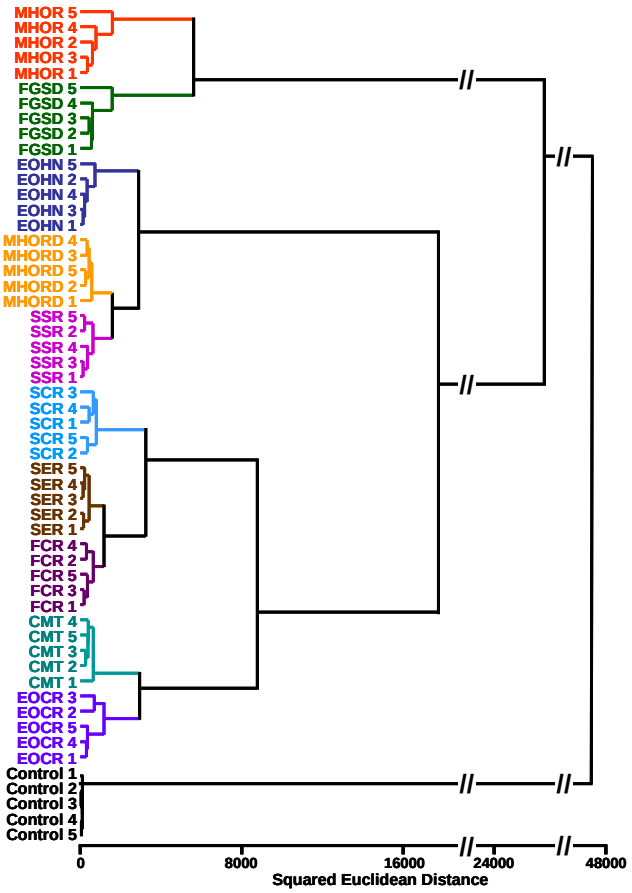

Figure 1.43 HCA for 10 commercial coffees and a control. All experiments were run in quintuplet trials; no confusions or errors in classification were observed in 55 trials. Abbreviations: Maxwell House Original Roast, MHOR; Folgers Grande Supreme Decaf, FGSD; Eight O'Clock Hazel Nut, EOHN; Maxwell House Original Roast Decaf, MHORD; Starbucks Sumatra Roast, SSR; Starbucks Columbian Roast, SCR; Starbucks Espresso Roast, SER; Folgers Columbian Roast, FCR; Café Mai Traditional, CMT; Eight O'Clock Columbian Roast, EOCR; the number indicates n^{th} trial; Control = no coffee present.

Zhang and Suslick had earlier applied a very similar approach to commercially available soft drinks using an early version of their array containing only 25 chemically responsive dyes printed on a hydrophobic membrane.[249] Fourteen commercial soft drinks were analyzed and facile identification of

all of the soft drinks was readily achieved using comparison of the color change profiles or a PCA score plot (Figure 1.44) Using a HCA dendrogram, the misclassification rate was < 2%, and even very similar sodas were easily differentiated. In addition, the monitoring of soft drinks as they degas or upon dilution also proved to be possible. This work demonstrated the potential of colorimetric sensor array technology for quality assurance/control applications of sodas and perhaps other beverages as well.

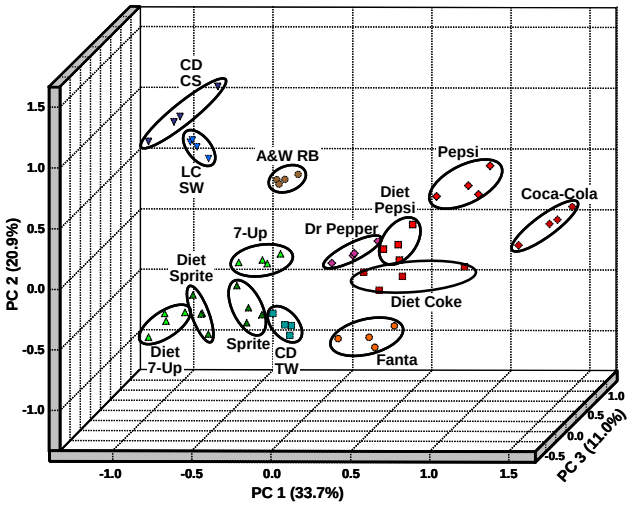

Figure 1.44 PCA score plot using the three most important principal components based on the data for the analysis of all soft drinks. The resolution between classes is in fact much better than can be shown by these three principal components which account for only 65.7% of the total variance. Abbreviations: A&W RB, A&W® Root Beer; CD TW, Canada Dry® Tonic Water; CD CS, Canada Dry® Club Soda; LC SW, LaCroix® Sparkling Water.

In a similar application, Zhang *et al.*[250] showed that colorimetric sensor arrays were able to differentiate among 18 brands of beer. Differentiation between ales and lagers (Figure 1.45) was without error, and even among very similar beers proved straightforward with an error rate of identification <3%. In addition, differentiation of pristine beer from the effects of watering or de-carbonation proved possible. These results suggest that colorimetric sensor arrays may prove useful for

QA/QC applications.

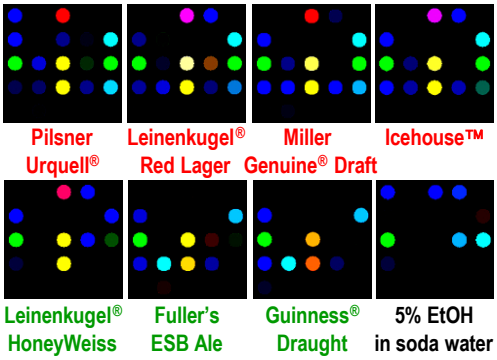

Figure 1.45 Colorimetric array analysis of a complex mixture: headspace analysis of various beers compared to 5% ethanol in carbonated water. Brands in red are lagers, brands in green are ales. Reproduced with permission from ref. [10].

Ya *et al.*[251] also analyzed five commercial baijiu (a Chinese distilled alcoholic beverage) using a simple colorimetric artificial nose. The presence of chemoresponsive dyes containing porphyrins and porphyrin derivatives provided a unique pattern of color changes in response to baijiu. With the aid of PCA and HCA, classification of types of baijiu was done according to their trace components. Using linear discriminant analysis (LDA), flavor styles were determined with 100% accuracy.

Y. T. Chang and co-workers have developed spectrophotometric microplate assays[252-256] for evaluation of tap and bottled water using 45 dyes including pH indicators, metal ion complexometric indicators, and substituted quinone dyes known to be responsive to various organic and inorganic species. By monitoring the optical spectra of the microwell plates, they were able to classify water samples in terms of their place of origin, metal ion content, and carbohydrate content.

Detection and quantification of sugars and sweeteners is very important in real-time food quality. Musto, Lim, and Suslick[226,257-258] have developed colorimetric sensor arrays for detection and quantification of sugars and artificial sweeteners by immobilizing suitable chemoresponsive dyes in

insoluble nanoporous pigments. The sensor array was able to accurately determine 14 sugars and sweeteners at millimolar concentrations at pH 7.4 (Figure 1.46). The concentrations of sugars and sweeteners could also be determined over at least a five-fold range, and glucose concentrations were measurable over the full range of clinical importance for blood sugar determinations. The sensor array worked as well in tea infusions. Ghosh *et al.*[259] applied the same concepts later to a microplate liquid ensemble of boronic acid derivatives and pH indicators with similar success and were able to show quantitative analysis of sugar concentrations.

Monitoring of food freshness, especially of meats, poultry and fish, are an obvious application of sensor arrays. Huang *et al.*[260] constructed a colorimetric sensor array by printing the nine chemoresponsive dyes on a reverse phase silica gel plate. These dyes were sensitive to volatile compounds produced during spoilage of fish. PCA and neural network techniques were applied for classification of the degree of spoilage, allowing evaluation of the fish freshness with the accuracy of 87.5%. Recently Salinas *et al.*[261] reported an optoelectronic nose constructed of 16 pigments able to identify the age of chicken meat.

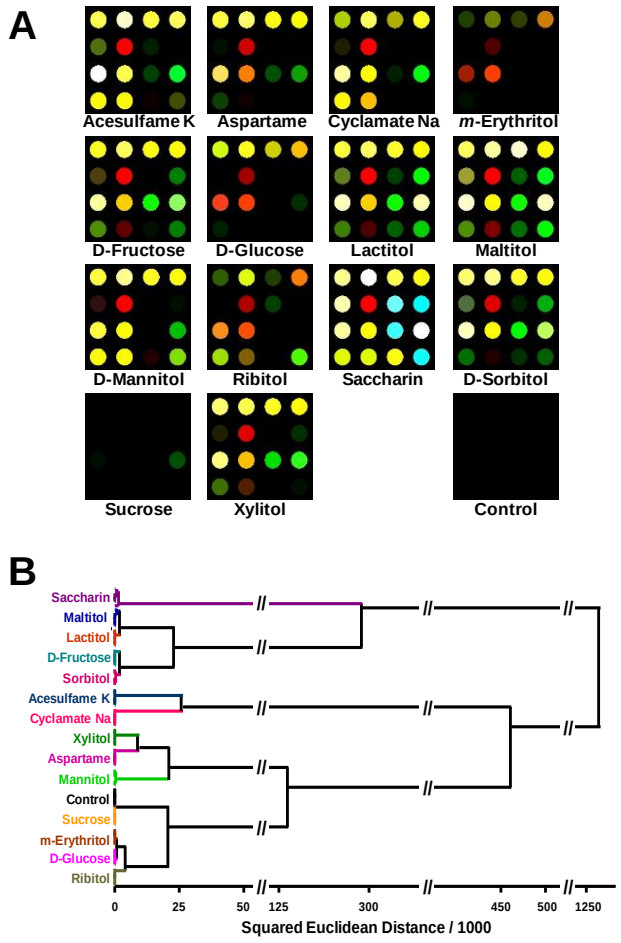

Figure 1.46 Colorimetric sensor array for sugars. a. Color difference maps for 14 representative natural and artificial sweeteners (10 mM) and one control. b. Hierarchical clustering analysis dendrogram for aforementioned sweeteners; zero misclassifications were observed in 100 trials. Reproduced with permission from ref. [226].

Indicator Displacement Assays

Anslyn and co-workers have developed a general displacement strategy using serum-albumin as a differentially selective receptor capable of binding both fluorescent reporters and a variety of non-polar analytes (e.g., fatty acids). The resultant probe was able to differentiate among fatty acids (palmitic acid, oleic acid, stearic acid, and linoleic acid) and among edible oils (sunflower oil, hazelnut oil, canola oil,

extra virgin olive oil, and peanut oil).[186] A graphical representation of their data using PCA is shown as Figure 1.47, showing clear distinction among analyte species. It is worth noting that the PCA is very strongly dominated by a single component (~90% of total variance), and that dimension essentially represents the hydrophobicity of the analytes.

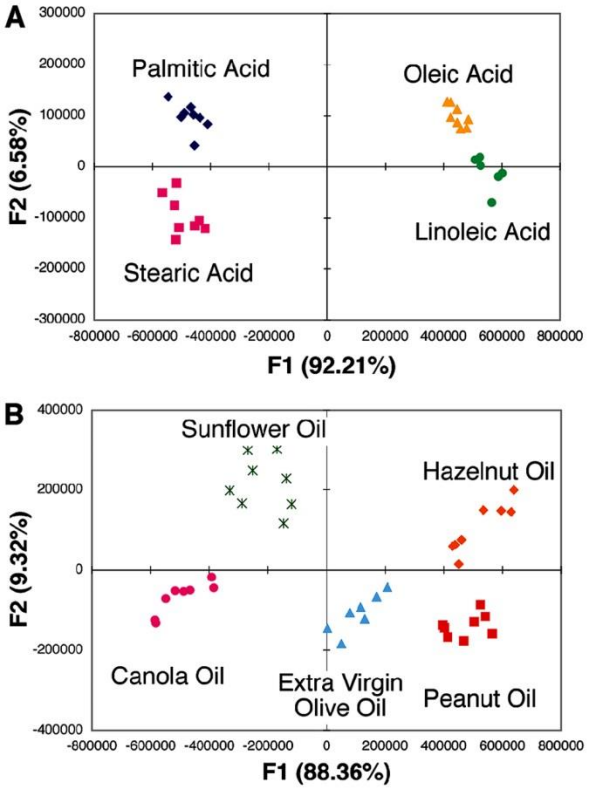

Figure 1.47 PCA plot showing differentiation among several fatty acids (A) and food oils (B). Reproduced with permission from ref. [186].

In a similar concept, Anslyn and coworkers used a set of metallo-histidine peptides in order to discriminate among polyphenol-based wine flavonoids.[262] In this indicator displacement assay, the probes were based on replacement of a catechol dye from a Cu^{2+} center bound to the peptide; the design strategy (shown as Figure 1.48) is quite straightforward and specific due to significant structural similarity between the indicator dye and chosen analytes. The resulting discrimination, however, was

only moderate.

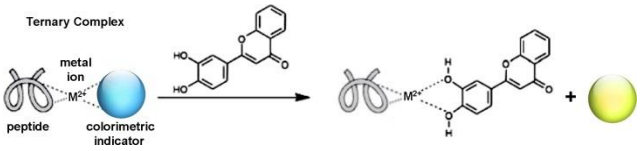

Figure 1.48 General scheme used for discrimination of wine flavonoids. Differential sensing ability is provided by several peptide sequences used with an indicator displacement strategy. Modified from ref. [262].

Much more impressive results were obtained by the same group using a diversified set of colorimetric indicators and synthetic boronic acid and guanidinium functionalized receptors.[263] The authors showed the ability of the array to discriminate malate, tartrate and citrate and then using spectrophotometric data at three wavelengths (the indicator maxima), they were able to discriminate accurately among six different red wines, as shown in Figure 1.49. In contrast with the earlier paper,[262] these more chemically diverse displacement assays provide a much higher dimensionality of data (three dimensions include 88% of the discriminatory power) and a much improved distinction between the wines.

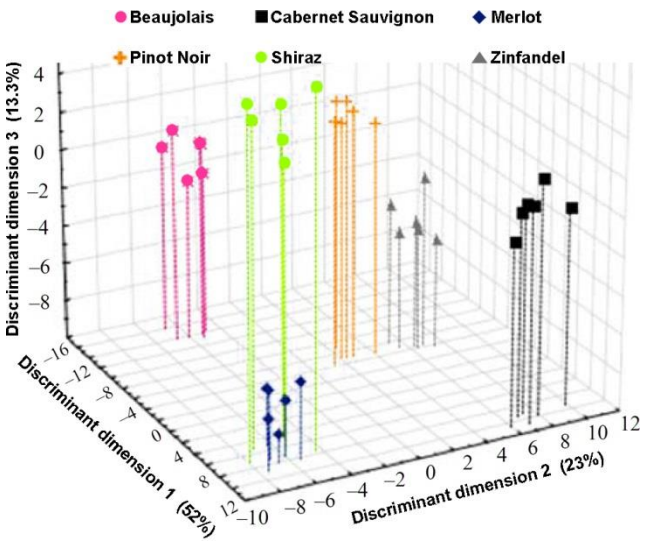

Figure 1.49 Linear discriminant score plot from spectroscopic data from synthetic receptor displacement indicator assays. Modified from ref. [263].

1.4.5.2 Proteins

There have been several recent studies reported on the optical sensor array identification of single proteins in solution. While it is not clear what application single protein identification may have, in some cases the approaches are intellectually clever. One may hope that such arrays might prove useful for detecting a specific rogue protein against a constant complex mixture as found in plasma; cross-reactive sensor arrays, however, are unlikely to be able to achieve such a goal at biomedically relevant concentrations. Such tests remain to be reported.

For colorimetric sensor arrays, Hou *et al.*[264] tested an array modeled closely on Suslick's work using a series of porphyrins and indicator dyes capable of rapid interaction with proteins. The array produced distinct patterns in response to each protein which permitted accurate identification of the pure and mixed proteins as well as denatured proteins. Figure 1.50 shows two dimensional PCA plots which show excellent discrimination among the proteins, especially given that only ~64 to 82% of the total variance is captured in a two dimensional plot. Remarkably, one is able to discriminate thermally denatured

proteins from the native form rather easily.

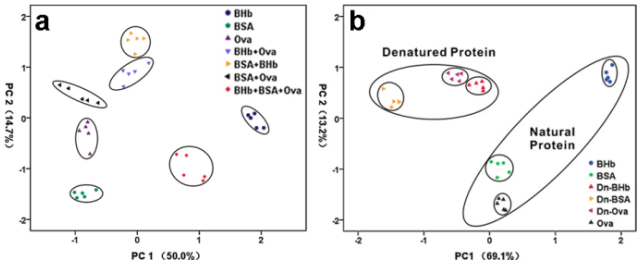

Figure 1.50 PCA from a 36 dye colorimetric sensor array (a) for seven individual and mixed proteins and (b) for six natural vs. thermally denatured (Dn) proteins. Reproduced with permission from ref. [264].

In another example of a pseudo-array data analysis using sequential array sensing of parallel solutions, displacement or differential assays have also been used to identify protein solutions. The Rotello group generated multiple differential sensing parallel arrays using gold nanoparticles with the aim of discriminating among a variety of biological samples; this work has been both succinctly[265-266] and exhaustively reviewed.[267-269] Several different fluorophores have been used. The interaction of analytes with nanoparticles adds additional unique characteristics, as shown schematically in Figure 1.51.

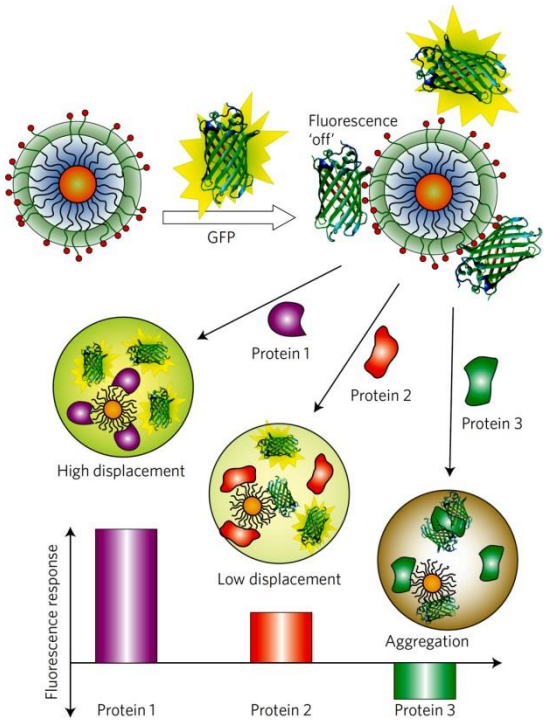

Figure 1.51 Illustration of competitive binding between protein and quenched green fluorescent protein-gold nanoparticle complexes and protein aggregation, which leads to fluorescence or further quenching. Reproduced with permission from ref. [270].

For detection of seven common proteins (bovine serum albumin, cytochrome c, alkaline phosphatase, acid phosphatase, subtilisin A, lipase, and β-galactosidase) Rotello *et al.*[271] prepared a sensor array based on six cationic functionalized gold nanoparticles (AuNPs) and an anionic PPE (poly(p-phenyleneethynylene)) polymer. The fluorescence of PPE polymer was quenched by interactions of AuNPs with polymer, but addition to a protein solution diplaced the polymer and enhanced the observed fluorescence. By using different functionalization, one could alter the protein affinity to the surface of nanoparticles and, thus, producing distinct fluorescence response patterns. Fluorescence responses to individual proteins were fingerprinted, giving a detection limit of 4 to 215 nM depending on protein size.

Of particular note, Rotello used a gold nanoparticle-fluorophore system made from gold

nanoparticles conjugated to green fluorescent protein (GFP-NP) to act as the displaced indicator. Using a protein as the displaced indicator is a straightforward method of discriminating among peptide-based analytes due to the molecular similarity between the incoming analyte and the displaced probe. This method was used for discrimination among several types of human serum proteins (Figure 1.52),[270] and then in a subsequent publication to mammalian cells,[272] as discussed in the last section.

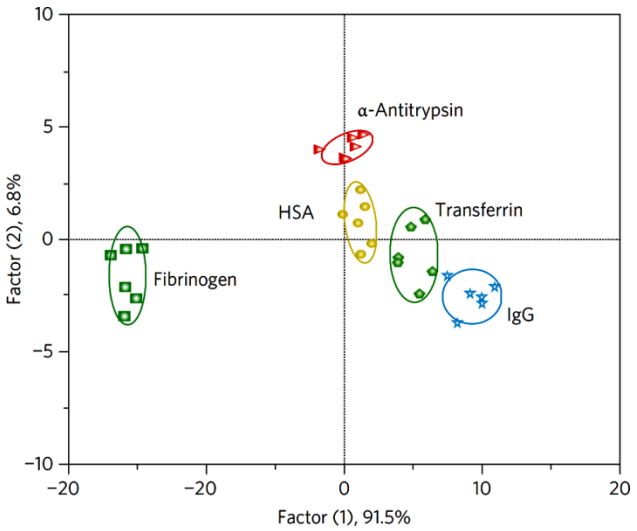

Figure 1.52 Fluorescent displacement sensing using multiple solutions doped with five GFP-NP sensors for five serum proteins (25 nM) at pH 7.4. Reproduced with permission from ref. [270].

Li *et al.*[273] used a set of functionalized Fe nanoparticles to discriminate among several proteins. This work used only two probes for discrimination, leading to an inherently low maximum dimensionality. In practice, the discrimination ability of the probes comes almost exclusively from a single dimension, as shown in Figure 1.53. The authors state that surface charge, protein size, and surface hydrophobicity all play roles in discrimination of these species; they may all contribute in a composite sense to the principal component, but the one-dimensional nature of the data establishes that this is not truly an array sensor. The origin of the specificity is not clear; proteins with very similar pI values are differentiated, and there is no correlation with protein size or surface charge. A more detailed data

about surface hydrophobicity may provide some further insight.

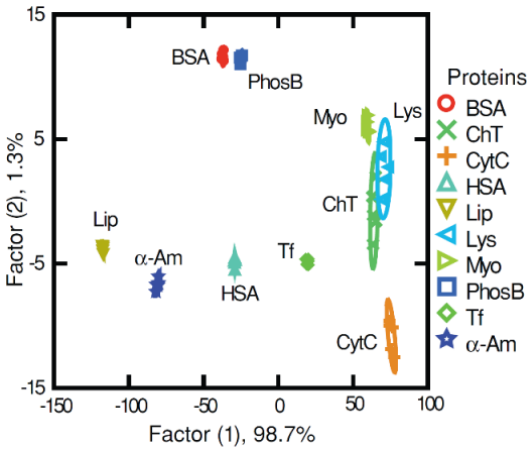

Figure 1.53 LDA score plot showing discrimination among 10 separate proteins. Note the complete dominance by one dimension (factor 1), showing that the discrimination ability comes nearly exclusively from a single dimension. Reproduced with permission from ref. [273].

1.4.5.3 Intra-cellular sensing using ratiometric fluorometry

In a sense, the use of two or more fluorophores in a single probe is also array sensing. So ratiometric fluorescent probes, where one has two fluorophores excited at the same wavelength, but emitting at different wavelengths, permits an array-like response that is self-calibrating. Let us examine a few recent examples of intra-cellular sensing using ratiometric fluorometry.

Intra-cellular temperature probes provide an interesting example. Small local temperature changes may have significant effects on the cellular signaling pathways and their nanoparticle uptakes;[274-277] thus, the development of novel temperature nanosensors may prove very useful for intra-cellular profiling and imaging. Peng *et al.*[278] prepared a ratiometric type of fluorescent nanoparticles with a green and a red fluorescence from a single wavelength excitation; these nanoparticles showed the capability of monitoring temperature variations in the physiological temperature range (i.e. 25°C-45°C),

as illustrated in Figure 1.54.

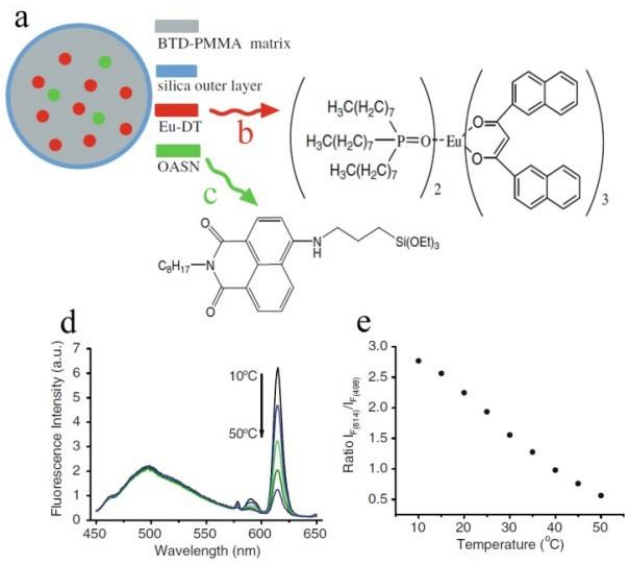

Figure 1.54 (a) Schematic representation of temperature-sensing nanoparticles containing a random dispersion of Eu-DT (structure shown as b) and OASN (structure shown as c) in a silylated poly(methyl methacrylate) matrix (BTD-PMMA), which is covered with a silica outer shell; (d) ratiometric fluorescence response; (e) temperature calibration plot. Reproduced with permission from ref. [278].

Monitoring of the pH inside live cells is also of importance for probing living cell functions.[279] Peng *et al.*[280] employed ratiometric fluorescent nanogels for monitoring pH variations (Figure 1.55). The hydrogel was prepared from polyurethane containing both hydrophilic and hydrophobic domains,[281] thus the nanogel chains rearranged to form a three-dimensionally stable nanostructures[282-283] when placed in water. It is noteworthy to mention that the volume of the nanogels were not affected by pH, so the efficiency of FRET was constant during in vitro pH sensing. The developed pH probe is suitable for montoring the pH in the range of 6-8. Figure 1.55b shows the fluorescence emission spectra of the nanogels at various pH values upon excitation at 450 nm. Calculation of the ratio of the observed emission intensities of the dyes in various pH values is presented in Figure 1.55, showing around nine

fold variation in the ratio on going from pH 5 to pH 9.

A final example simultaneously measured oxygen content and pH value in bacterial cultures (*Pseudomonas putida*), Kocincova *et al.*[284] prepared and employed a "dual" sensor based on organosilica microparticles (for oxygen sensing) and polymethacrylate derivative embedded into a polyurethane hydrogel (for pH sensing).

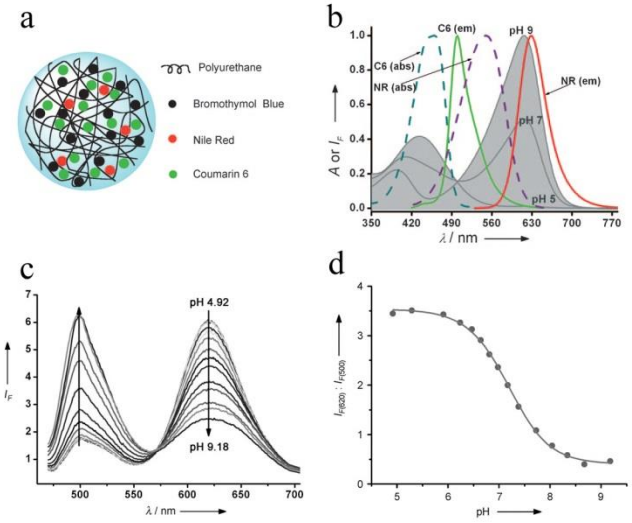

Figure 1.55 (a) Schematic representation of the ratiometric pH sensing nanogel; (b) spectrum showing the pH-dependent absorption of bromothymol blue in aqueous solution at pH 5.0, 7.0, and 9.0 (gray curves), and absorption and emission spectra of coumarin 6 (C6) and Nile Red (NR) in ethanol; (c) fluorescence spectra of the ratiometric pH-responsive nanogels at 450 nm excitation at various pH values from 4.92 to 9.18; d) pH calibration plot from the ratio of the fluorescence intensities at 620 nm and 500 nm of the ratiometric nanogels. Reproduced with permission from ref. [280].

1.4.5.4 Detection and identification of bacteria

The detection and identification of bacteria are pressing problems in both medicine and industry. Bacterial infections are involved in food poisoning, hospital-acquired infections, and other areas that are

of great concern for public health, and sepsis remains one of the leading causes of death even among first world nations.[285-286] In industry, many products must be screened after manufacture for bacterial contamination before they may be released and as a consequence regulation of the food industry must be particularly stringent.[287-288] Existing methods for identification of pathogenic bacteria are limited by the necessity of long culturing times, the need for highly trained laboratory personnel, or the requirement of expensive and high-maintenance equipment.[289-294]

Bacteria stink: that is, they produce volatile organic compounds (VOCs) to which the mammalian olfactory system is highly responsive. Consequently, an experienced microbiologist can readily identify many bacteria by smell. Applications of prior electronic nose technology, however, have been limited by the low dimensionality of traditional sensor arrays (e.g., metal oxides) and have achieved only modest success, even when attempting to classify small numbers of bacterial species.[295-297]

Using a disposable colorimetric sensor array, Carey *et al.*[298] were able to identify different species and specific strains of human pathogenic bacteria based on volatile compounds produced during bacterial growth. In 164 trials monitoring bacterial growth as a function of time, they were able to identify 10 strains of bacteria including Enterococcus faecalis and Staphylococcus aureus and their antibiotic-resistant strains during 10 hours of culture time with 98.8% accuracy as evaluated by jackknifed LDA using timestacked data. Figure 1.56 shows the color difference maps and time evolution of the array response to the head-gas mixture produced in sealed Petri dishes. Figure 1.57 shows a PCA score plot using the three most important dimensions, which account for only 79% of the total variance.

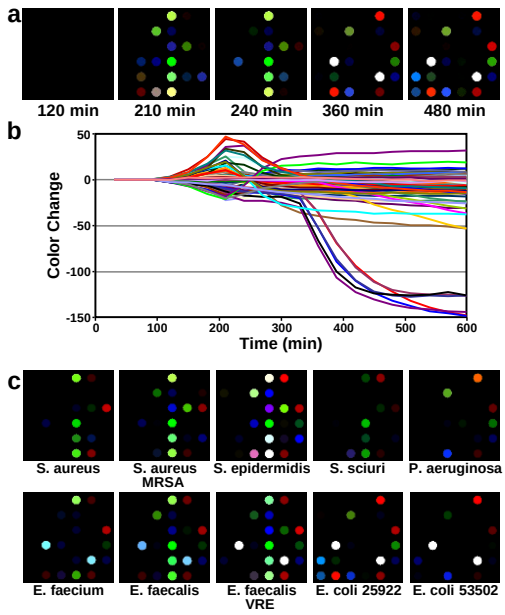

Figure 1.56 (a) Color difference maps and time response profile resulting from colorimetric sensor array exposure to a growing culture of *E. coli*, American Type Culture Collection (ATCC) #25922. (b) The color change values versus time plotted for all color channels (ΔR, ΔG, and ΔB values for each spot, i.e., 108 color channels) at each time point. (c) Color difference maps for 10 different bacterial strains resulting from colorimetric sensor array exposure to Petri dish growing cultures after 480 min. Reproduced with permission from ref. [298].

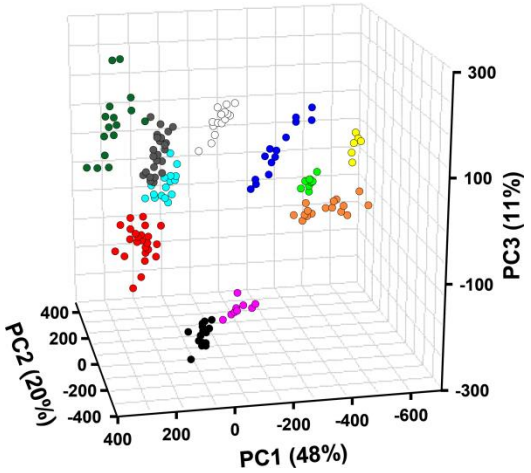

Figure 1.57 PCA score plot using the three most important principal components based on 164 trials of 10 bacterial strains and controls. The resolution between bacterial classes is in fact much better than can be shown by any three-dimensional PCA plot because the first three principal components account for only 79% of the total variance.

● *S. aureus*; ● MRSA; ● *S. epidermidis*; ● *S. sciuri*; ● *P. aeruginosa*;

o *E. faecium*; ● *E. faecalis*; ● E. faecalis VRE; ● *E. coli* 25922; ● *E. coli* 53502; ● Control. Reproduced with permission from ref. [298].

Rotello and co-workers used an aqueous solution based displacement assay to identify bacteria in liquid growth media using the fluorescence quenching of fluorophores attached to gold nanoparticles.[299] They made use of cationic gold nanoparticles with conjugated polymer fluorophores as their differential fluorescence probe, whose response is dictated by the binding strength of the bacterium to the gold nanoparticle. By manipulating the surface chemistry of gold nanoparticles and the constitution of the conjugated polymer, they generated array-like data (albeit one solution at a time). Nine bacterial species and 3 strains of *E. coli* were examined in 64 trials with a 95% accuracy of classification by LDA (Figure 1.58).

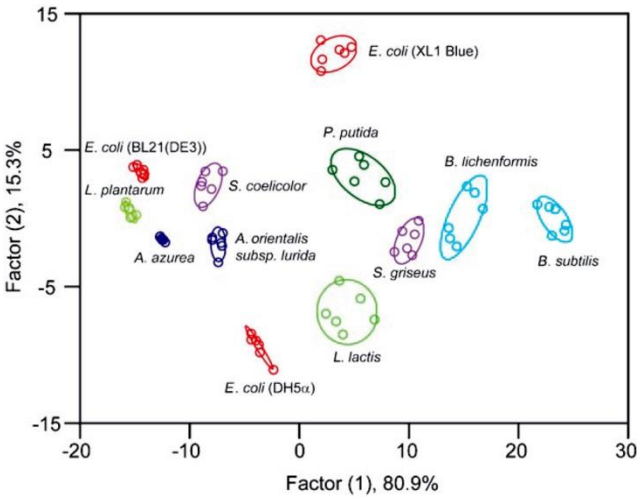

Figure 1.58 LDA score plot for the fluorescence response patterns to bacteria as determined from solution displacement assays using gold nanoparticle displacement assays. The first two dimensions contain 96.2% of the variance. Reproduced with permission from ref. [299].

The immobilized fluorescent bead strategy that Walt developed for use with microwelled optical fiber bundles (discussed earlier) has also been recently applied to bacterial identification. Fixed arrays of this sort are difficult to reuse multiple times, in part due to photobleaching. Walt and coworkers have attempted to address this problem by using a free bead strategy; [300] using optical trapping, the arrays are re-created between each use. Since the methods of signal transduction are identical to those used in the immobilized bead strategy, it is expected that performance will be similar. A false-color image showing raw data output using this method is shown as Figure 1.59 for detection of three strains of *E. coli*.

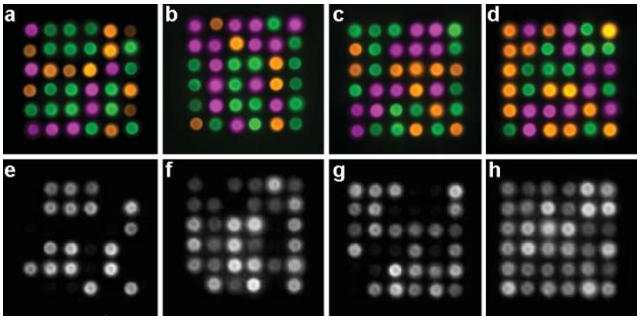

Figure 1.59 False color images of raw three-component microbead array responses to three strains of *E. coli*. Each column is one strain. Top row (a-d) shows the identity of the beads from their fluorescence, while bottom row (e-h) shows intensity response to the exposed analyte as a gray scale. The array is ~25x25 µm. Modified from ref. [300].

1.4.5.5 Cancer and disease diagnosis

Optical sensor arrays also have begun to find applications to medical diagnosis of disease. Different cell line produce different volatile metabolites, as discussed early with bacteria; this applies to any rapidly growing cells, and in principle the breath is in equilibrium with the volatiles produced within the body. Breath analysis has a long history as an underutilized diagnostic tool;[301-303] limitations in analytical tools that are sufficiently sensitive, specific, or inexpensive have limited this approach in clinical or hospital applications. Electronic noses[301,303-304] have certainly been examined for breath analysis, especially for diagnosis of lung cancer and of respiratory infections with some limited success. Colorimetric sensor arrays of the type developed in Suslick's lab for bacterial identification[298] too, have had some preliminary clinical success for breath diagnosis. Point of care diagnosis of bacterial sinusitis, as one example, has achieved classification accuracy as high as 90% in initial studies at the University of Pennsylvania medical school.[305] Lung cancer screening using breath analysis has also been reported by Mazzone *et al.*[304] at the Cleveland Clinic with promising initial results. In a study with 229 subjects (92 with lung cancer), individuals with different histologies could be accurately distinguished from one

another (86.4% for adeno-carcinoma vs. squamous cell carcinoma), and the accuracy of breath biosignatures could be optimized by incorporating clinical risk factors. [304]

In an entirely different approach to cell differentiation, it is not surprising that different cell lines interact differently with different nanoparticles[306-308] and that those interactions are strongly affected by the chemical nature of the nanoparticle surfaces, particularly as biomolecules adsorb onto nanoparticle surfaces forming a "protein corona".[309-311]

Taking advantage of nanoparticle-whole cell interaction, the parallel soluble fluorescent displacement assays that Rotello *et al*. [272,312-313] have developed for protein identification also have been applied to differentiation between normal and cancerous whole cells. For example, green fluorescent protein coated gold nanoparticles array were used to differentiate types of mammalian cancer cells (HeLa (cervical), HepG2 (liver), MCF-7 (breast), and NT2 (testis))[312]. The nanoparticle suface ligand structures for mammalian cell discrimination are shown as Figure 1.60. A score plot summarizing the array's discrimination ability[272] is shown as Figure 1.61.

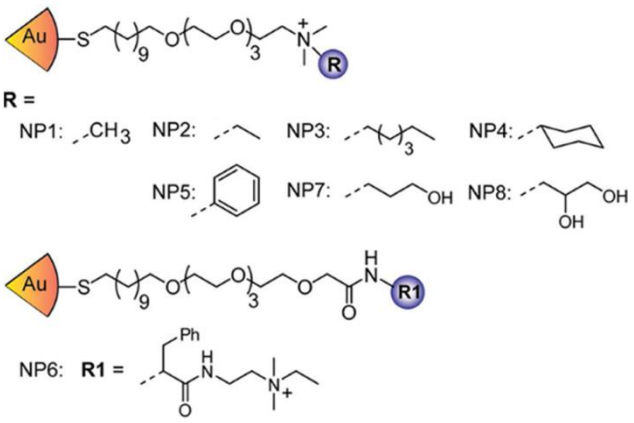

Figure 1.60 The six nanoparticle ligand structures used for mammalian cell discrimination. Differential sensing ability derives from displacement of GFP from the nanoparticles to release GFP in the presence of species with differential relative affinities for the gold nanoparticle with various surface ligands (NP1 through NP6). Reproduced with permission from ref. [272].

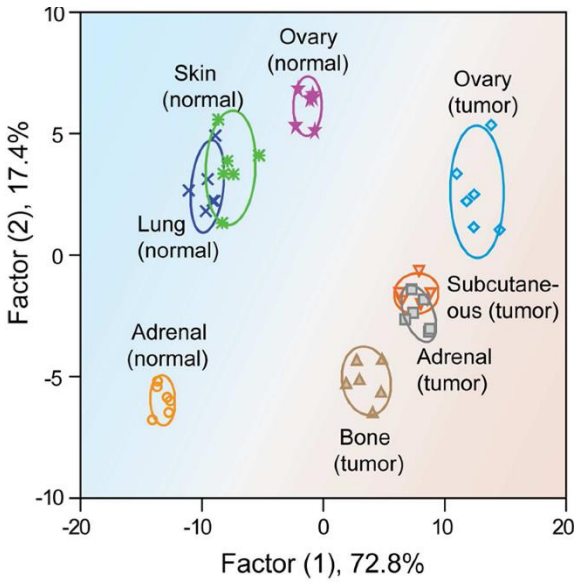

Figure 1.61 LDA score plot showing clear differentiation between healthy and metastatic mammalian cells and among cells from various organs. The blue/red shading is meant to delineate healthy/normal and metastatic/tumor cells. Reproduced from ref. [272].

1.5 Limitations, opportunities, and future challenges

The primary limitation of a sensor array, including the mammalian nose, is that it gives a composite response to complex mixtures. One does not get a component by component analysis from cross-reactive sensor arrays. Most chemists naturally assume that the goal with any complex mixture is to achieve a complete quantitative analysis of each component. But in fact, for multi-component analytes, there are generally multiple analytical goals: one often wants to know is this mixture the same as that one, is there one (or a few) component(s) that have changed against a constant complex mixture, is this mixture genuine or counterfeit, was this material processed correctly or not?

The primary strength of a sensor array, including the mammalian nose, is that it gives a composite response to complex mixtures. The ability to fingerprint complex mixtures is often greatly simplified by such a composite response. With recent advances in optical sensor arrays, exquisite fingerprinting of extremely similar mixtures or single analytes has been achieved over a wide range of analyte types.

Another characteristic of sensor arrays that probes chemical properties of analytes, rather than physical properties, is non-uniform intrinsic response to analytes. This too is a good news-bad news story. The good news is that most analytes of concern (e.g., toxic gases) are, essentially by definition, highly reactive and therefore easily detected, even at sub-ppm concentrations. This eliminates many of the problems of false-positives associated with traditional electronic nose and solid state chemical sensors. The bad news is that some analyses are interested in less reactive analytes. One solution, developed only recently, is to pre-react the analyte stream to produce, for example, partial oxidation products that are more reactive and therefore more easily analyzed by chemoresponsive sensors.[19] More selective methods of "activating" these analytes, especially in the presence of a high concentration of interferents, would add significantly to the capabilities of current optical sensor arrays for gas analysis.

The alternative of incorporating even more promiscuous optical sensors has some merit as well; the

difficulty is that the weak interactions usually used in monitoring such properties (e.g., physisorption onto surfaces, absorption into polymers) generally lead to lower sensitivity (e.g., solvatochromic shifts of polymer adsorbents are typically undetectable below ~0.1% of the saturation vapor pressure of an analyte).

For heterogeneous optical arrays designed for liquid sensing, contamination of analyte solutions due to probe solubility is a major problem. One is caught in a dilemma for solid state optical arrays that are to be immersed in liquids: the solvates must have access to the sensor medium, but the sensor dyes must not dissolve into the liquid. In principle, one may overcome this problem by immobilization of dyes into sol-get formulations, but in practice immobilization is sometimes imperfect.

Solution phase array sensing is carried out by a parallel analysis of multiple aliquots of the analyte solution, each with an added, different homogeneous probe, e.g. using microwell plates. This is a cumbersome procedure, and one that should yield to improved technology using heterogenization of the soluble probes, including covalent attachment to the probe substrate.

All in all, however, one can only be impressed by the development of optical sensor arrays over the past decade.[17] Colorimetric sensor arrays have demonstrated excellent potential for complex systems analysis in real-world applications and provide a novel method for discrimination among closely similar complex mixtures.

The commercialization of optoelectronic nose technology is underway in several companies and one expects that significant markets are likely to develop in the future.

1.6 Acknowledgments

This work was supported through the NIH Genes, Environment and Health Initiative (U01ES016011), the Department of Defence (Contract N41756-12-R-4767), and the NSF (CHE 1152232).

1.7 References

(1) Buck, L.; Axel, R. *Cell* **1991**, *65*, 175.

(2) Hawkes, C. H. D., R. L. *The Neurology of Olfaction*; Cambridge Univ. Press, 2009.

(3) Mombaerts, P. *Science* **1999**, *286*, 707.

(4) Hierlemann, A.; Gutierrez-Osuna, R. *Chem. Rev.* **2008**, *108*, 563.

(5) Suslick, K. S. *Current Opinion in Chemical Biology* **2012**, *16*, 557.

(6) Stitzel, S. E.; Aernecke, M. J.; Walt, D. R. *Annual Review of Biomedical Engineering* **2011**, *13*, 1.

(7) Paolesse, R.; Monti, D.; Dini, F.; Di Natale, C. In *Luminescence Applied in Sensor Science*; Prodi, L., Montalti, M., Zaccheroni, N., Eds. 2011; Vol. 300, p 139.

(8) Rock, F.; Barsan, N.; Weimar, U. *Chemical Reviews* **2008**, *108*, 705.

(9) Nakamoto, T.; Ishida, H. *Chemical Reviews* **2008**, *108*, 680.

(10) Suslick, K. S.; Rakow, N. A.; Sen, A. *Tetrahedron* **2004**, *60*, 11133.

(11) Turner, A. P. F.; Magan, N. *Nature Reviews Microbiology* **2004**, *2*, 161.

(12) Lewis, N. S. *Accounts of Chemical Research* **2004**, *37*, 663.

(13) Janata, J. *Principles of Chemical Sensors, Second Edition*, 2009.

(14) Suslick, K. S. *MRS Bulletin* **2004**, *29*, 720.

(15) Persaud, K.; Dodd, G. *Nature* **1982**, *299*, 352.

(16) Lim, S. H.; Feng, L.; Kemling, J. W.; Musto, C. J.; Suslick, K. S. *Nature Chemistry* **2009**, *1*, 562.

(17) Rakow, N. A.; Suslick, K. S. *Nature* **2000**, *406*, 710.

(18) Suslick, K. S.; Bailey, D. P.; Ingison, C. K.; Janzen, M.; Kosal, M. E.; McNamara III, W. B.; Rakow, N. A.; Sen, A.; Weaver, J. J.; Wilson, J. B.; Zhang, C.; Nakagaki, S. *Quimica Nova* **2007**, *30*, 677.

(19) Lin, H.; Jang, M.; Suslick, K. S. *Journal of the American Chemical Society* **2011**, *133*, 16786.

(20) Borisov, S. M.; Wolfbeis, O. S. *Chemical Reviews* **2008**, *108*, 423.

(21) Kemling, J. W.; Qavi, A. J.; Bailey, R. C.; Suslick, K. S. *Journal of Physical Chemistry Letters* **2011**, *2*, 2934.

(22) Anker, J. N.; Hall, W. P.; Lyandres, O.; Shah, N. C.; Zhao, J.; Van Duyne, R. P. *Nature Materials* **2008**, *7*, 442.

(23) Jeon, S.; Ahn, S. E.; Song, I.; Kim, C. J.; Chung, U. I.; Lee, E.; Yoo, I.; Nathan, A.; Lee, S.; Robertson, J.; Kim, K. *Nature Materials* **2012**, *11*, 301.

(24) Kubo, W.; Fujikawa, S. *Nano Letters* **2011**, *11*, 8.

(25) Lu, Y.; Peng, S.; Luo, D.; Lal, A. *Nature Communications* **2011**, *2*.

(26) Wang, S.; Ota, S.; Guo, B.; Ryu, J.; Rhodes, C.; Xiong, Y.; Kalim, S.; Zeng, L.; Chen, Y.; Teitell, M. A.; Zhang, X. *Nano Letters* **2011**, *11*, 3431.

(27) Wang, S.; Pile, D. F. P.; Sun, C.; Zhang, X. *Nano Letters* **2007**, *7*, 1076.

(28) Gründler, P. *Chemical Sensors, An Introduction for Scientists and Engineers*; Springer-Verlag: Berlin Heidelberg, 2007.

(29) Janata, J. *Analytical Chemistry* **2001**, *73*, 150 A.

(30) Buck, L. B. *Angewandte Chemie International Edition* **2005**, *44*, 6128.

(31) Katada, S.; Hirokawa, T.; Oka, Y.; Suwa, M.; Touhara, K. *Journal of Neuroscience* **2005**, *25*, 1806.

(32) Stetter, J. R.; Li, J. *Chem. Rev.* **2008**, *108*, 352.

(33) Ahmed, M. U.; Hossain, M. M.; Tamiya, E. *Electroanalysis* **2008**, *20*, 616.

(34) Tomchenko, A. A.; Harmer, G. P.; Marquis, B. T.; Allen, J. W. *Sensors and Actuators B: Chemical* **2003**, *93*, 126.

(35) Ho, G. W. *Science of Advanced Materials* **2011**, *3*, 150.

(36) Potyrailo, R. A.; Surman, C.; Nagraj, N.; Burns, A. *Chemical Reviews* **2011**, *111*, 7315.

(37) James, D.; Scott, S. M.; Ali, Z.; O'Hare, W. T. *Microchimica Acta* **2005**, *149*, 1.

(38) Janata, J.; Josowicz, M. *Journal of Solid State Electrochemistry* **2009**, *13*, 41.

(39) Ronkainen, N. J.; Halsall, H. B.; Heineman, W. R. *Chemical Society Reviews* **2010**, *39*, 1747.

(40) Nambiar, S.; Yeow, J. T. W. *Biosensors & Bioelectronics* **2011**, *26*, 1825.

(41) Zanardi, C.; Terzi, F.; Seeber, R. *Analytical and Bioanalytical Chemistry* **2013**, *405*, 509.

(42) Grate, J. W. *Chem. Rev.* **2000**, *100*, 2627.

(43) Snow, E. S.; Perkins, F. K.; Houser, E. J.; Badescu, S. C.; Reinecke, T. L. *Science* **2005**, *307*, 1942.

(44) Park, S.; Vosguerichian, M.; Bao, Z. A. *Nanoscale* **2013**, *5*, 1727.

(45) Cui, Y.; Wei, Q.; Park, H.; Lieber, C. M. *Science* **2001**, *293*, 1289.

(46) Patolsky, F.; Zheng, G.; Lieber, C. M. *Nanomedicine* **2006**, *1*, 51.

(47) Sharma, S.; Madou, M. *Philosophical Transactions of the Royal Society a-Mathematical Physical and Engineering Sciences* **2012**, *370*, 2448.

(48) Zhu, Z. G.; Garcia-Gancedo, L.; Flewitt, A. J.; Xie, H. Q.; Moussy, F.; Milne, W. I. *Sensors* **2012**, *12*, 5996.

(49) Gan, T.; Hu, S. S. *Microchimica Acta* **2011**, *175*, 1.

(50) Ma, Q.; Su, X. G. *Analyst* **2011**, *136*, 4883.

(51) Pumera, M.; Ambrosi, A.; Bonanni, A.; Chng, E. L. K.; Poh, H. L. *Trac-Trends in Analytical Chemistry* **2010**, *29*, 954.

(52) Bakker, E.; Qin, Y. *Analytical Chemistry* **2006**, *78*, 3965.

(53) Privett, B. J.; Jae, H. S.; Schoenfisch, M. H. *Analytical Chemistry* **2008**, *80*, 4499.

(54) Privett, B. J.; Shin, J. H.; Schoenfisch, M. H. *Analytical Chemistry* **2010**, *82*, 4723.

(55) Kimmel, D. W.; LeBlanc, G.; Meschievitz, M. E.; Cliffel, D. E. *Analytical Chemistry* **2011**, *84*, 685.

(56) Brett, C. M. A. *Pure and Applied Chemistry* **2007**, *79*, 1969.

(57) Hanrahan, G.; Patil, D. G.; Wang, J. *Journal of Environmental Monitoring* **2004**, *6*, 657.

(58) Campas, M.; Garibo, D.; Prieto-Simon, B. *Analyst* **2012**, *137*, 1055.

(59) Parellada, J.; Narváez, A.; López, M. A.; Domínguez, E.; Fernández, J. J.; Pavlov, V.; Katakis, I. *Analytica Chimica Acta* **1998**, *362*, 47.

(60) Solé, S.; Alegret, S. *Environmental Science and Pollution Research* **2001**, *8*, 256.

(61) Dalbasti, T.; Kilinc, E. *Methods in Enzymology* **2005**, *396*, 584.

(62) Wang, Y.; Xu, H.; Zhang, J.; Li, G. *Sensors* **2008**, *8*, 2043.

(63) Hahn, C. E. W. *Analyst* **1998**, *123*, 57R.

(64) Pedrero, M.; Campuzano, S.; Pingarron, J. M. *Analytical Methods* **2011**, *3*, 780.

(65) Laschi, S.; Centi, S.; Mascini, M. *Bioanalytical Reviews* **2011**, *3*, 11.

(66) Shiddiky, M. J. A.; Torriero, A. A. J. *Biosensors and Bioelectronics* **2011**, *26*, 1775.

(67) Song, S.; Xu, H.; Fan, C. *International journal of nanomedicine* **2006**, *1*, 433.

(68) Serra, B.; Reviejo, Á. J.; Pingarrón, J. M. In *Comprehensive Analytical Chemistry*; Alegret, S., Merkoçi, A., Eds.; Elsevier: 2007; Vol. Volume 49, p 255.

(69) Pedrero, M.; Campuzano, S.; Pingarrón, J. M. *Electroanalysis* **2012**, *24*, 470.

(70) Danielsson, B.; Mosbach, K.; Winquist, F.; Lundström, I. *Sensors and Actuators* **1988**, *13*, 139.

(71) Barsony, I.; Ducso, C.; Furjes, P. *Thermometric Gas Sensing*; Springer: New York, 2009.

(72) Ramanathan, K.; Jönsson, B. R.; Danielsson, B. *Analytical Chemistry* **2000**, *72*, 3443.

(73) Ramanathan, K.; Jönsson, B. R.; Danielsson, B. *Analytica Chimica Acta* **2001**, *427*, 1.

(74) Yakovleva, M.; Bhand, S.; Danielsson, B. *Analytica Chimica Acta* **2013**, *766*, 1.

(75) Mandenius, C. F.; Bülow, L.; Danielsson, B.; Mosbach, K. *Applied Microbiology and Biotechnology* **1985**, *21*, 135.

(76) Xie, B.; Ramanathan, K.; Danielsson, B. *TrAC Trends in Analytical Chemistry* **2000**, *19*, 340.

(77) Xie, B.; Mecklenburg, M.; Danielsson, B.; Öhman, O.; Winquist, F. *Analytica Chimica Acta* **1994**, *299*, 165.

(78) Bataillard, P.; Steffgen, E.; Haemmerli, S.; Manz, A.; Widmer, H. M. *Biosensors and Bioelectronics* **1993**, *8*, 89.

(79) Zhang, Y.; Tadigadapa, S. *Biosensors and Bioelectronics* **2004**, *19*, 1733.

(80) Shimohigoshi, M.; Karube, I. *Sensors and Actuators, B: Chemical* **1996**, *30*, 17.

(81) Mecklenburg, M.; Lindbladh, C.; Li, H.; Mosbach, K.; Danielsson, B. *Analytical Biochemistry* **1993**, *212*, 388.

(82) Scheller, F.; Siegbahn, N.; Danielsson, B.; Mosbach, K. *Analytical Chemistry* **1985**, *57*, 1740.

(83) Wolf, A.; Weber, A.; Hüttl, R.; Lerchner, J.; Wolf, G. *Thermochimica Acta* **2002**, *382*, 89.

(84) Xie, B.; Mecklenburg, M.; Danielsson, B.; Ohman, O.; Norlin, P.; Winquist, F. *Analyst* **1995**, *120*, 155.

(85) Jerónimo, P. C. A.; Araújo, A. N.; Conceição B.S.M. Montenegro, M. *Talanta* **2007**, *72*, 13.

(86) Nassau, K. *The Physics and Chemistry of Color*; Wiley: New York, 2001.

(87) Lakowicz, J. R. *Principles of Fluorescence Spectroscopy, 3rd ed.*; 4th Printing: New York, 2006.

(88) *Lakowicz J. R. Principles of fluorescence spectroscopy, 3rd ed. Springer, New York, (2006), 4th Printing, 2006, XXVI, 954 p, 1255 illus.*

(89) Podbielska, H.; Ulatowska-Jarza, A.; Muller, G.; Eichler, H. J. In *Optical Chemical Sensors*; Baldini, F., Chester, A. N., Homola, J., Martellucci, S., Eds.; Springer: Erice, Italy, 2006.

(90) Orellana, G. In *Optical Chemical Sensors*; Baldini, F., Chester, A. N., Homola, J., Martellucci, S., Eds. 2006, p 99.

(91) Bonacchi, S.; Genovese, D.; Juris, R.; Montalti, M.; Prodi, L.; Rampazzo, E.; Sgarzi, M.; Zaccheroni, N. In *Topics in Current Chemistry: Luminescence Applied in Sensor Science*; Prodi, L., Montalti, M., Zaccheroni, N., Eds.; Springer Berlin / Heidelberg: 2011; Vol. 300, p 93.

(92) dos Santos, C. M. G.; Harte, A. J.; Quinn, S. J.; Gunnlaugsson, T. *Coordination Chemistry Reviews* **2008**, *252*, 2512.

(93) Thomas, S. W.; Joly, G. D.; Swager, T. M. *Chemical Reviews* **2007**, *107*, 1339.

(94) de Silva, A. P.; Gunaratne, H. Q. N.; Gunnlaugsson, T.; Huxley, A. J. M.; McCoy, C. P.; Rademacher, J. T.; Rice, T. E. *Chemical Reviews* **1997**, *97*, 1515.

(95) Newman, R. H.; Fosbrink, M. D.; Zhang, J. *Chemical Reviews* **2011**, *111*, 3614.

(96) Wade, C. R.; Broomsgrove, A. E. J.; Aldridge, S.; Gabbaï, F. o. P. *Chemical Reviews* **2010**, *110*, 3958.

(97) Lee, J. Y.; Kim, S. K.; Jung, J. H.; Kim, J. S. *The Journal of Organic Chemistry* **2005**, *70*, 1463.

(98) Turkewitsch, P.; Wandelt, B.; Darling, G. D.; Powell, W. S. *Analytical Chemistry* **1998**, *70*, 2025.

(99) Wiskur, S. L.; Ait-Haddou, H.; Lavigne, J. J.; Anslyn, E. V. *Accounts of Chemical Research* **2001**, *34*, 963.

(100) Pinalli, R.; Dalcanale, E. *Accounts of Chemical Research* **2013**, *46*, 399.

(101) Nguyen, B. T.; Anslyn, E. V. *Coordination Chemistry Reviews* **2006**, *250*, 3118.

(102) Umali, A. P.; Anslyn, E. V. *Current Opinion in Chemical Biology* **2010**, *14*, 685.

(103) Wright, A. T.; Anslyn, E. V. *Chemical Society Reviews* **2006**, *35*, 14.

(104) Meng, L.-Z.; Mei, G.-X.; He, Y.-B.; Zeng, Z.-Y.; Liu, S.-Y. *Acta Chimica Sinica* **2005**, *63*, 416.

(105) Anslyn, E. V. *J. Org. Chem.* **2007**, *72*, 687.

(106) Atwood, J. L.; Davies, J. E. D.; MacNicol, D. D.; Vogtle, F. *Comprehensive Supramolecular Chemistry*; Pergamon: Oxford, 1996.

(107) Wang, K.; Yang, X.; Yang, R. *Sensors and Actuators B: Chemical* **2000**, *66*, 263.

(108) Hunter, C. A. *Angewandte Chemie-International Edition* **2004**, *43*, 5310.

(109) Rigby, M.; Smith, E. B.; Wakeham, W. A.; Maitland, G. C. *The Forces Between Molecules*; Clarendon: Oxford, 1986.

(110) Müller-Dethlefs, K.; Hobza, P. *Chemical Reviews* **1999**, *100*, 143.

(111) Jungreis, E. *Spot Test Analysis 2nd ed.*; J. Wiley: New York, 1997.

(112) Feigle, F.; Anger, V. *Spot Tests in Organic Chemistry*; Elsevier: New York, 1966.

(113) Kolthoff, I. M. *Acid Base Indicators*; Macmillan: New York, 1937.

(114) Janzen, M. C.; Ponder, J. B.; Bailey, D. P.; Ingison, C. K.; Suslick, K. S. *Analytical Chemistry* **2006**, *78*, 3591.

(115) El-Desouki, M.; Deen, M. J.; Fang, Q. Y.; Liu, L.; Tse, F.; Armstrong, D. *Sensors* **2009**, *9*, 430.

(116) Meier, R. J.; Fischer, L. H.; Wolfbeis, O. S.; Schaferling, M. *Sensors and Actuators B-Chemical* **2013**, *177*, 500.

(117) Hsieh, M. D.; Zellers, E. T. *Analytical Chemistry* **2004**, *76*, 1885.

(118) Healey, B. G.; Walt, D. R. *Analytical Chemistry* **1997**, *69*, 2213.

(119) Lavigne, J. J.; Anslyn, E. V. *Angewandte Chemie - International Edition* **2001**, *40*, 3118.

(120) Devos, M.; Patte, F.; Rouault, J.; Laffort, P.; Gemert, L. J. V. *Standardized Human Olfactory Thresholds*; IRL Press, Oxford University Press: Oxford, 1990.

(121) Wang, J.; Luthey-Schulten, Z. A.; Suslick, K. S. *Proceedings of the National Academy of Sciences* **2003**, *100*, 3035.

(122) Duan, X. F.; Block, E.; Li, Z.; Connelly, T.; Zhang, J.; Huang, Z. M.; Su, X. B.; Pan, Y.; Wu, L. F.; Chi, Q. Y.; Thomas, S.; Zhang, S. Z.; Ma, M. H.; Matsunami, H.; Chen, G. Q.; Zhuang, H. Y. *Proceedings of the National Academy of Sciences of the United States of America* **2012**, *109*, 3492.

(123) Rakow, N. A.; Suslick, K. S. In *Artificial Chemical Sensing: Olfaction and the Electronic Nose*; Stetter, J. R., Pensrose, W. R., Eds. Pennington, NJ, 2001, p 8.

(124) Suslick, K. S.; Rakow, N. A. *"Colorimetric Artificial Nose Having an Array of Dyes and Method for Artificial Olfaction" U.S. Patent 6,368,558; April 9, 2002.* **2002**.

(125) Dini, F.; Magna, G.; Martinelli, E.; Paolesse, R.; Filippini, D.; Lundstrcm, I.; Di Natale, C. In *Procedia Engineering* 2012; Vol. 25, p 1413.

(126) Amao, Y. *Microchimica Acta* **2003**, *143*, 1.

(127) Collman, J. P.; Fu, L. *Accounts of Chemical Research* **1999**, *32*, 455.

(128) Cook, B. R.; Reinert, T. J.; Suslick, K. S. *Journal of the American Chemical Society* **1986**, *108*, 7281.

(129) Suslick, K. S.; Fox, M. M. *Journal of the American Chemical Society* **1983**, *105*, 3507.

(130) Bhyrappa, P.; Vaijayanthimala, G.; Suslick, K. S. *Journal of the American Chemical Society* **1999**, *121*, 262.

(131) Bhyrappa, P.; Young, J. K.; Moore, J. S.; Suslick, K. S. *Journal of the American Chemical Society* **1996**, *118*, 5708.

(132) Fang, M.; Wilson, S. R.; Suslick, K. S. *Journal of the American Chemical Society* **2008**, *130*, 1134.

(133) Sen, J.; Suslick, K. S. *Journal of the American Chemical Society* **2000**, *122*, 11565.

(134) Rakow, N. A.; Sen, A.; Janzen, M. C.; Ponder, J. B.; Suslick, K. S. *Angewandte Chemie - International Edition* **2005**, *44*, 4528.

(135) Sessler, J. L.; Gale, P. A.; Cho, W.-S. *Anion Receptor Chemistry*; RSC Publishing: Cambridge, UK, 2006.

(136) Gunnlaugsson, T.; Glynn, M.; Tocci, G. M.; Kruger, P. E.; Pfeffer, F. M. *Coordination Chemistry Reviews* **2006**, *250*, 3094.

(137) O'Neil, E. J.; Smith, B. D. *Coordination Chemistry Reviews* **2006**, *250*, 3068.

(138) Kim, S. K.; Lee, D. H.; Hong, J. I.; Yoon, J. *Accounts of Chemical Research* **2009**, *42*, 23.

(139) Duke, R. M.; Veale, E. B.; Pfeffer, F. M.; Kruger, P. E.; Gunnlaugsson, T. *Chemical Society Reviews* **2010**, *39*, 3936.

(140) Li, A. F.; Wang, J. H.; Wang, F.; Jiang, Y. B. *Chemical Society Reviews* **2010**, *39*, 3729.

(141) Garcia, J. M.; Garcia, F. C.; Serna, F.; de la Pena, J. L. *Polymer Reviews* **2011**, *51*, 341.

(142) Du, J. J.; Hu, M. M.; Fan, J. L.; Peng, X. J. *Chemical Society Reviews* **2012**, *41*, 4511.

(143) Chifotides, H. T.; Dunbar, K. R. *Accounts of Chemical Research* **2013**, *46*, 894.

(144) Liu, Z. P.; He, W. J.; Guo, Z. J. *Chemical Society Reviews* **2013**, *42*, 1568.

(145) Kim, D.-S.; Chung, Y.-M.; Jun, M.; Ahn, K. H. *The Journal of Organic Chemistry* **2009**, *74*, 4849.

(146) Lehn, J. M. *Supramolecular Chemistry: Concepts and Perspectives*; VCH: Weinhiem, 1995.

(147) Kaur, N.; Kumar, S. *Tetrahedron* **2011**, *67*, 9233.

(148) Flaschka, H.; Schwarzenbach, G. *Complexometric Titrations*; Methuen: London, 1969.

(149) Steinberg, I. M.; Lobnik, A.; Wolfbeis, O. S. *Sensors and Actuators B: Chemical* **2003**, *90*, 230.

(150) Qazi, M. A.; Qureshi, I.; Memon, S. *Journal of Molecular Structure* **2010**, *975*, 69.

(151) Feng, L.; Zhang, Y.; Wen, L.; Chen, L.; Shen, Z.; Guan, Y. *Chemistry - A European Journal* **2011**, *17*, 1101.

(152) Mayr, T.; Igel, C.; Liebsch, G.; Klimant, I.; Wolfbeis, O. S. *Analytical Chemistry* **2003**, *75*, 4389.

(153) Hunger, K., ed. *Industrial Dyes. Chemistry, Properties, Applications.*; Wiley-VCH: Weinheim, 2003.

(154) Zollinger, H. *Color Chemistry. Synthesis, Properties and Applications of Organic Dyes and Pigments, 3rd ed.*; Wiley-VCH: Weinheim, 2003.

(155) Garfield, S. *Mauve: How One Man Invented a Color That Changed the World*; Faber and Faber: London, 2000.

(156) Rottman, C.; Grader, G.; De Hazan, Y.; Melchior, S.; Avnir, D. *Journal of the American Chemical Society* **1999**, *121*, 8533.

(157) El-Nahhal, I.; Zourab, S.; Qudeh, A. *Sol-Gel Optical pH Sensors: Thin film sol-gel optical pH indicators using surfactants* LAP LAMBERT Köln, 2012.

(158) Green, F. J. *The Sigma-Aldrich Handbook of Stains, Dyes and Indicators*; Aldrich Chemical Co., Inc.: Milwaukee, WI, 1990.

(159) Reichardt, C.; Welton, T. *Solvents and solvent effects in organic chemistry, 4th ed.*; Wiley-VCH: Weinheim, 2010.

(160) Reichardt, C. *Solvent Effects in Organic Chemistry, 2nd ed.*; Verlag Chemie: Weinheim, 1988.

(161) Reichardt, C. *Chemical Reviews* **1994**, *94*, 2319.

(162) Reichardt, C. *Green Chemistry* **2005**, *7*, 339.

(163) Reichardt, C. *Organic Process Research & Development* **2007**, *11*, 105.

(164) Kamlet, M. J.; Abboud, J. L. M.; Taft, R. W. *Prog. Phys. Org. Chem.* **1981**, *13*, 485.

(165) Taft, R. W.; Abboud, J. L. M.; Kamlet, M. J.; Abraham, M. H. *Journal of Solution Chemistry* **1985**, *14*, 153.

(166) Cabot, R.; Hunter, C. A. *Chemical Society Reviews* **2012**, *41*, 3485.

(167) Mancini, P. M.; Adam, C. G.; Fortunato, G. G.; Vottero, L. R. *Arkivoc* **2007**, 266.

(168) Marini, A.; Muñoz-Losa, A.; Biancardi, A.; Mennucci, B. *The Journal of Physical Chemistry B* **2010**, *114*, 17128.

(169) Matyushov, D. V.; Schmid, R.; Ladanyi, B. M. *Journal of Physical Chemistry B* **1997**, *101*, 1035.

(170) Buncel, E.; Rajagopal, S. *Accounts of Chemical Research* **1990**, *23*, 226.

(171) Katritzky, A. R.; Fara, D. C.; Yang, H. F.; Tamm, K.; Tamm, T.; Karelson, M. *Chemical Reviews* **2004**, *104*, 175.

(172) Walt, D. R. *Science* **2000**, *287*, 451.

(173) Walt, D. R. *Chemical Society Reviews* **2010**, *39*, 38.

(174) Zhang, X.; Li, B.; Chen, Z. H.; Chen, Z. N. *Journal of Materials Chemistry* **2012**, *22*, 11427.

(175) Buss, C. E.; Mann, K. R. *Journal of the American Chemical Society* **2002**, *124*, 1031.

(176) Hudson, Z. M.; Sun, C.; Harris, K. J.; Lucier, B. E. G.; Schurko, R. W.; Wang, S. N. *Inorganic Chemistry* **2011**, *50*, 3447.

(177) Cich, M. J.; Hill, I. M.; Lackner, A. D.; Martinez, R. J.; Ruthenburg, T. C.; Takeshita, Y.; Young, A. J.; Drew, S. M.; Buss, C. E.; Mann, K. R. *Sensors and Actuators B-Chemical* **2010**, *149*, 199.

(178) Wolfbeis, O. S. *Analytical Chemistry* **2008**, *80*, 4269.

(179) Wolfbeis, O. S. *Fiber Optic Chemical Sensors and Biosensors*; CRC Press: Boca Raton, 1991.

(180) Lobnik, A.; Čajlaković, M. *Sensors and Actuators B: Chemical* **2001**, *74*, 194.

(181) Lin, H.; Suslick, K. S. *Journal of the American Chemical Society* **2010**, *132*, 15519.

(182) Rosi, N. L.; Mirkin, C. A. *Chemical Reviews* **2005**, *105*, 1547.

(183) Xie, X. J.; Xu, W.; Liu, X. G. *Accounts of Chemical Research* **2012**, *45*, 1511.

(184) Perfezou, M.; Turner, A.; Merkoci, A. *Chemical Society Reviews* **2012**, *41*, 2606.

(185) Basabe-Desmonts, L.; Reinhoudt, D. N.; Crego-Calama, M. *Chemical Society Reviews* **2007**, *36*, 993.

(186) Kubarych, C. J.; Adams, M. M.; Anslyn, E. V. *Org. Lett.* **2010**, *12*, 4780.

(187) Stephenson, C. J.; Shimizu, K. D. *Polymer International* **2007**, *56*, 482.

(188) Allender, C. J.; Brain, K. R.; Heard, C. M. *Chirality* **1997**, *9*, 233.

(189) Greene, N. T.; Shimizu, K. D. *Journal of the American Chemical Society* **2005**, *127*, 5695.

(190) Vetrichelvan, M.; Nagarajan, R.; Valiyaveettil, S. *Macromolecules* **2006**, *39*, 8303.

(191) Valero-Navarro, A.; Medina-Castillo, A. L.; Fernandez-Sanchez, J. F.; Fernandez-Gutierrez, A. *Biosensors & Bioelectronics* **2011**, *26*, 4520.

(192) Ng, S. M.; Narayanaswamy, R. *Analytical and Bioanalytical Chemistry* **2006**, *386*, 1235.

(193) Chen, Y. C.; Brazier, J. J.; Yan, M. D.; Bargo, P. R.; Prahl, S. A. *Sensors and Actuators B-Chemical* **2004**, *102*, 107.

(194) Sergeyeva, T. A.; Gorbach, L. A.; Piletska, E. V.; Piletsky, S. A.; Brovko, O. O.; Honcharova, L. A.; Lutsyk, O. D.; Sergeeva, L. M.; Zinchenko, O. A.; El'skaya, A. V. *Analytica Chimica Acta* **2013**, *770*, 161.

(195) Hsu, H. C.; Chen, L. C.; Ho, K. C. *Analytica Chimica Acta* **2004**, *504*, 141.

(196) Long, J.; Xu, J.; Yang, Y.; Wen, J.; Jia, C. *Materials Science and Engineering B: Solid-State Materials for Advanced Technology* **2011**, *176*, 1271.

(197) Feng, L.; Musto, C. J.; Kemling, J. W.; Lim, S. H.; Zhong, W.; Suslick, K. S. *Analytical Chemistry* **2010**, *82*, 9433.

(198) Suslick, K. S.; Bailey, D. P.; Ingison, C. K.; Janzen, M.; Kosal, M. A.; III, W. B. M.; Rakow, N. A.; Sen, A.; Weaver, J. J.; Wilson, J. B.; Zhang, C.; Nakagaki, S. *Quimica Nova* **2007**, *30*, 677.

(199) Zhang, C.; Suslick, K. S. *Journal of the American Chemical Society* **2005**, *127*, 11548.

(200) Kemling, J. W.; Suslick, K. S. *Nanoscale* **2011**, *3*, 1971.

(201) Lukowiak, A.; Strek, W. *Journal of Sol-Gel Science and Technology* **2009**, *50*, 201.

(202) Podbielska, H.; Ulatowska-Jarza, A.; Muller, G.; Eichler, H. J. *Sol-Gels for Optical Sensors*; Springer: Erice, Italy, 2006.

(203) Lim, S. H.; Kemling, J. W.; Feng, L.; Suslick, K. S. *Analyst* **2009**, *134*, 2453.

(204) Feng, L.; Musto, C. J.; Kemling, J. W.; Lim, S. H.; Suslick, K. S. *Chemical Communications* **2010**, *46*, 2037.

(205) Bang, J. H.; Lim, S. H.; Park, E.; Suslick, K. S. *Langmuir* **2008**, *24*, 13168.

(206) Bang, J. H.; Suslick, K. S. *Advanced Materials* **2010**, *22*, 1039.

(207) LaFratta, C. N.; Walt, D. R. *Chemical Reviews* **2008**, *108*, 614.

(208) Pantano, P.; Walt, D. R. *Chemistry of Materials* **1996**, *8*, 2832.

(209) Walt, D. R. *BioTechniques* **2006**, *41*, 529.

(210) Dickinson, T. A.; Michael, K. L.; Kauer, J. S.; Walt, D. R. *Analytical Chemistry* **1999**, *71*, 2192.

(211) Steemers, F. J.; Ferguson, J. A.; Walt, D. R. *Nature Biotechnology* **2000**, *18*, 91.

(212) Epstein, J. R.; Ferguson, J. A.; Lee, K. H.; Walt, D. R. *Journal of the American Chemical Society* **2003**, *125*, 13753.

(213) Rissin, D. M.; Walt, D. R. *Nano Letters* **2006**, *6*, 520.

(214) Rissin, D. M.; Walt, D. R. *Journal of the American Chemical Society* **2006**, *128*, 6286.

(215) Taylor, L. C.; Walt, D. R. *Analytical Biochemistry* **2000**, *278*, 132.

(216) Kuang, Y.; Walt, D. R. *Analytical Biochemistry* **2005**, *345*, 320.

(217) Brogan, K. L.; Walt, D. R. *Current Opinion in Chemical Biology* **2005**, *9*, 494.

(218) Tam, J. M.; Song, L.; Walt, D. R. *Biosensors and Bioelectronics* **2009**, *24*, 2488.

(219) Bjerketorp, J.; Håkansson, S.; Belkin, S.; Jansson, J. K. *Current Opinion in Biotechnology* **2006**, *17*, 43.

(220) Magrisso, M.; Etzion, O.; Pilch, G.; Novodvoretz, A.; Perez-Avraham, G.; Schlaeffer, F.; Marks, R. *Biosensors and Bioelectronics* **2006**, *21*, 1210.

(221) Haswell, S. J. *Practical guide to chemometrics*; CRC Press, 1992.

(222) Donoho, D. L. *AMS Math Challenges Lecture* **2000**, 1.

(223) Johnson, R. A.; Wichern, D. W. *Applied Multivariate Statistical Analysis*; 6th ed.; Prentice Hall: Upper Saddle River, NJ, 2007.

(224) Hair, J. F.; Black, B.; Babin, B.; Anderson, R. E.; Tatham, R. L. *Multivariate data analysis*; 6th ed.; Prentice Hall: Upper Saddle River, NJ, 2005.

(225) Massart, D. L., Kaufman, L. *The Interpretation of Analytical Chemical Data by the Use of Cluster Analysis*; John Wiley & Sons: New York, 1983.

(226) Musto, C. J.; Lim, S. H.; Suslick, K. S. *Analytical Chemistry* **2009**, *81*, 6526.

(227) De, M.; Rana, S.; Akpinar, H.; Miranda, O. R.; Arvizo, R. R.; Bunz, U. H. F.; Rotello, V. M. *Nature Chemistry* **2009**, *1*, 461.

(228) Li, B.; M.K., K.; Altman, N. *Ann. Statist.* **2010**, *38*, 1094.

(229) Zeng, P.; Zhong, W. In *Topics in Applied Statistics: 2012 Symposium of the International Chinese Statistical Association (Springer Proceedings in Mathematics & Statistics)*; Hu, M., Liu, Y., Lin, J., Eds.; Springer: New York, 2013.

(230) Zhong, W.; Suslick, K. S. *Technometrics*, *55*, in press (2013).
http://publish.illinois.edu/wenxuan/files/2012/12/matrix_clust.pdf

(231) Tang, Z.; Yang, J.; Yu, J.; Cui, B. *Sensors* **2010**, *10*, 6436.

(232) Luo, X. G.; Liu, P.; Hou, C. J.; Huo, D. Q.; Dong, J. L.; Fa, H. B.; Yang, M. *Review of Scientific Instruments* **2010**, *81*.

(233) Byrnes, M. E.; King, D. A.; Tierno Jr, P. M. *Nuclear, Chemical, and Biological Terrorism: Emergency Response and Public Protection*; CRC Press, 2003.

(234) Armour, S. J. *International Task Force 40: Toxic Industrial Chemicals (TICs)-Operational and Medical Concerns*; US GPO: Washington, DC., 2001.

(235) Sen, A.; Albarella, J. D.; Carey, J. R.; Kim, P.; McNamara III, W. B. *Sensors and Actuators B: Chemical* **2008**, *134*, 234.

(236) Kim, P.; Albarella, J. D.; Carey, J. R.; Placek, M. J.; Sen, A.; Wittrig, A. E.; McNamara III, W. B. *Sensors and Actuators B: Chemical* **2008**, *134*, 307.

(237) Hou, C.; Li, J.; Huo, D.; Luo, X.; Dong, J.; Yang, M.; Shi, X. *Sensors and Actuators, B: Chemical* **2012**, *161*, 244.

(238) Laine, D. F.; Roske, C. W.; Cheng, I. F. *Analytica Chimica Acta* **2008**, *608*, 56.

(239) Dubnikova, F.; Kosloff, R.; Zeiri, Y.; Karpas, Z. *The Journal of Physical Chemistry A* **2002**, *106*, 4951.

(240) Kostesha, N. V.; Alstrøm, T. S.; Johnsen, C.; Nilesen, K. A.; Jeppesen, J. O.; Larsen, J.; Jakobsen, M. H.; Boisen, A. *Proc. SPIE* **2010**, *7673*, 76730I.

(241) Alstrøm, T. S.; Larsen, J.; Kostesha, N. V.; Jakobsen, M. H.; Boisen, A. In *21st IEEE International Workshop on Machine Learning for Signal Processing* Beijing, 2011, p 6064615.

(242) Huo, D.-Q.; Zhang, G.-P.; Hou, C.-J.; Dong, J.-L.; Zhang, Y.-C.; Liu, Z.; Luo, X.-G.; Fa, H.-B.; Zhang, S.-Y. *Chinese Journal of Analytical Chemistry* **2010**, *38*, 1115.

(243) Corradini, R.; Paganuzzi, C.; Marchelli, R.; Pagliari, S.; Sforza, S.; Dossena, A.; Galaverna, G.; Duchateau, A. *Journal of Materials Chemistry* **2005**, *15*, 2741.

(244) Corradini, R.; Paganuzzi, C.; Marchelli, R.; Pagliari, S.; Dossena, A.; Duchateau, A. *Journal of Inclusion Phenomena and Macrocyclic Chemistry* **2007**, *57*, 625.

(245) Illy, E. *Scientific American* **2002**, *286*, 86.

(246) Clarke, R. J.; Vitzthum, O. G. *Coffee: Recent Developments*; Blackwell Science: Oxford, 2001.

(247) Flament, I. *Coffee Flavor Chemistry*; J. Wiley & Sons: Chichester, 2002.

(248) Suslick, B. A.; Feng, L.; Suslick, K. S. *Analytical Chemistry* **2010**, *82*, 2067.

(249) Zhang, C.; Suslick, K. S. *Journal of Agricultural and Food Chemistry* **2007**, *55*, 237.

(250) Zhang, C.; Bailey, D. P.; Suslick, K. S. *Journal of Agricultural and Food Chemistry* **2006**, *54*, 4925.

(251) Ya, Z.; He, K.; Lu, Z. M.; Yi, B.; Hou, C. J.; Shan, S.; Huo, D. Q.; Luo, X. G. *Flavour and Fragrance Journal* **2012**, *27*, 165.

(252) Vendrell, M.; Zhai, D.; Er, J. C.; Chang, Y. T. *Chem. Rev.* **2012**, *112*, 4491.

(253) Lee, J. W.; Lee, J. S.; Kang, M.; Su, A. I.; Chang, Y. T. *Chemistry-a European Journal* **2006**, *12*, 5691.

(254) Lee, J. W.; Lee, J. S.; Chang, Y. T. *Angewandte Chemie-International Edition* **2006**, *45*, 6485.

(255) Lin, Y. S.; Tu, G. M.; Lin, C. Y.; Chang, Y. T.; Yen, Y. P. *New Journal of Chemistry* **2009**, *33*, 860.

(256) Chan, S. A.; Lee, J. S.; Chang, Y. T. *Australian Journal of Chemistry* **2009**, *62*, 1040.

(257) Lim, S. H.; Musto, C. J.; Park, E.; Zhong, W.; Suslick, K. S. *Organic Letters* **2008**, *10*, 4405.

(258) Musto, C. J.; Suslick, K. S. *Current Opinion in Chemical Biology* **2010**, *14*, 758.

(259) Ghosh, K. K.; Yap, E.; Kim, H.; Lee, J. S.; Chang, Y. T. *Chemical Communications* **2011**, *47*, 4001.

(260) Huang, X.; Xin, J.; Zhao, J. *Journal of Food Engineering* **2011**, *105*, 632.

(261) Salinas, Y.; Ros-Lis, J. V.; Vivancos, J. L.; Martínez-Máñez, R.; Marcos, M. D.; Aucejo, S.; Herranz, N.; Lorente, I. *Analyst* **2012**, *137*, 3635.

(262) Umali, A. P.; LeBoeuf, S. E.; Newberry, R. W.; Kim, S.; Tran, L.; Rome, W. A.; Tian, T.; Taing, D.; Hong, J.; Kwan, M.; Heymann, H.; Anslyn, E. V. *Chemical Science* **2011**, *2*, 439.

(263) Gallagher, L. T.; Heo, J. S.; Lopez, M. A.; Ray, B. M.; Xiao, J.; Umali, A. P.; Zhang, A.; Dharmarajan, S.; Heymann, H.; Anslyn, E. V. *Supramolecular Chemistry* **2012**, *24*, 143.

(264) Hou, C.; Dong, J.; Zhang, G.; Lei, Y.; Yang, M.; Zhang, Y.; Liu, Z.; Zhang, S.; Huo, D. *Biosensors and Bioelectronics* **2011**, *26*, 3981.

(265) Miranda, O. R.; Creran, B.; Rotello, V. M. *Current Opinion in Chemical Biology* **2010**, *14*, 728.

(266) Bunz, U. H. F.; Rotello, V. M. *Angewandte Chemie International Edition* **2010**, *49*, 3268.

(267) Mout, R.; Moyano, D. F.; Rana, S.; Rotello, V. M. *Chemical Society Reviews* **2012**, *41*, 2539.

(268) Saha, K.; Agasti, S. S.; Kim, C.; Li, X.; Rotello, V. M. *Chemical Reviews* **2012**, *112*, 2739.

(269) Moyano, D. F.; Rana, S.; Bunz, U. H. F.; Rotello, V. M. *Faraday Discussions* **2011**, *152*, 33.

(270) De, M.; Rana, S.; Akpinar, H.; Miranda, O. R.; Arvizo, R. R.; Bunz, U. H. F.; Rotello, V. M. *Nat Chem* **2009**, *1*, 461.

(271) You, C. C.; Miranda, O. R.; Gider, B.; Ghosh, P. S.; Kim, I. B.; Erdogan, B.; Krovi, S. A.; Bunz, U. H. F.; Rotello, V. M. *Nature Nanotechnology* **2007**, *2*, 318.

(272) Rana, S.; Singla, A. K.; Bajaj, A.; Elci, S. G.; Miranda, O. R.; Mout, R.; Yan, B.; Jirik, F. R.; Rotello, V. M. *ACS Nano* **2012**, *6*, 8233.

(273) Li, X.; Wen, F.; Creran, B.; Jeong, Y.; Zhang, X.; Rotello, V. M. *Small* **2012**, *8*, 3589.

(274) Xiao, R.; Zhang, B.; Dong, Y.; Gong, J.; Xu, T.; Liu, J.; Xu, X. Z. S. *Cell* **2013**, *152*, 806.

(275) Conti, B.; Hansen, M. *Cell* **2013**, *152*, 671.

(276) Mahmoudi, M.; Shokrgozar, M. A.; Behzadi, S. *Nanoscale* **2013**, *5*, 3240.

(277) Mahmoudi, M.; Lohse, S.; Murphy, C. J.; Suslick, K. S. *NanoLetters* **2013**, *submitted*.

(278) Peng, H.-S.; Huang, S.-H.; Wolfbeis, O. S. *Journal of Nanoparticle Research* **2010**, *12*, 2729.

(279) Surana, S.; Bhat, J. M.; Koushika, S. P.; Krishnan, Y. *Nature Communications* **2011**, *2*, 340.

(280) Peng, H. S.; Stolwijk, J. A.; Sun, L. N.; Wegener, J.; Wolfbeis, O. S. *Angewandte Chemie* **2010**, *122*, 4342.

(281) Emami, S. H.; Orang, F.; Mahmoudi, M.; Rafienia, M. *Polymers for Advanced Technologies* **2008**, *19*, 167.

(282) Nayak, S.; Andrew Lyon, L. *Angewandte Chemie - International Edition* **2005**, *44*, 7686.

(283) Peppas, N. A.; Hilt, J. Z.; Khademhosseini, A.; Langer, R. *Advanced Materials* **2006**, *18*, 1345.

(284) Kocincová, A. S.; Nagl, S.; Arain, S.; Krause, C.; Borisov, S. M.; Arnold, M.; Wolfbeis, O. S. *Biotechnology and bioengineering* **2008**, *100*, 430.

(285) Riedel, S.; Carroll, K. C. *Journal of Infection and Chemotherapy* **2010**, *16*, 301.

(286) Martin, G. S.; Mannino, D. M.; Eaton, S.; Moss, M. *New England Journal of Medicine* **2003**, *348*, 1546.

(287) Lazcka, O.; Del Campo, F. J.; Munoz, F. X. *Biosensors & Bioelectronics* **2007**, *22*, 1205.

(288) Savov, A. V.; Kouzmanov, G. B. *Biotechnology & Biotechnological Equipment* **2009**, *23*, 1462.

(289) Miller, M. B.; Tang, Y. W. *Clinical Microbiology Reviews* **2009**, *22*, 611.

(290) Weile, J.; Knabbe, C. *Analytical and Bioanalytical Chemistry* **2009**, *394*, 731.

(291) Peters, R. P. H.; Savelkoul, P. H. M.; Vandenbroucke-Grauls, C. M. J. E. *Lancet* **2010**, *375*, 1779.

(292) Seng, P.; Drancourt, M.; Gouriet, F.; La Scola, B.; Fournier, P. E.; Rolain, J. M.; Raoult, D. *Clinical Infectious Diseases* **2009**, *49*, 543.

(293) Klouche, M.; Schroder, U. *Clinical Chemistry and Laboratory Medicine* **2008**, *46*, 888.

(294) Raoult, D.; Fournier, P. E.; Drancourt, M. *Nature Reviews Microbiology* **2004**, *2*, 151.

(295) Karasinski, J.; Andreescu, S.; Sadik, O. A.; Lavine, B.; Vora, M. N. *Analytical Chemistry* **2005**, *77*, 7941.

(296) Setkus, A.; Kancleris, Z.; Olekas, A.; Rimdeika, R.; Senuliene, D.; Strazdiene, V. *Sensors and Actuators B-Chemical* **2008**, *130*, 351.

(297) Dutta, R.; Das, A.; Stocks, N. G.; Morgan, D. *Sensors and Actuators B-Chemical* **2006**, *115*, 17.

(298) Carey, J. R.; Suslick, K. S.; Hulkower, K. I.; Imlay, J. A.; Imlay, K. R. C.; Ingison, C. K.; Ponder, J. B.; Sen, A.; Wittrig, A. E. *Journal of the American Chemical Society* **2011**, *133*, 7571.

(299) Phillips, R. L.; Miranda, O. R.; You, C. C.; Rotello, V. M.; Bunz, U. H. F. *Angewandte Chemie-International Edition* **2008**, *47*, 2590.

(300) Manesse, M.; Phillips, A. F.; LaFratta, C. N.; Palacios, M. A.; Hayman, R. B.; Walt, D. R. *Lab on a Chip* **2013**, *13*, 2153.

(301) Montuschi, P.; Mores, N.; Trove, A.; Mondino, C.; Barnes, P. J. *Respiration* **2013**, *85*, 72.

(302) Amann, A.; Corradi, M.; Mazzone, P.; Mutti, A. *Expert Review of Molecular Diagnostics* **2011**, *11*, 207.

(303) Thaler, E. R.; Hanson, C. W. *Expert Review of Medical Devices* **2005**, *2*, 559.

(304) Mazzone, P. J. *Journal of Thoracic Oncology* **2008**, *3*, 774.

(305) Thaler, E. R.; Lee, D. D.; Hanson, C. W. *Journal of Breath Research* **2008**, *2*, 030716.

(306) Åkerman, M. E.; Chan, W. C. W.; Laakkonen, P.; Bhatia, S. N.; Ruoslahti, E. *Proceedings of the National Academy of Sciences of the United States of America* **2002**, *99*, 12617.

(307) Dubertret, B.; Skourides, P.; Norris, D. J.; Noireaux, V.; Brivanlou, A. H.; Libchaber, A. *Science* **2002**, *298*, 1759.

(308) Wu, X.; Liu, H.; Liu, J.; Haley, K. N.; Treadway, J. A.; Larson, J. P.; Ge, N.; Peale, F.; Bruchez, M. P. *Nature Biotechnology* **2003**, *21*, 41.

(309) Salvati, A.; Pitek, A. S.; Monopoli, M. P.; Prapainop, K.; Bombelli, F. B.; Hristov, D. R.; Kelly, P. M.; Åberg, C.; Mahon, E.; Dawson, K. A. *Nature Nanotechnology* **2013**, *8*, 137.

(310) Mirshafiee, V.; Mahmoudi, M.; Lou, K.; Cheng, J.; Kraft, M. L. *Chemical Communications* **2013**.

(311) Laurent, S.; Mahmoudi, M. *International Journal of Molecular Epidemiology and Genetics* **2011**, *2*, 367.

(312) Bajaj, A.; Rana, S.; Miranda, O. R.; Yawe, J. C.; Jerry, D. J.; Bunz, U. H. F.; Rotello, V. M. *Chemical Science* **2010**, *1*, 134.

(313) Bajaj, A.; Miranda, O. R.; Kim, I. B.; Phillips, R. L.; Jerry, D. J.; Bunz, U. H. F.; Rotello, V. M. *Proceedings of the National Academy of Sciences of the United States of America* **2009**, *106*, 10912.

Chapter 2: Liquid-phase sensing

2.1 Background

Exposure to waterborne toxins is a concern in most developed countries, and enforced by a combination of environmental and health protection agencies (US EPA, OSHA, etc). The US military also has significant concern due the likelihood of being required to use foreign water sources when performing operations overseas.

A list of relevant toxins and suggested maximum exposure levels for military personnel was provided in 2005 after years of revision of old, defunct toxin tables.[1] The list ranked toxins based on a combination of hazard severity (i.e., toxicity, flammability, and reactivity) and encounter probability (i.e., physical state and difficulty of transport, worldwide rarity, and infamy with regards to historical events); the product of the two scores was used to rank toxins roughly objectively using the criteria set for each score. The list was also partially subjective, as it removed specific compounds due to their relatively low toxicity toward humans (e.g., benzene, which is very toxic to rabbits but fairly innocuous to humans) or previous omission and lack of study (e.g., pesticides). A subselection of this list was targeted for study with colorimetric sensor arrays, provided in Table 2.1.

Table 2.1 Aqueous toxins chosen for investigation and their suggested maximum exposure levels.

	Species	MEG (5 day)	MEG (1 year)	EPA
Metal Cations	Hg^{2+}		155 nM	10 nM
	Cd^{2+}	500 nM	62 nM	44 nM
	Cu^{2+}	2 μM	2 μM	20 μM
Anions	CN^-	231 mM	11 μM	8 μM
	AsO_2^-	4 μM	800 nM	133 nM
Organophosphate Pesticides	Methamidophos		5 nM	5 nM
	Acephate		300 nM	300 nM
	Methyl Parathion			13 nM
Organics	Nicotine	2.5 μM		

The selected analytes represent a relatively broad selection of physical and physiological properties. Mercury (Hg^{2+}) and cadmium (Cd^{2+}) both have toxicity owing to the physiological replacement of Zinc (Zn^{2+}) in various enzymes crucial to human respiration; their reactivity is otherwise fairly low, however, and detection would require some sort of chelating dye. Copper (Cu^{2+}), on the other hand, simply promotes production of reactive oxygen species in the body, and its corresponding toxicity is significantly higher than other heavy metals; chelating dyes are also likely the best candidates for detection. Cyanide (CN^-) is toxic due to its poisoning of cytochrome *c* oxidase, a protein crucial for human cellular respiration (specifically, processing oxygen); it is also somewhat more reactive than many chemical species and has a high affinity for heavy metals, so exploiting this provides the most likely route for detection. Arsenite (AsO_2^-) toxicity is the primary source of toxicity for all arsenic-containing species, and is derived from inhibition of pyruvate dehydrogenase (Acetyl-CoA synthesis) and

succinic dehydrogenase by interfering with thiol redox reactions; the best candidate for detection in this case will exploit its redox properties. Organophosphate toxicity is derived from poisoning of acetylcholine esterase; organophosphate reactivity is especially low, and detection will likely require a similar environment as in an affected enzyme. Nicotine is toxic due to its poorly reversible interactions with nicotinic receptors in the brain; there are well-known colorimetric tests for nicotine, but adapting these to a colorimetric sensor array in an aqueous environment constitutes a significant challenge.

The most common potential interferents are from divalent alkali earth metals (i.e., "hard water") which could potentially interact with sensors designed for divalent Hg^{2+}, Cd^{2+}, and Cu^{2+} as well as Cl^-, which could potentially interact with sensors designed for CN^-. Interferent concentrations range from water that is considered extremely "hard", such as the water in Turkey, and water that is considered extremely "soft", such as the water in Nigeria. Relevant concentrations of these interferents are listed in Table 2.2.

Table 2.2 Interferent concentrations in both "hard" and "soft" water conditions.

Species	**Turkey[2]**	**Nigeria[3]**
Ca^{2+}	1.4 mM	0.08 mM
Mg^{2+}	0.7 mM	0.1 mM
Cl^-	1.2 mM	-

2.2 Experimental procedures

A flow setup for aqueous sensing was created using a sealed cell originally developed for gas sensing. Arrays were printed on the appropriate substrate (PVDF or PET), then adhered to a silicone backer. This silicone-cartridge composite was then adhered to the underside of the flow cell (which itself

had silicone elastomer seals and needle entry ports attached), thereby sealing the sensor components inside the flow cell; the flow cell was then attached to a rigid cartridge via clasps in order to help prevent leakage during operation. The flow cell was then used upside-down on an Epson V600 flatbed scanner for imaging; pictures of the setup are shown in Figure 2.1. The overall volume of the flow cell was approximately 500 μL, with the volume directly around the chemical sensor array being approximately 100 μL.

This setup was attached to a pair of peristaltic pumps via needles inserted into the elastomer-sealed ports. One pump was attached to the inlet, and one was attached to the outlet; this was necessary to minimize pressure differences (and thus liquid or air leakage) on the inside of the flow cell. This setup was still prone to leakage, but was an improvement over a single-pump system; leakage in this case would ruin an experimental trial, as water on the scanner (caused by too-high pressure in the cell) would change the optical properties of the scan, and bubbles in the cell (caused by too-low pressure in the cell) would obscure imaging and obstruct liquid flow. The experimental setup was not optimized, and had approximately 25% failure rate with regards to leakage.

Arrays were initially equilibrated with deionized water for 1 minute while flowing at 1.5 mL/minute (i.e., total cell replacement approximately every 20 seconds). A "before exposure" scan was collected, and then the cell was switched to an analyte flow by briefly pausing the pumps and moving the inlet line to a vial containing the analyte solution. These were then imaged at the time points further specified (typically 3 and 10 minutes).

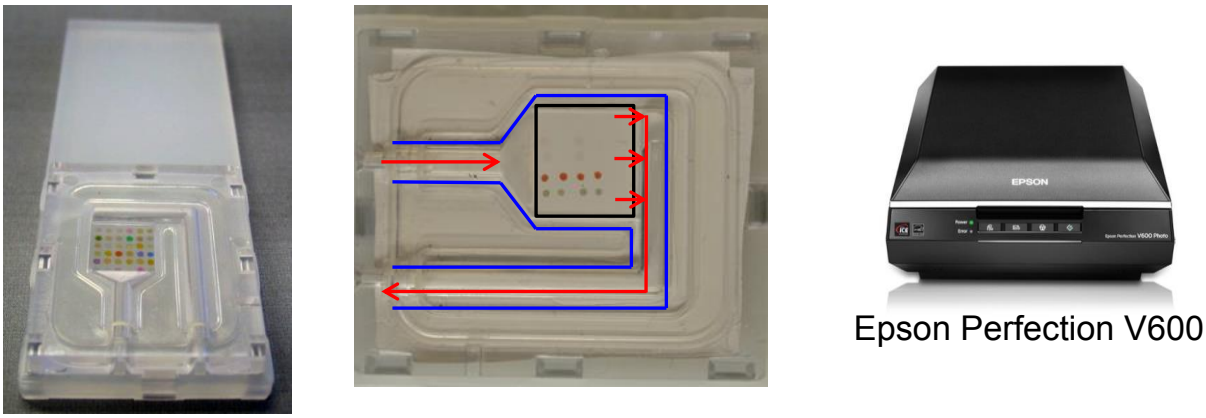

Figure 2.1 Sealed cartridge (left), sealed cartridge with PVDF array affixed and marked flow path (center), flatbed scanner used for imaging (right). In the center image, red arrows indicate the liquid flow path, blue lines indicate the edges of the sealed chamber, and the black box indicates the colorimetric sensor array.

2.3 Array Development

2.3.1 Array Development - General Considerations

The first questions asked when starting an applied project like colorimetric aqueous toxin sensing is "Can we use a system that already exists, and if not, why?". Evaluation of an array developed for studying toxic industrial chemicals (TICs) in the gas phrase[4-6] revealed several key differences between gas-phase sensing and liquid-phase sensing. Sensor spots that are not optimized for use in aqueous conditions will often dissolve into the ambient medium and cause a variety of effects. In order from least-to-most overt, these are blooming, leaching, disassociation, and disintegration.

Blooming is a chromatographic effect where a poorly-soluble dye migrates along the substrate; the spot becomes larger and often decreases in intensity. Blooming is caused when the immobilization matrix has a low but non-negligible partition coefficient between the ambient medium and substrate

(i.e., the matrix is poorly soluble in the ambient medium, but also has a relatively high affinity for the substrate), and the ambient medium has an affinity for the substrate. Blooming most commonly occurs when using a substrate with similar polarity to the ambient medium (e.g., sensing aqueous analytes with a cellulose substrate) and only rarely occurs when using a substrate with opposite polarity (e.g., sensing aqueous analytes with a PVDF substrate). This problem is avoided in aqueous conditions by using either a strongly hydrophobic substrate (e.g., PVDF) or a hydrophilic substrate with an insoluble matrix (e.g., sol-gel).

Leaching is a process where the dye in the sensor spot dissolves into the ambient medium; the spot becomes significantly less intense, and can sometimes leave only the insoluble matrix behind after the dye completely migrates out of the sensor spot. This effect can be observed in Figure 2.2; blue circles indicate spots that underwent significant leaching. Leaching is caused when a sensor dye is very soluble in the ambient medium and the immobilization matrix has an affinity for the ambient medium but is insoluble; in this case, the matrix stays in place, but the dye diffuses out of the spot. Leaching occurs very commonly as most colorimetric dyes are highly soluble in water and most immobilization matrices are at least somewhat hydrophilic. This problem can be decreased or eliminated in aqueous media by using highly hydrophobic matrices, but this also eliminates one of the necessary conditions for sensing species that have a similar polarity to the ambient medium (e.g., chloride ions in water). A more direct solution would be to attach the dye to the matrix through covalent modification or ion pairing, but this was not fully explored. Leaching manifests as a non-zero background response which changes as a function of time. Using negative controls, the magnitude of the leaching effect was quantified and used in an identical method to non-leaching arrays, such as those using gas-phase analytes. It was determined that leaching contributed significantly to the noise in the control samples, which in turn resulted in worse (i.e., higher) detection limits; this is one of the primary weaknesses of the method.

Disassociation is a physical process where a sensor spot actually lifts away from the substrate in its entirety. These spots will typically drift downstream and attach to the end of the flow cell or another sensor spot. Disassociation is caused when the immobilization matrix has low affinity for the substrate but has an affinity for the ambient medium and is insoluble; in this case, the sensor spot will become briefly suspended in the ambient medium induced by turbulent conditions and detach from the substrate. Disassociation is common when using low surface area substrates (e.g., PET sheets) but extremely rare when using high surface area substrates (e.g., PVDF, cellulose, or any porous membrane). This problem is trivially avoided in aqueous media by using porous substrates.

Disintegration is caused when the immobilization matrix dissolves into the ambient medium. This is caused when the immobilization matrix is soluble in the ambient medium. This effect can be observed in Figure 2.2; red circles indicate spots that disintegrated upon exposure to water. The entire spot simply dissolves into the ambient medium; insoluble dyes are either solubilized by the matrix or suspended as particles. Disintegration is common in aqueous media when using hydrophilic matrices (e.g., PEG, glycerol, or surfactants). This problem is avoided in aqueous media by using poorly soluble or insoluble matrices (e.g., sol-gel or BBP).

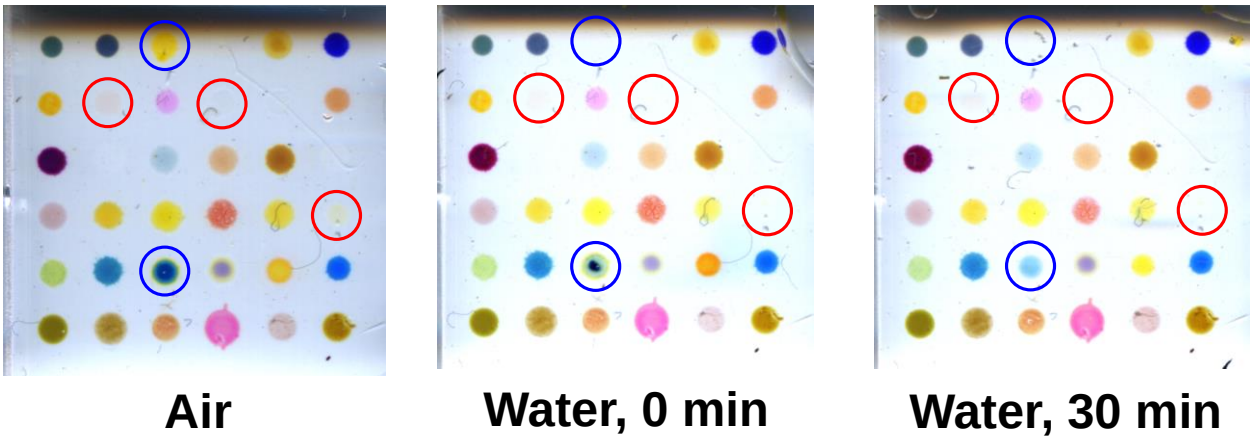

Figure 2.2 TICs array on PET upon exposure to air (left), immediate exposure to deionized water (center), and 30 minutes of exposure to deionized water (right). Several problems are clearly evident, inluding dye leaching and probable spot disassociation.

Sensor arrays also experience non-chemical problems when switching from a gas to a liquid environment. For the array in aqueous media shown in Figure 2.3, it is evident that matrices require time to become fully wetted by the media (red circles); as diffusion in liquids is significantly slower than in gas, it is also expected that mass transfer from the analyte stream to the sensor spots will be slower. Additionally, bubbles (blue circles) have a tendency to become trapped between the substrate and the flow cell as the spots are sufficiently hydrophobic so as to stabilize the hydrophobic air bubble against the surface of the hydrophobic flow cell (the analyte stream in this case was behind the array, away from the camera).

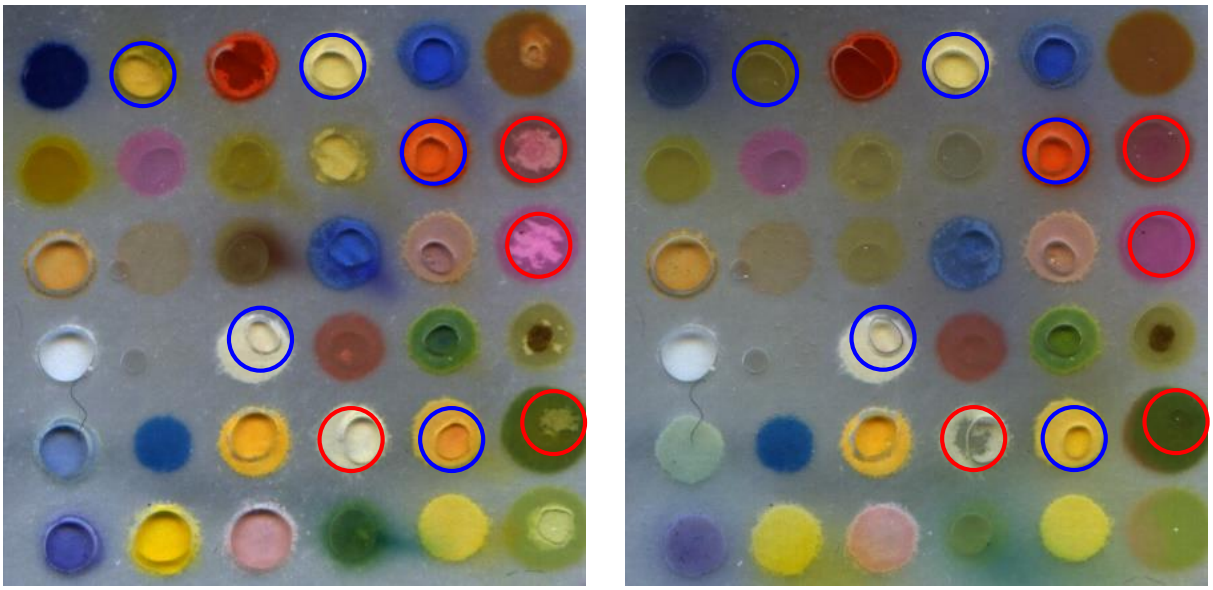

Figure 2.3 TICs array on hydrophilic PVDF (i.e., PVDF/cellulose composite membrane) upon immediate exposure to deionized water (left) and 30 minutes of exposure to deionized water (right). Problems with air bubbles and incomplete spot saturation are clearly evident, as well as significant dye leaching.

Briefly sonicating these arrays in an ultrasonic cleaning bath (e.g., 15 seconds or less) removed bubbles and ensured that spots were saturated with ambient media, but also enhanced problems with leaching and blooming, as shown in Figure 2.4. From this, is is clear that the TICs array is not suitable for use in aqueous environments, though some of the spots (especially spots using strongly hydrophobic octyl-TEOS sol-gel matrices) were largely unaffected by the aqueous environment.

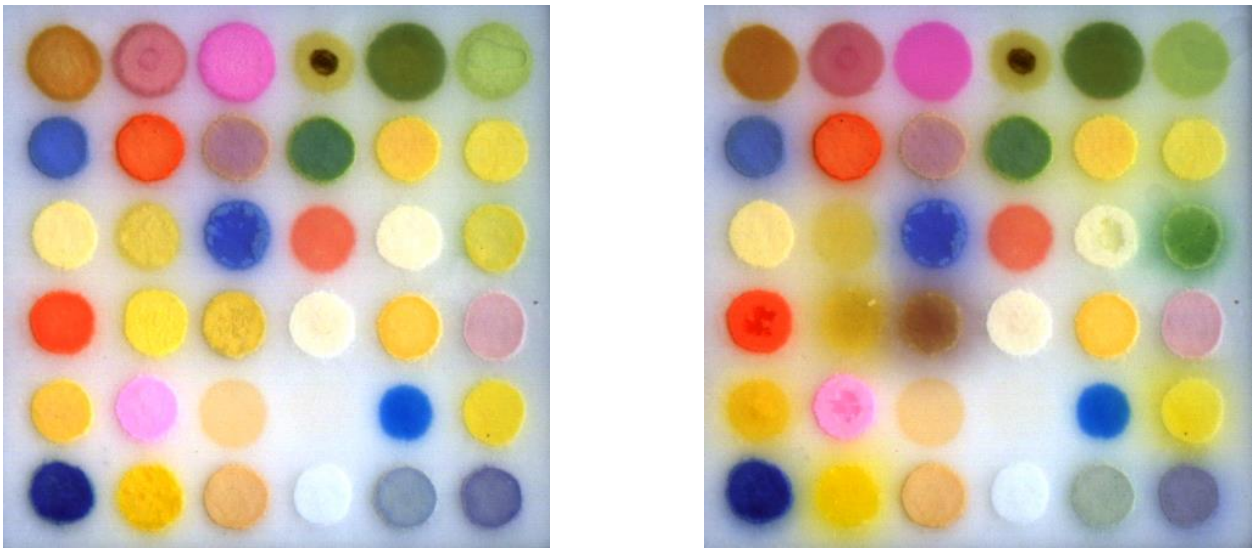

Figure 2.4 Sonicated TICs arrays printed on hydrophilic PVDF. Leaching and blooming effects are clearly evident.

In order to address these problems, one must look back to initial development of gas-phase sensor arrays (e.g., the TICs array) and examine solutions to related problems. Whereas the primary problems in gas-phase sensing are dye or matrix volatility, an analogous problem in aqueous sensing exists as dye or matrix solubility. Sensor array design must then consider solubility as well as volatility. This problem is more often encountered with aqueous-phase sensing due to the relatively high solubility of most compounds compared to their volatility: most compounds are soluble to a certain extent in water due to water's incredible ability to act as a solvent. Further, even insoluble particles can be suspended (especially when in close association with a partially soluble compound such as a surfactant), which causes similar problems. Flow also amplifies this effect due to the constant depletion of the

dissolved dye and matrix near the surface of the sensor spot. Thus, special care must be taken so as to reduce solubility while still maintaining reactivity.

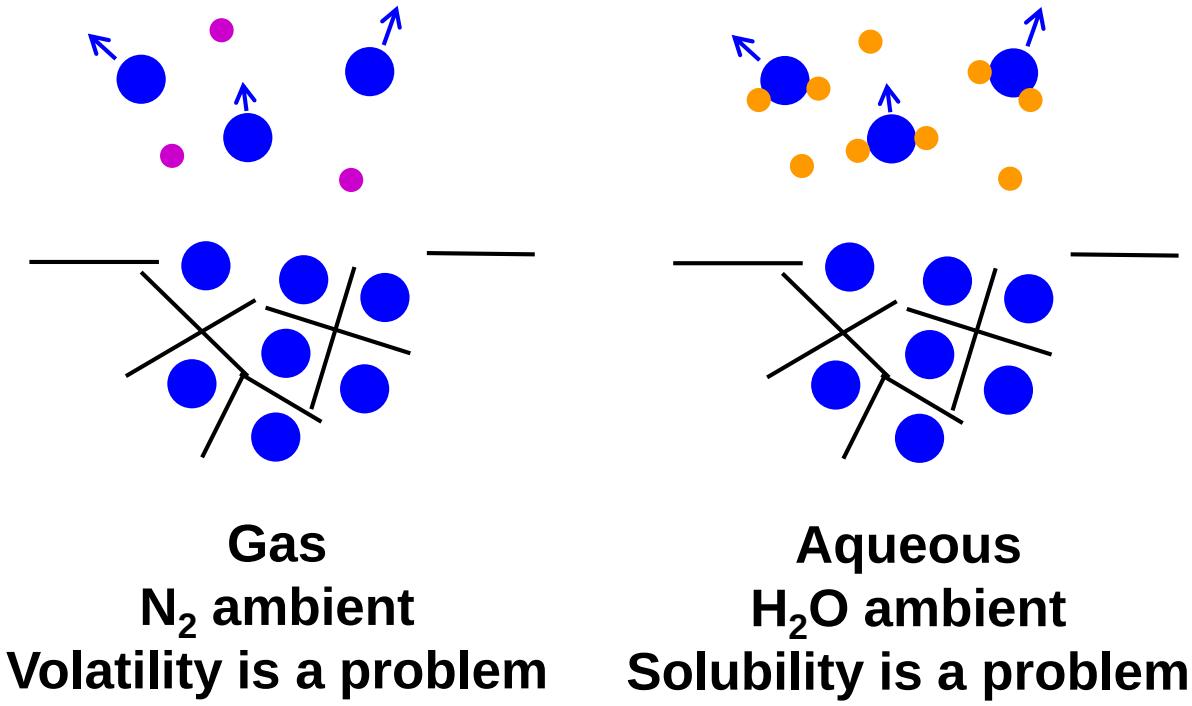

Figure 2.5 Cartoon showing analogy between gas-phase problems with volatility and aqueous-phase problems with solubility.

2.3.2 Array development - CN^- detection using enzymatic sensors

An early attempt at sensing CN^- was made by investigating its ability to inhibit horseradish peroxidase (HRP), a well-studied peroxidase enzyme. In the presence of hydrogen peroxide, HRP will oxidize a wide variety of organic substrates, such as o-dianisidine, a chromogenic dye that turns green upon 1-e^- oxidation and brown-black upon 2-e^- oxidation. This is a turn-off method, in which the sensor

response is maximal when there is no cyanide present. Initial proof-of-concept experiments using hydrogen peroxide directly turned out to be troublesome, however; the spots tended to react unevenly (as too-high concentrations of peroxide irreversibly damaged the enzymes) and hydrogen peroxide also reacted with other spots on the array, which made inclusion of a peroxide-consuming spot in a larger sensor array impossible.

Instead, hydrogen peroxide was generated *in situ* by including glucose oxidase (GOx) in sensor spots alongside HRP. Glucose oxidase produces hydrogen peroxide (and D-glucono-δ-lactone) when exposed to glucose. Despite being able to reach theoretically higher concentrations of hydrogen peroxide, this two-enzyme method was found to be significantly more reproducible and gave higher total response than using hydrogen peroxide directly. It was assumed that having equal concentrations of the two enzymes (in reactive units per mL; reactive units are equivalent to 1 micromol turnovers per minute) would give the best behavior, as the stoichiometry of the reaction is 1:1. Enzyme concentrations were tested in order to determine the minimum amounts necessary to give a suitable control response; these trials are shown in figure 2.6, showing that 150 u/mL of both enzymes was necessary to get the minimum acceptable response. Since this is a turn-off sensor, minimizing the enzyme concentration was desirable so as to not consume the organic chromogen too quickly. A response over time plot is shown as Figure 2.7, giving the total squared euclidean distance (i.e., the sum of every dimensions' response squared) as a function of time. This plot is for all tested concentrations together, but it is also worth noting that the plot looks very similar for any one particular chosen concentration. As shown, the sensor response decreased significantly on exposure to aqueous KCN.

Table 2.3 Vital properties for GOx and HRP screen

Matrix Formulation	
TMOS	7.5% by volume
Methyl TMOS	7.5% by volume
2-MeOEtOH	45% by volume
H_2O	40% by volume
o-dianisidine	2.5 mg/mL
HCl	~ 10 mM
MES buffer	10 mM, pH 5.5
Drying/Curing	5 days at 4 °C
Membrane	Nitrocellulose, 0.22 μm
Procedure	MES buffer (as above) for 1 minute 100 mM Glucose in MES buffer after 1 minute

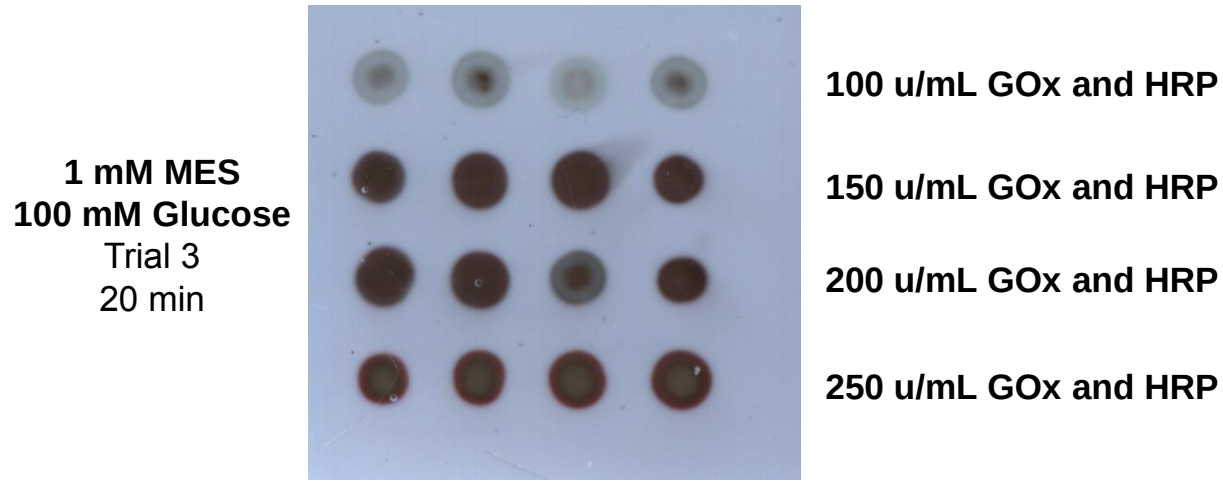

Figure 2.6 Screen of different GOx and HRP concentrations in order to determine optimal enzyme concentration.

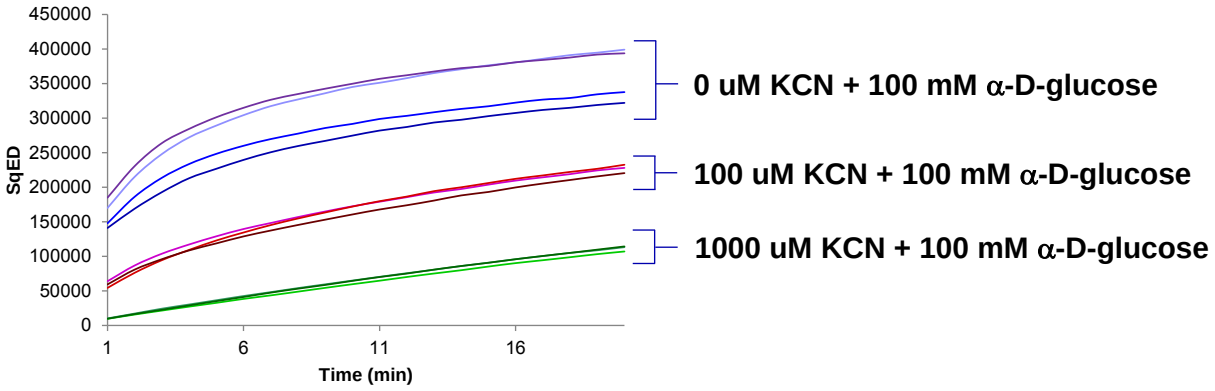

Figure 2.7 Sensor response for entire array described above.

This sensor response data was processed using a second order kinetic fit in order to give a linearized temporal response by assuming that the squared euclidean distance was proportional to the concentration of the oxidized dye. This approximation is purely empirical; proper determination of analyte concentration using this system would require normalization and calibration. By plotting against KCN concentration, it was observed that the intercept (which is roughly inversely proportional to the catalytic rate coefficient k_{cat}) had a linear relationship with [KCN], as shown in Figure 2.9. Solving for [KCN] where the intercept was equal to 3x the standard deviation of the control data (i.e., [KCN] = 0), an estimated limit of detection was calculated to be approximately 18 μM.

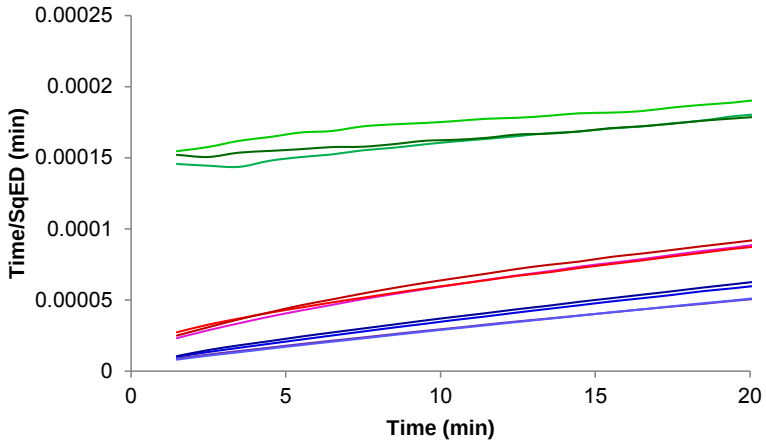

$$SqED = \frac{At}{B+t}$$

$$t/SqED = t/A + B/A$$

Figure 2.8 Processed sensor response. The data was fit using a second-order kinetic equation to give a linear response over time.

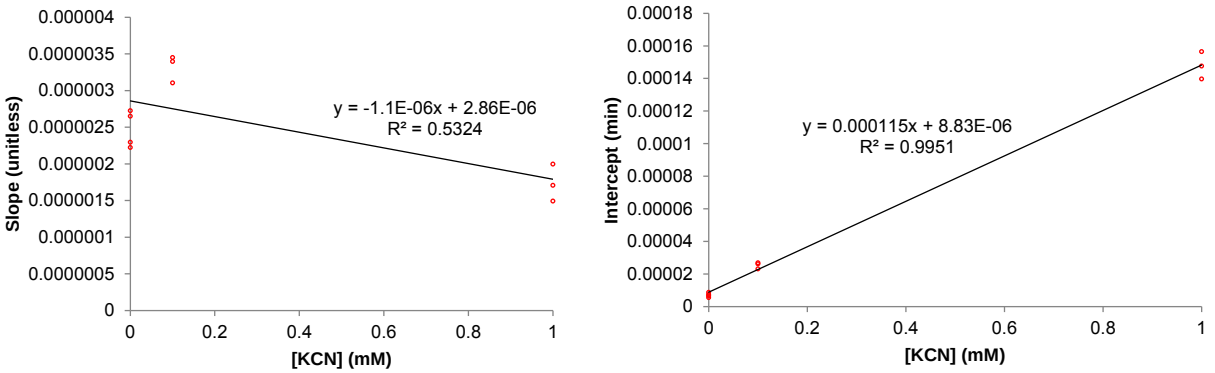

Figure 2.9 Approximation of detection limit using a linear fit of the kinetic parameters determined using a 2nd order kinetic approximation.

During these experiments, significant amounts of variability were observed. It was eventually found that the curing/drying time of the array had a strong effect on its behavior, so a study was performed comparing different drying times with a selection of immobilization matrices, as shown in Figures 2.10 and 2.11. Of the matrices listed below, the 7.5% isv TMOS/MeTMOS mixture is identical to

that described above. H_2O only indicates that there were no matrix components; the buffered components were printed directly on the membrane, with dramatic reduction in print quality. PvA-SbQ is a water soluble photocurable polymer that was used in the hopes of eliminating any problems with cross-reactivity between the sol-gel matrix and enzymes during the sol-gel curing process; it was cured using a short-term exposure to UV light generated with an Ar lamp. The 15% isv TMOS mixture listed below is similar to the 7.5% TMOS/MeTMOS matrix except that MeTMOS was replaced with TMOS, increasing its hydrophilicity.

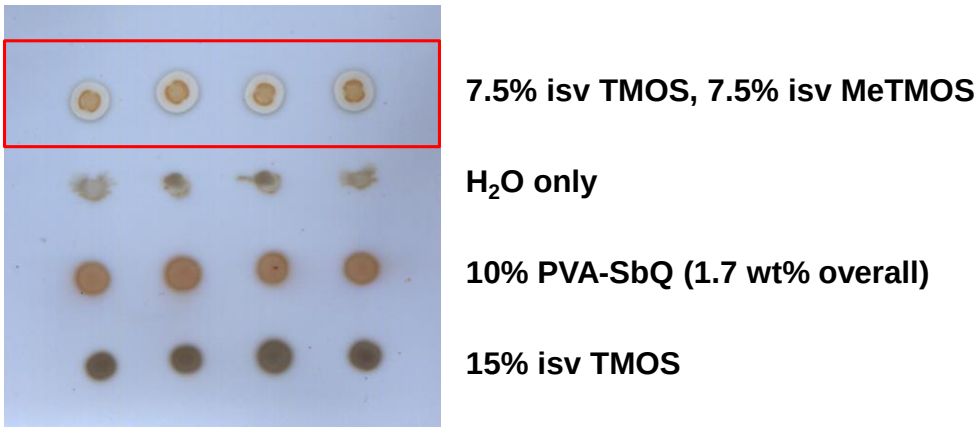

Figure 2.10 Drying study of HRP and GOx-containing spots with 4 different immobilization matrices.

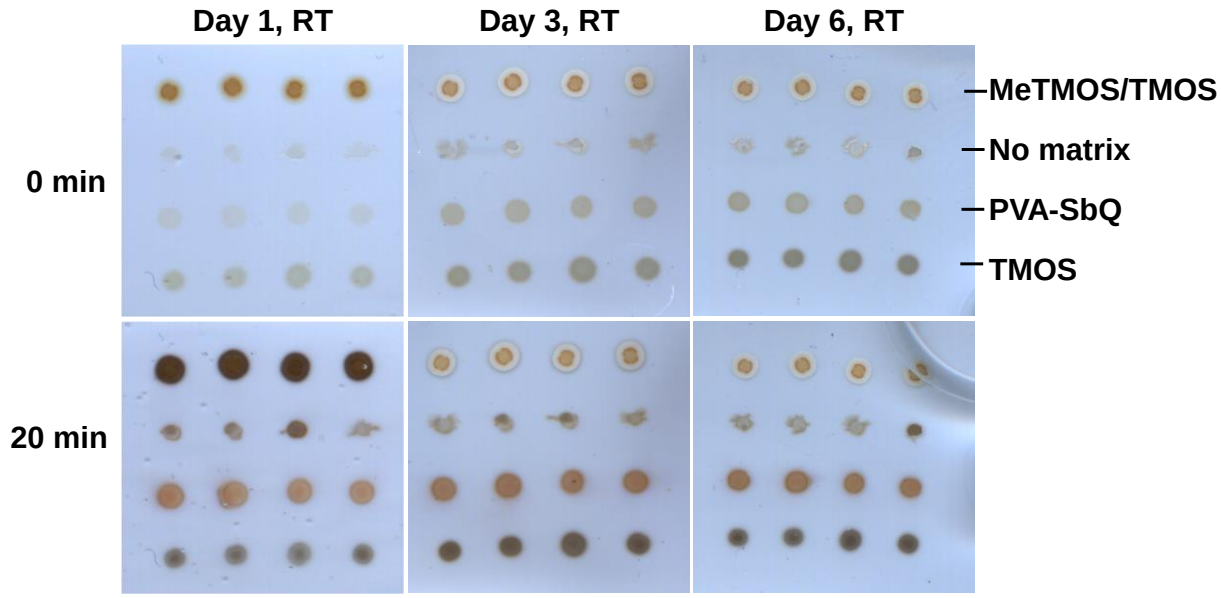

Figure 2.11 Effects of array curing/drying at room temperature and in a refrigerator at 4 °C. As observed, the dye became increasingly oxidized in un-exposed arrays as drying time and temperature increased, and subsequent array response decreased on exposure to glucose.

Unfortunately this experiment generated two fatal results for this project: (1) curing caused the organic dye to oxidize over time, even in samples without a matrix, and (2) curing dramatically decreased the responsiveness of the spots toward glucose after only 3 days. Since this is a turn-off sensor designed for low analyte concentrations, reproducibility and high response are paramount in order to reliably detect minor decrease in signal upon exposure to inhibitors such as CN^-. Because the shelf life of this array was only approximately 3 days (essentially aspect of the array suffered significant degradation upon even this short-term curing/drying), the enzymatic approach to CN^- detection was shelved indefinitely.

To replace this sensor, it was decided to investigate previously-developed chemical-based sensors instead and improve their performance in aqueous conditions: compared to this HRP/GOx

system, chemical sensors are cheaper, easier to prepare, significantly more tolerant to curing/drying conditions, would not likely require an additive in the media (e.g., glucose), and (most importantly) are turn-on sensors.

2.3.3 Array development - initial probe choices

Probes for CN^- took advantage of the high stability of certain metal-cyanide bonds, specifically Hg^{2+}-CN and Ag^+-CN. A probe for CN^- incorporating Hg^{2+} is essentially the opposite of a probe meant to detect Hg^{2+}; interaction with CN^- effectively pulls Hg^{2+} out of a sensor spot meant to detect it, forming unreactive $HgCN_2$ or an intermediate salt. One such dye initially chosen was the chelating dye diphenylcarbazone (DPC), shown in Figure 2.12, which forms a yellow spot that turns purple on exposure to Hg^{2+}; this color change is the opposite when DPC-Hg is exposed to CN^-.

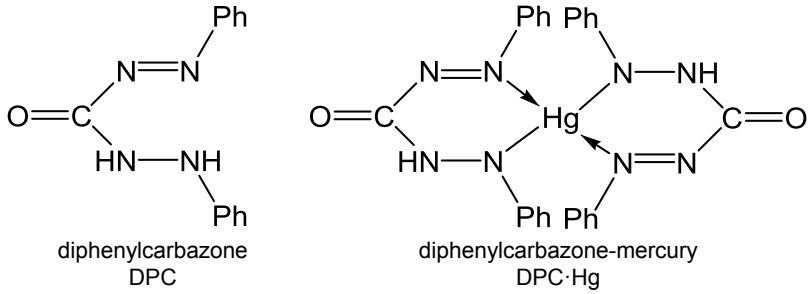

Figure 2.12 Probes chosen for Hg^{2+} (i.e., DPC) and CN^- (i.e., DPC-Hg).

DPC is poorly soluble in water, and DPC-Hg is essentially insoluble; the interaction between DPC and Hg^{2+} is reversible, however, and it could potentially cause problems to include Hg^{2+} in a sensor array that is also designed to *detect* Hg^{2+}. Thus, sensors based on Hg^{2+} were largely abandoned in favor of probes based on Ag^+, which also has a strong interaction with CN^- . A strongly hydrophobic spot

containing $AgNO_3$ and a pH indicator (either Bromophenol Blue [BPB] or Bromocresol Green [BCG], as shown in Figure 2.13) was on the TICs array, and these spots showed a response to KCN and immunity to a NaCl interferent, as shown in Figure 2.14. Importantly, these spots were also resistant to blooming and dissolution, unlike many spots on the TICs array. It is generally speculated that these spots work by converting HCN to HNO_3 which then acidifies the pH indicator; essentially, it allows HCN to act as a strong acid, which is contrary to its weak acidity in solution.

Development of arrays including DPC-Hg is especially troublesome, as the dye's insolubility makes it impossible to prepare normally; instead, aqueous $HgCl_2$ is printed on top of a DPC spot. This makes the spot especially problematic with regards to reproducibility and potential Hg^{2+} contamination. As such, once Ag^+-containing spots proved to be effective, DPC-Hg was abandoned as a sensor choice; this spot will not be discussed further, as reproducibility was poor and quite frustrating.

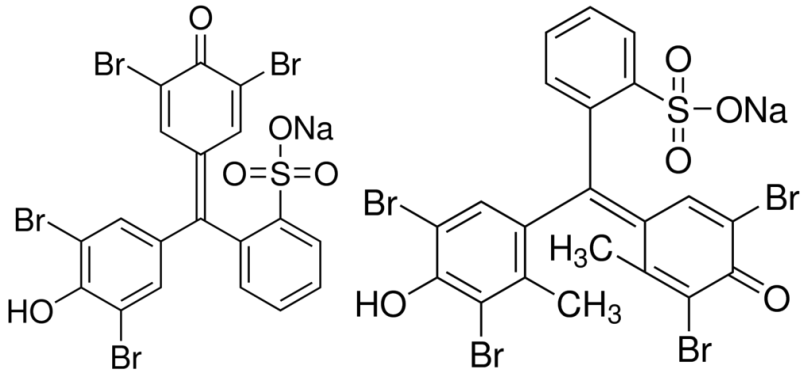

Figure 2.13 Bromophenol Blue sodium salt (BPB, left) and Bromocresol Green sodium salt (BCG, right). These dyes were chosen as a pH indicators for probing the interaction between $AgNO_3$ and CN^-.

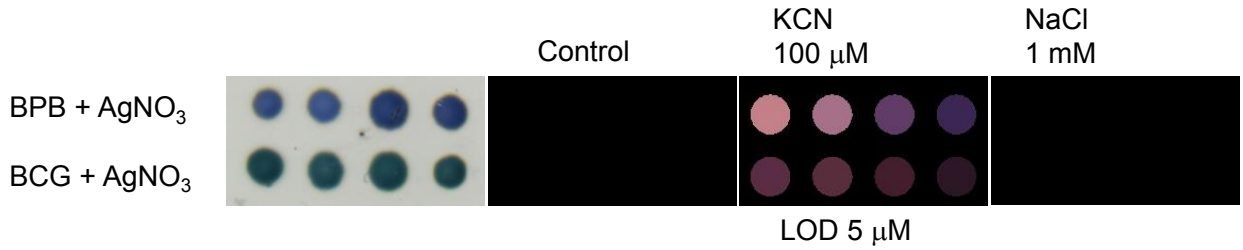

Figure 2.14 Response of $AgNO_3$-containing sensors toward aqueous KCN. The estimated detection limit was 5 μM. Signals were scaled from (1,16) to (0,255).

Other chelating dyes were chosen for detection of other metal ions, including Cd^{2+} and Cu^{2+}. Their structures are shown in Figure 2.15. These dyes are traditionally-used dyes in titration experiments for quantitation of these and other metal ions. Note also that dithizone was investigated and seemed to be a very sensitive probe, but it was found to be unstable upon exposure to air and was abandoned.

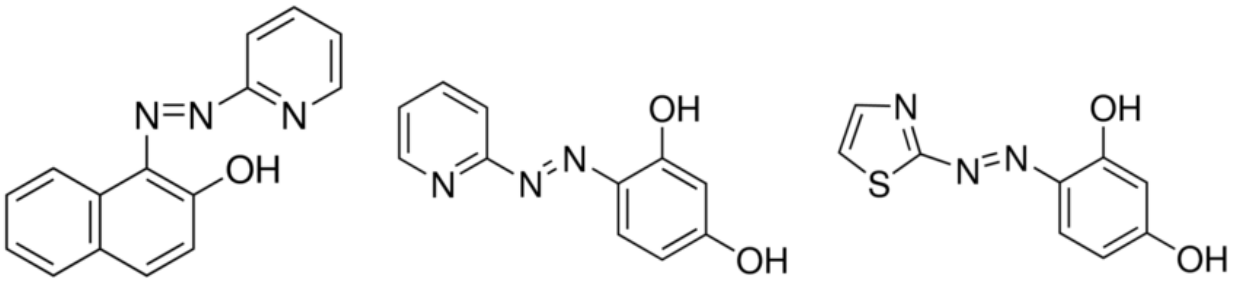

1-(2-pyridylazo)-2-naphthol
PAN

4-(2-pyridylazo)-resorcinol
PAR

4-(2-thiazolylazo)-resorcinol
TAR

Figure 2.15 Structures of chelating dyes investigated for detection of aqueous Cd^{2+} and Cu^{2+}.

2.3.4 Array development - substrate, matrix, and dye choices

Based on previous experiments with the TICs array (section 2.3.1), hydrophobic PVDF membrane was chosen as an ideal substrate for aqueous sensing: non-porous PET sheets did not provide adequate adhesion for the sensor spots, and hydrophilic membranes had significant problems with bleeding. Of the substrates tested, only PVDF sufficiently maintained integrity of the sensor spots; PVDF also dramatically reduced problems with bubbles preferentially adhering to spot surfaces.

After testing several matrix formulations, a set of general truisms was established for the best-working sensors:

1. The matrix must have a similar polarity to the probed species
    - KCN is highly polar, but freely converts to the volatile HCN, which is nonpolar.
    - All metal salts are highly polar.
2. The matrix must be accessible to the ambient medium
    - PVDF is hydrophobic and has small pores which trap air (i.e., inaccessible to water)
    - The ambient medium for soluble species is water, which is hydrophilic
    - The ambient medium for volatile species is air, which is hydrophobic
3. Any matrix which is accessible to water will leach soluble dyes
4. All dyes are partially soluble in water

The last two points are especally difficult for aqueous sensor development, as it essentially guarantees that any effective dye will also eventually dissolve into the aqueous medium. Covalent attachment of the dye to the matrix or substrate would almost certainly solve this problem, but this was not pursued.

2.3.5 Array design finalization and results

Results for the ultimate array design are described below. Both arrays are described in order to discuss the effectiveness of DPC-Hg (as a CN^- sensor) as well as PAN and TAN (primarily included to detect Cd^{2+}). The design of array JA-2.3.5 is shown in Figure 2.16. A table with relevant spot formulations is shown in Table 2.4.

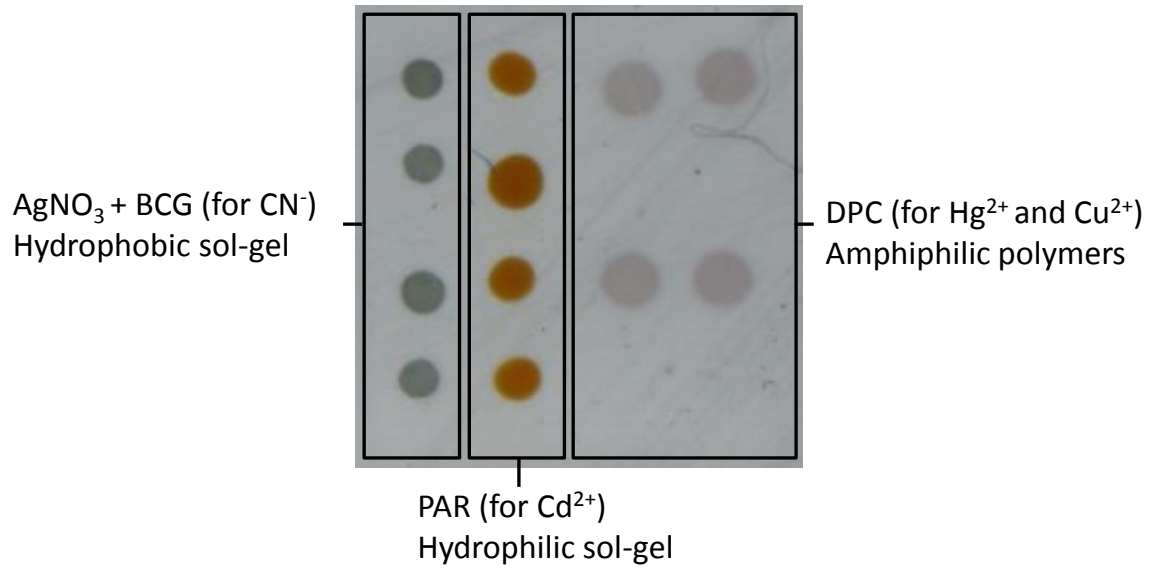

Figure 2.16 Picture of array JA-2.3.5.1 before exposure. The array uses 4 different colorimetric probes and immobilization agents optimized for use in aqueous conditions.

Table 2.4 Spot and formulation list for Array JA-2.3.5.

Spot	**Dye Amount**	**Formulation**
DPC	8 mg/mL	PEG 400 (50 mg) + BBP (200 μL) + MeOEtOH (750 μL)
PAR	4 mg/mL	JA197D
BCG + $AgNO_3$	2 mg/mL BCG 5 mg/mL $AgNO_3$	SLII-042A

Difference map at relevant analyte concentrations are shown in figure 2.17. Though there is significant overlap between the Hg^{2+} and Cu^{2+} signals, the analytes are able to be easily differentiated by the change in the red channel, as evidenced by the difference maps showing yellow spots for Hg^{2+} and green spots for Cu^{2+} (i.e., Hg-DPC and Cu-DPC are different shades of purple). The sensor array showed no response to interferents, as shown in Figure 2.18.

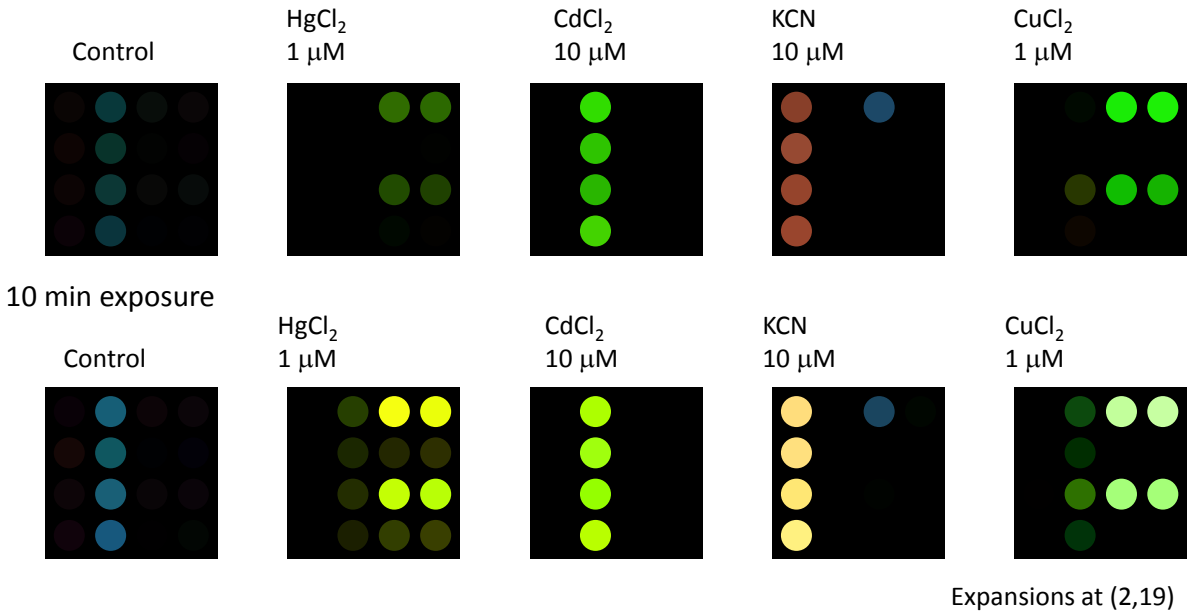

Figure 2.17 Average difference maps of relevant analyte concentrations. For visualization, responses were scaled so that the range of (2-19) was projected onto 8-bit color space (i.e., 0-255). Note that the control response was subtracted from each of the non-control analytes.

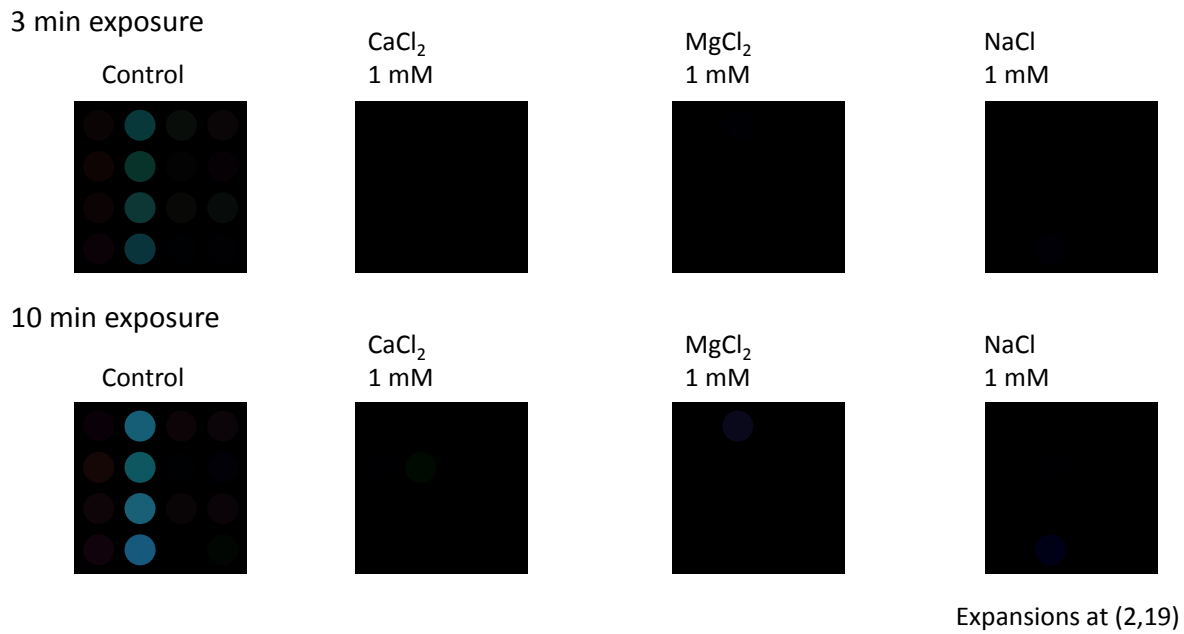

Figure 2.18 Average difference maps of a control sample and relevant interferants. For visualization, responses were scaled so that the range of (2-19) was projected onto 8-bit color space (i.e., 0-255). Note that the control response was subtracted from each of the non-control analytes.

Results measuring the sensitivity of this array are shown in Table 2.5. The sensor array compares well to published values for similar colorimetric or portable methods, but in general has a few major flaws. The sensitivity of the array toward Hg^{2+} is very nearly on-target, and is easily capable of detecting Hg^{2+} in water just above drinking water limits (i.e., very long-term exposure). Limits of detection for CN^- and Cd^{2+} are lower than published values, but is still suitable only for detection of acutely toxic water (detection limits are still higher than the EPA limits). In the opposite direction, the array's limit of detection for Cu^{2+} is several orders of magnitude lower than desired; the array is too sensitive, which could cause problems as Cu^{2+} could be considered a potential interferent for Hg^{2+} due to overlapping sensor response.

Table 2.5 Results of sensor array sensitivity (i.e., limit of detection, LOD) as compared to relevant values: maximum exposure guidelines for acute (i.e., 5 day) exposure, chronic (i.e., 1 year) exposure, EPA drinking water guidelines, and published limits for similar sensors.s

	Species	MEG (5 day)	MEG (1 year)	EPA	LOD	Lit
	Hg^{2+}		155 nM	10 nM	33 nM	100 nM[7]
Metals	Cd^{2+}	500 nM	62 nM	44 nM	250 nM	1 mM[8]
	Cu^{2+}	2 μM	2 μM	20 μM	17 nM	160 nM[9]
Anions	CN^-	231 μM	11 μM	8 μM	175 nM	1.6 mM[10]

2.4 References

(1) Hauschild, V. D.; Bratt, G. M. *Journal of Toxicology and Environmental Health, Part A* **2005**, *68*, 857.

(2) Soylak, M.; Armagan Aydin, F.; Saracoglu, S.; Elci, L.; Dogan, M. *Polish Journal of Environmental Studies* **2011**, *11*, 151.

(3) Kolo, B.; Dibal, J. M.; Ndakawa, I. I. *European Journal of Applied Sciences* **2009**, *1*, 26.

(4) Lim, S. H.; Feng, L.; Kemling, J. W.; Musto, C. J.; Suslick, K. S. *Nature Chemistry* **2009**, *1*, 562.

(5) Feng, L.; Musto, C. J.; Kemling, J. W.; Lim, S. H.; Suslick, K. S. *Chemical Communications* **2010**, *46*, 2037.

(6) Feng, L.; Musto, C. J.; Kemling, J. W.; Lim, S. H.; Zhong, W.; Suslick, K. S. *Analytical Chemistry* **2010**, *82*, 9433.

(7) Wang, B.; Zhu, Q.; Liao, D.; Yu, C. *Journal of Materials Chemistry* **2011**, *21*, 4821.

(8) Li, G.; Zhang, L.; Li, Z.; Zhang, W. *Journal of Hazardous Materials* **2010**, *177*, 983.

(9) Yang, P.; Zhao, Y.; Lu, Y.; Xu, Q.-Z.; Xu, X.-W.; Dong, L.; Yu, S.-H. *ACS Nano* **2011**, *5*, 2147.

(10) Mashraqui, S. H.; Betkar, R.; Chandiramani, M.; Estarellas, C.; Frontera, A. *New Journal of Chemistry* **2011**, *35*, 57.

Chapter 3: Handheld reader for colorimetric sensor arrays

This chapter taken in large part from the following references:

Askim, J.R.; Suslick, K.S. "A Handheld Reader for Colorimetric Sensor Arrays" *Accepted, Analytical Chemistry.* **2015**

Suslick, K.S. "User's Manual. PROJECT JAWBREAKER: A Handheld Optoelectronic System." *Progress report to TSWG.* **2014**

3.1 Introduction

Development of rapid, sensitive, portable and inexpensive systems for identification of gaseous analytes has become an urgent societal need and has important applications ranging from the chemical workplace to security screening to even health monitoring of the general population. The use of colorimetric sensor arrays has proven to be a fast, sensitive, and versatile method of liquid, vapor, and gas analysis where the specificity derives from the pattern of response from cross-reactive sensor arrays rather than individual sensors for specific analytes.[1-5] Colorimetric sensor arrays have been successfully used to differentiate among diverse families of analytes, ranging from toxic industrial chemicals,[6-9] to various foods and beverages,[10-17] to pathogenic bacteria and fungi.[18-23] Unfortunately, these methods have generally been limited to use in laboratory settings due to the fragility and bulk of the instrumentation.

The use of colorimetric sensor arrays would benefit greatly from a portable, low-noise optical reader with onboard processing capability. To that end, we have developed a handheld reader to analyze colorimetric sensor arrays that is a self-contained, truly portable analytical device. The handheld reader uses a color contact image sensor (CIS) that contains a linear CMOS sensor array for optical transduction;[24,25] due to their short focal distances, CIS devices are commonly used as business card scanners and in some flatbed scanners. The handheld reader also incorporates a disposable sealed cartridge, a diaphragm micropump for analyte flow control, and onboard electronics that provide rapid,

low-noise measurement of red, green, and blue reflectivity of a linearly-arranged colorimetric sensor array during exposure to gaseous analytes. The handheld reader is also capable of performing statistical evaluation (e.g., classification) in real-time.

Because machine learning and pattern recognition terminology is less commonly used by chemists, we have included Table 3.1 below with definitions of some of the common terms used in our discussions in this and following sections.

Table 3.1. Definitions of pattern analysis terminology

Sample	A single data point consisting of one measurement of each sensor element. For us, this would be the color change vector measured from a single cartridge exposure at a given time.
Class, Cluster	A collection of multiple samples all assigned the same identity. For example, 35 scans of Hydrochloric Acid gas would all be assigned the class "HCl".
Group	A collection of one or more classes; a supercluster.
Supervised learning	Supervised (“biased”) learning infers a function from labeled training data. The training data consists of a set of pre-known examples, i.e., a name/class/output value linked with an input object (typically a data vector). A supervised learning algorithm analyzes the training data and produces function that can be used for mapping new examples into the pre-existing known classes.
Unsupervised learning	Unsupervised (“unbiased”) learning is the task of finding structure in unlabeled data. The observations given to the learner are not predetermined (“unlabeled”) and there is no bias (error or reward) in the number of possible classes generated. Cluster analysis is typically unsupervised.
Classifier	A function that can separate two or more already known groups.
HCA, Hierarchical Cluster Analysis	A function that groups a set of objects so that objects in the same group (a cluster or class) are more similar to each other than to those in other clusters. Hierarchical cluster analysis (HCA) is an unsupervised (“unbiased”) connectivity model for clustering that is based on distance connectivity in some high dimensional space and presents a resultant dendrogram of connectivity.
LDA, Linear Discriminant Analysis; PCA, Principal Component Analysis	LDA (also Fisher’s LDA) uses a training set of data to find a linear combination of dimensions to separate two or more classes of objects so as to maximize the separation between the classes. LDA is related to principal component analysis (PCA) in that they both look for linear combinations of variables that best explain the data. LDA is a supervised method that explicitly attempts to model the difference between the classes of data. PCA on the other hand is unsupervised and does not take into account any difference in class.

Table 3.1 (continued)

SVM, Support Vector Machine	SVMs (also called support vector networks) are a supervised ("biased") learning model used for classification. Given a set of training examples in pre-assigned groups, SVM builds a model that assigns new examples to one category or another (one-against-one or one-against-the rest) using a non-probabilistic binary classifier algorithm. SVMs can efficiently perform a non-linear classification using what is called the kernel trick, implicitly mapping their inputs into high-dimensional feature spaces.
Kernel methods	Kernel methods are a class of algorithms for pattern analysis and are closely associated with support vector machine classification. Kernel functions permit the operation of high dimensional data without ever computing the coordinates of the data in that space; rather, inner products (scalar value from the dot product of two vectors) of all pairs of vector data are used (i.e., the "kernel trick"). Processing data into a form that can easily be separated in a linear fashion (a vector between two groups). A "linear kernel" is not further processed; it is assumed that the incoming data is already able to be separated in a linear fashion. A common example of a non-linear kernel is the radial kernel, which is often used to measure distance from a fixed point. Kernels can be tailored to suit the overall shape of data that is to be classified, if necessary.
One-against-one	A method where one classifier is created for each pair of classes. This means that there are N*(N-1)/2 total pairs, where N is the number of classes. This sort of method can easily use a linear kernel as long as each class is distributed evenly around a central point (a center for each class).
One-against-the-rest	A method where one classifier is created for each class. This means that there are N total pairs, where N is the number of classes. This sort of method cannot easily use a linear kernel, as class will often be "surrounded" by other classes, except in very special cases. A radial kernel is often used for this method.

3.2 Methods and materials

3.2.1 Handheld reader construction

M116 CIS modules were purchased from CMOS Sensor Inc. (Mountain View, CA, USA).[25] Diaphragm micropumps were purchased from Schwarzer Precision (Essen, NRW, Germany).[26] Onboard processing and device operation were controlled using custom-designed electronics (D3 Engineering, Rochester, NY, USA) centered around a TMS320DM6437 Digital Signal Processor as the CPU (Texas Instruments, Dallas, TX, USA). Other components (chassis, flow manifolds, etc.) were custom-designed (iSense Systems/Metabolomx, Mountain View, CA, USA and Intelligent Product Solutions, Hauppage, NY, USA). The component costs of the handheld reader are modest: M116 CIS module ($80, CMOS Sensor

Inc), NHD-042H1Z LCD screen ($18, Newhaven Display), 2 position membrane switch ($10, SSI Electronics), and SP-100-EC-LC diaphragm micropump ($80, Schwarzer Precision). Prototype components consisted of the digital processor and chassis; we estimate that the digital processor could be replaced with commercially-available components for < $100, and a plastic chassis could be mass-produced for < $10.

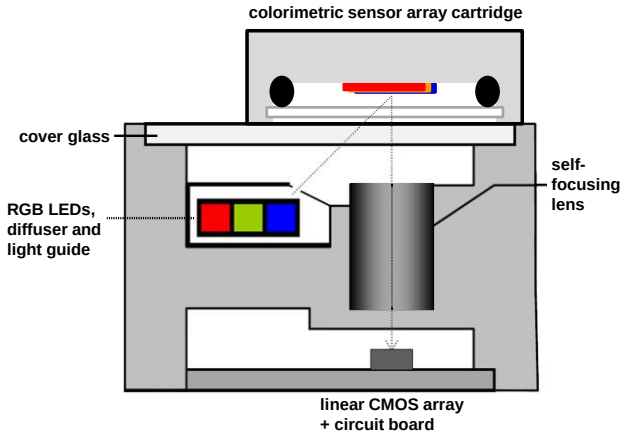

Figure 3.1 Schematic of the important optical components present in the handheld reader. The reader uses a CMOS Sensor Inc M116-A8C1 contact image sensor (i.e., 2.4 inch wide business card scanner) to read a custom-designed colorimetric sensor array cartridge. Components of the CIS are adapted from http://www.csensor.com/M116_CIS.htm (accessed 28 January, 2014).

3.2.2 Colorimetric sensor array cartridge

A custom linear cartridge was designed to fit the handheld reader and provide a narrow flow path for analyte exposure of a colorimetric sensor array. Polypropylene membranes (0.2 µm) were used as printing substrates for the array and were purchased from Sterlitech Corporation (Kent, WA, USA). The polypropylene was mounted to an injection-molded low-volatility white polycarbonate cartridge (Dynamic Plastics, Chesterfield Twp, MI, USA) using a solvent-weld (dichloromethane).

The colorimetric sensor array then robotically printed on the substrate using procedures described previously.[8] Arrays used for evaluation of the handheld reader used 28 to 48 colored spots printed at 1.0 or 1.2 mm center-to-center distances; 1.2 mm spacing provided more consistent physical separation of the sensor elements. All reagents were analytical-reagent grade, purchased from Sigma-Aldrich and used without further purification.

After colorimetric sensor arrays were printed, they were thoroughly dried under nitrogen. A glass microscope slide was then snapped into the cartridge, providing a gas-tight seal against a Viton O-ring, as shown in Figure 3.2. This provides a nearly ideal flow path for the analyte stream with a flow volume of ~85 µL. The arrangement of the CIS and the linear colorimetric sensor array is shown in Figure 3.1.

Figure 3.2 Photographs of the cartridge and a colorimetric sensor array showing side and array views. The sensor array shown here has 40 sensor elements at 1.2 mm center-to-center spacing and represents typical printing quality.

3.2.3 CIS calibration

As designed, the CIS outputs an analog signal between ~0-3.4V that is fed into a 12-bit analog-digital converter (ADC) with a 5V reference voltage. Initially, illumination parameters (i.e., LED voltage and pulse widths) were set to their maximum allowed values in order to determine the optimal pixel

clock rate; a pixel clock of 500 kHz (1478 total pixels, which gives a 3.0 ms capture window for each of the red, green, and blue LEDs) was found to be ideal for maximizing the signal from a white substrate without significant over-exposure. To minimize response variability between pixels and to maximize sensitivity, illumination levels were further optimized by varying the voltage for each of the red, green, and blue LEDs; these optimized illumination levels are a one-time calibration of the CIS and were used for all further experiments with all five instruments constructed. Individual pixels vary slightly in responsivity; pixels (and by extension, separate scanner units) were calibrated by normalizing from data obtained using a cartridge containing a blank polypropylene substrate for a 100% reflectance standard and turning off all illumination for a 0% reflectance standard. These calibration standards are an additional one-time calibration for each individual handheld reader.

3.2.4 Array testing

All tests were performed using a built-in diaphragm micropump (approximately 580 cm^3/min flow rate). For laboratory-controlled gas sampling, air was drawn through a bubbler containing deionized water to generate 100% relative humidity (RH) flow for the control gas stream. The analyte gas stream was generated by drawing air through a bubbler containing dilute aqueous ammonia to generate an NH_3 gas stream, whose concentration was confirmed by in-line analysis using an FTIR multi-gas analyzer, MKS Instruments model 2030; typical concentration was 50 ppm. The humidity control is not a requirement for use of these colorimetric sensor arrays, whose insensitivity to changes in humidity have already been well established.[6,8,9,27-32] Control and analyte gas streams were pulled through cartridges with the onboard micropump and scanned at 1.0 Hz. The arrays were initially exposed to the control gas line for 10 min before being switched to the analyte line for 10 min. The colorimetric sensor array response is sufficient for analysis even after only a few seconds of exposure, but the exposure times were intentionally made extremely long (i.e., 10 min) in order to guarantee total equilibration

with the analyte gas stream and thus eliminate any potential for change in the sensor array response during the gathering of noise and statistical data using multiple scans over a short period of time.

3.2.5 Data processing

All data processing on the handheld device was done using custom-designed software. Spot location followed a two-step process: first, the array is initially assumed to have perfectly-defined spacing and then those initial position are further refined. Spot locations were initially estimated algorithmically by sweeping over the array in order to locate an appropriate number of adjacent spot centers with a 24 pixel (approximately equal to 1.0 mm) center-to-center distance that gave the highest total deviation from the background color (i.e., this assumes ideal printing of the array) as defined by total sum of the squared Euclidean distance of pixel responses. Due to minor imperfections in printing positions inherent in pin-printing, however, spot distances are not perfectly uniformly spaced; the software thus further refined positions to account for individual variation in the center location of each printed spot by finding the pixel which gave the minimum in spatial variance over a 9-pixel window (i.e., the center of the spot is where the color is most uniform, and changes the least over a short distance). To evaluate the effectiveness of this protocol, spot widths were varied manually in order to examine the effect of feature size on resultant S/N; nine pixel minimization proved optimal.

Data processing for 2-dimensional images (DSLR, iPhone, and flatbed scanner) was performed using proprietary spot-finding software designed by iSense, Inc. (Mountain View, CA); using this software, spot centers and sizes are initially set manually, and the software optimizes these spot locations in a batch process after data collection across all images in an individual experimental trial.

3.2.6 Spot finding algorithm

The custom spot finding alogorithm for our one-dimensional data from the CIS functions as follows. A background reflectance threshold was set to 85% of the maximum reflectance observed from a blank cartridge. Pixels with red, green, or blue reflectance less than that threshold were assigned to dye spots (i.e., colored pixels); the leading and trailing edges of each sensor spot were used to identify the spot. The spatial variance in RGB values for each dye spot pixel (i.e., comparing data from adjacent pixels) was calculated using a radius of 3 pixels (i.e., 7 total pixels) and gave a measure of the local color uniformity for each pixel. For each spot, the spot center was set to the colored pixel with the minimum variance over a 23 total pixel span (i.e., the pixel in the middle of the most color-uniform environment over a center-to-center spacing of spots in the sensor array).

3.2.7 Device comparison and characterization

Four separate imaging devices were compared, and their relevant parameters are described in Table 3.2: the handheld reader (which uses a stationary linear CMOS-based CIS), a high-end consumer-grade flatbed scanner (Epson V600, which uses Epson ReadyScan LED technology, i.e., a white LED illumination bar), a high-end consumer-grade DSLR camera (Canon EOS 5D Mark II), and a high-end consumer-grade smartphone (Apple iPhone 5S). The DSLR and smartphone methods required external illumination ("natural white" LED light strips, purchased from SuperBrightLEDs.com, used with a current controlled power supply) and had different non-zero focal distances; the focal distances used were the minimum necessary in order to ensure appropriate illumination of the chemical sensor arrays (e.g., elimination of shadows obscuring sensor elements and elimination of unwanted specular reflection).

Noise statistics for each of these imaging methods were quantified by comparing images taken of a colorimetric sensor array that was equilibrated with the ambient environment (i.e., an un-exposed colorimetric sensor array). Images from each device were collected by scanning at least 20 frames of the

colorimetric sensor array. The last 10 frames obtained in each experiment were then used to obtain color data; each spot's color values consisted of a Red, Green, and Blue (RGB) values which are themselves composed of data averaged from multiple pixels depending on the spot size: i.e., each spot's RGB values resulted in 87 separate values (dimensions) for a 29-spot array. Standard deviations for each dimension were calculated from the 10 scans, and the noise parameter for each imaging methodology was quantified by using the average of these standard deviations among all dimensions.

The edges of any colorimetric sensor spot represent, of course, a discontinuity in the measured RGB values. As a consequence,, colors measured near the edges of a spot show increased variability (among sequential scans) when subjected to small variations in center position (i.e., physical jitter) compared to measurements near spot centers. This increased variability is due to changes in the alignment of physical location on the sensor array to specific pixels in the imager from scan to scan and is therefore sensitive to physical motion (jitter). In order to investigate the magnitude and effect of physical jitter in each of these methods, spot center positions were shifted across the image horizontally (i.e., all digital spot centers are shifted simultaneously by N pixels in the X direction, and N is varied) and noise was calculated as a function of this shift by comparison among multiple scans. Two-dimensional methods (smartphone, flatbed scanner, and video camera) used a 4-pixel radius circular spot from the measurement center point (resulting in 13 pixels), while the one-dimensional data obtained from the CIS used a 4-pixel linear spot from the measurement center point (resulting in 4 pixels). All appropriate gas flow apparatuses were active during these scans (i.e., the diaphragm micropump for the handheld device and mass flow controllers for the smartphone, flatbed scanner, and video camera). The handheld reader was further characterized by obtaining the response profiles upon varying illumination intensity.

Table 3.2 Summary of parameters used in compared imaging methods.*

Method	Sensor Type	Focal Dist.	Pixel Res.	Scan Rate
Handheld Reader	CIS CMOS	≈ 2 mm	600 ppi	2.0 Hz
Flatbed Scanner	CIS CCD	≈ 2 mm	590 ppi	0.02 Hz
DSLR Camera	2D CMOS	30 cm	900 ppi	30 Hz
Smartphone	2D CMOS	10 cm	560 ppi	30 Hz

* Pixel resolution (i.e., pixels per inch, ppi) was calculated using known 1.0 mm reference distances.

3.3 Results and discussion

3.3.1 Background

Colorimetry initially evolved as a slow, bulky, qualitative analysis method; techniques such as colorimetric titration and spot tests involved multiple milligrams of material and were evaluated with little more than inspection by eye.[33] Improvements in microelectronics have allowed for significant miniaturization of optical transduction components which in turn allows for faster, smaller, quantitative analyses that are evaluated electronically. The imaging methods used to evaluate gas-phase colorimetric sensor arrays involve the use of flatbed scanners,[6,8,9,27,28,30-32,34] digital cameras,[35-42] and smartphone cameras (often with associated analysis software).[43-47] These methods are inexpensive, powerful, and significant improvements over classical qualitative techniques; nonetheless the use of off-the-shelf hardware leaves much room for additional improvement and optimization. The analyses still generally require manual data processing with a separate device, and the complete apparatuses themselves are also bulky due to the size of both the imaging instrumentation and essential auxiliaries (i.e., gas flow controllers, illumination sources, and external devices required for data processing).

In a similar vein, portable instrumentation for liquid-phase analytes has found some success in urine, saliva, and pH sensing.[18,19,48,49] These methods use only single-point measurements (vs. continuous

monitoring) and usually require significant operator input, e.g., manual dipstick testing or downloading and manual processing of collected data on a separate computer.

In order to create a portable reader designed for gas phase analysis with colorimetric sensor arrays, we have developed a handheld reader. The device is a self-contained, truly portable analytical device with a portable, low-noise optical reader and onboard processing capability.

3.3.2 Device construction

The handheld reader was designed with a compact form factor in which a CIS optically images the reflectance from a colorimetric sensor array rigidly held ≈2 mm from its surface. The CMOS array present in the CIS is a broadband photodetector; RGB reflectance values are measured by sequentially illuminating the array with red, green, and blue LEDs. A general schematic for operation with a sealed colorimetric sensor array cartridge is shown in the supporting information as Figure 3.1, light emission profiles are provided as Figure 3.6, and an illumination timing chart for the CIS is given in Figure 3.7. Additionally, the chassis itself minimized stray light exposure.

One primary application of colorimetric sensor arrays is monitoring and analysis of gaseous analytes.[1] To accommodate this, a cartridge was designed to fit the handheld reader and provide a low-volume flow path for analyte exposure of a colorimetric sensor array. The array is printed on a substrate (e.g., polypropylene membrane) and mounted to the cartridge, which is then sealed using a glass microscope slide that sits against a Viton O-ring, as shown in Figure 3.2. A flow system using a diaphragm micropump was incorporated to allow for gas exposure at ambient pressure without the need for external attachments; the cartridge outflow port was sealed to a gas flow manifold by compression of an O-ring upon closure of the top latch (Figure 2). The micropump can produce a static pressure of ~500 mbar and was powerful enough to pull vapor analytes through bubblers and loosely packed tubes of silica gel.

Critical to the advancement of this project, linearization of the array was successfully completed. Using a line imager such as a CCIS (color contact image sensor) requires a linear rather than a two-dimensional (e.g., 6x6) array. In addition, a linear array greatly reduces the dead volume inside a cartridge and substantially improves the analyte gas stream flow over the sensor array by eliminating stagnant pockets of poorly mixed gases (e.g., corners in a square array). We therefore designed a linear sensor cartridge with the goals of easy assembly, inexpensive production, minimal dead volume, and optimization of gas flow path, with special attention to minimization of entrance length before gas analytes hit the sensor array. Figure 3.3 show the resulting design. Injection molded cartridges (Figure 3.3) are mounted with a linear printed colorimetric sensor array and a microscope slide is snapped in place as cover (Figure 3.4).

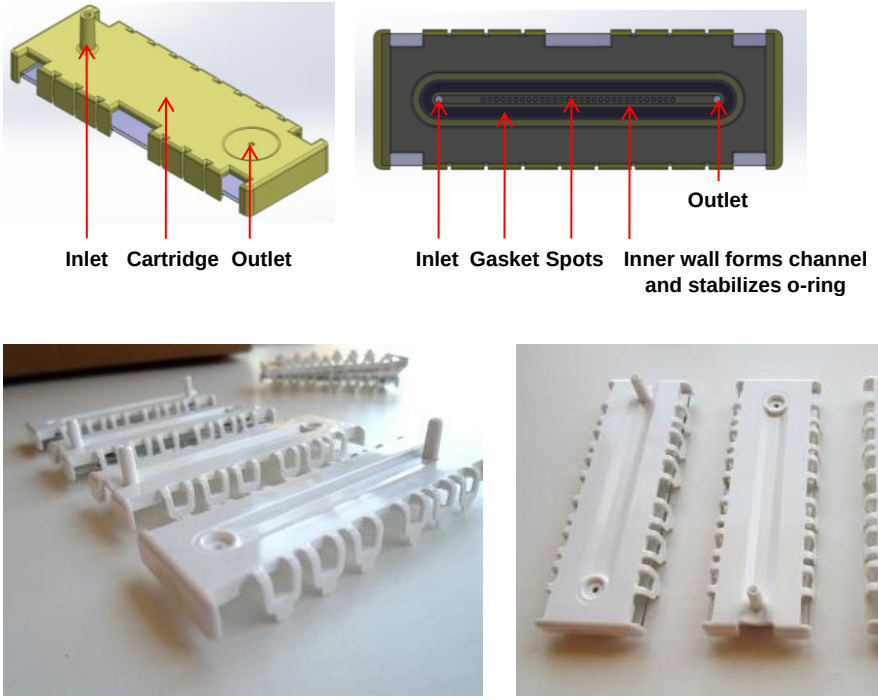

Figure 3.3 Injection molded cartridges. The inlet tube can be attached to a flexible "snout" (e.g., Teflon tubing) for sniffing of specific locations. The cartridge design minimizes dead volume and improves gas

flow path substantially with a linear channel, 1.2 x 0.5 x 77 mm (<50 µL).

Figure 3.4 JawBreaker sensor array, consisting of DNT-sensitive, general Lewis/Brønsted TICS-sensitive, metal-containing, ketone-specific, vapochromic/solvatochromic, and redox-sensitive colorimetric sensors. Upper image: sensor array in cartridge but without glass slide in place. Middle image: array with glass microscope slide cover in place. The sensor array itself is housed in the injection molded

snap-on cartridges requires no adhesive for sealing the standard microscope slide as a cover. Bottom image: enlarged annotated set of the 40 chemically responsive dyes that make up the array in its final formulation. The array is 50 mm long and 4 mm wide. The cartridges are stored under nitrogen in aluminized Mylar pouch to maximize shelf-life.

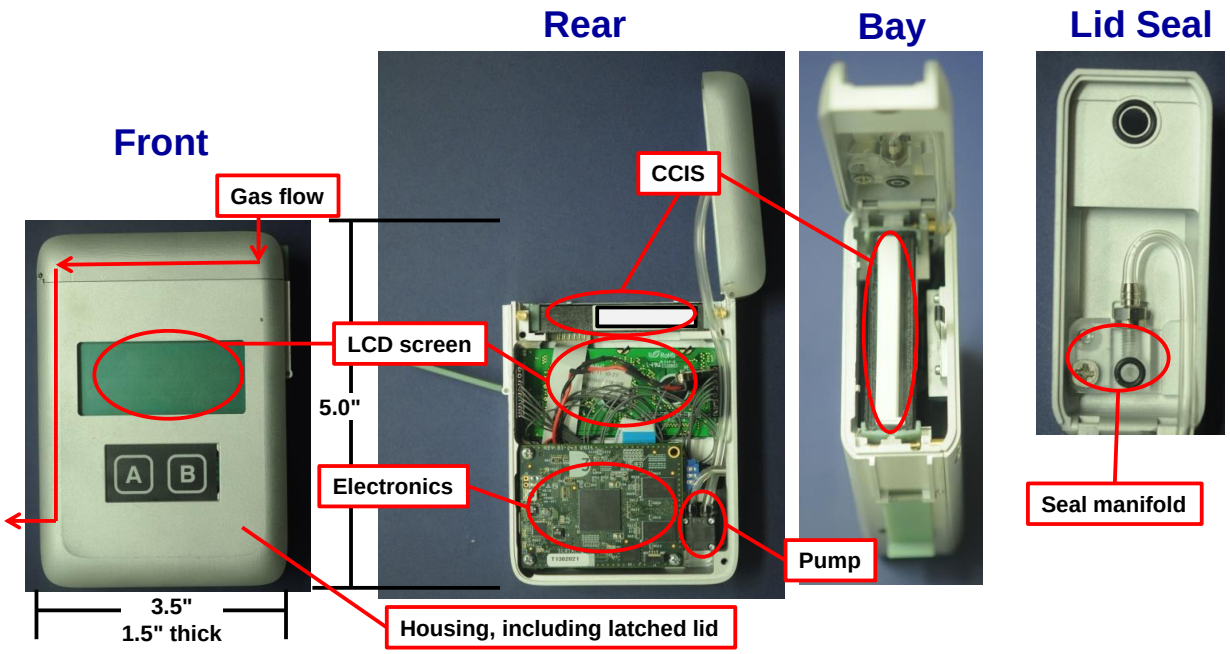

Figure 3.5 Photographs of the handheld reader including front, rear, and cartridge bay views. Dimensions are 12.5 cm tall by 9.5 cm wide by 4.0 cm thick. The rear panel and 9 V battery were removed in order to provide a better view of the internal electronics and diaphragm micropump (located in rear image, lower right). Left: front view. Left center: rear view, case cover removed. Top right and lower center right: top view with lid open showing top of sensor cartridge in place (the sensor array itself is not visible here). Lower right: top view of the lid with lid open showing the sealing manifold to the cartridge that is connected to the micropump inside the case. The handheld reader is powered by external power supply or standard 9V battery (red & black wires to battery connector shown in lower left-center photo, but battery removed to show internal view).

Digital data was produced from the analog output of the CIS using a 12-bit ADC. The onboard processor used a 700 MHz CPU to control component behavior and image processing; the internal bus and CPU are capable of transferring images and performing these relatively simple analyses at rates much greater than the 48 Hz scan rate. A database of relevant sensor responses is stored on the handheld sensor enabling classification in real-time. User control for autonomous modes (e.g., real-time monitoring and comparison to known databases) was provided by a simple LCD screen and two-button control scheme. Relevant specifications are shown in Table 3.3.

Table 3.3. Relevant component parameters of the handheld reader.

Scanner Size	12.8 cm x 9.5 cm x 4.0 cm
Scanner Weight	460 g + battery + cartridge
Cartridge Size	7.9 cm x 2.8 cm x 1.0 cm
Cartridge Weight	11 g
Battery Weight	48 g
Static Pressure[26]	550 mbar
Pump Rate[26]	50-580 cm^3/min, adjustable
Current Draw	~400 mA at 100% duty
Battery Charge	1200 mAh
Scan Time	11 ms

3.3.3 Further device characterization

The device was characterized further in order to assess its operational parameters. The emission spectra for the RGB LED light sources are shown as Figure 3.6. Illumination and timing profiles are shown in Figure 3.7; it is important to note that there are blank scan cycles separating each illumination cycle. The effects of scan rate and scan position on the measured noise are shown in Figure 3.8 and S5 respectively.

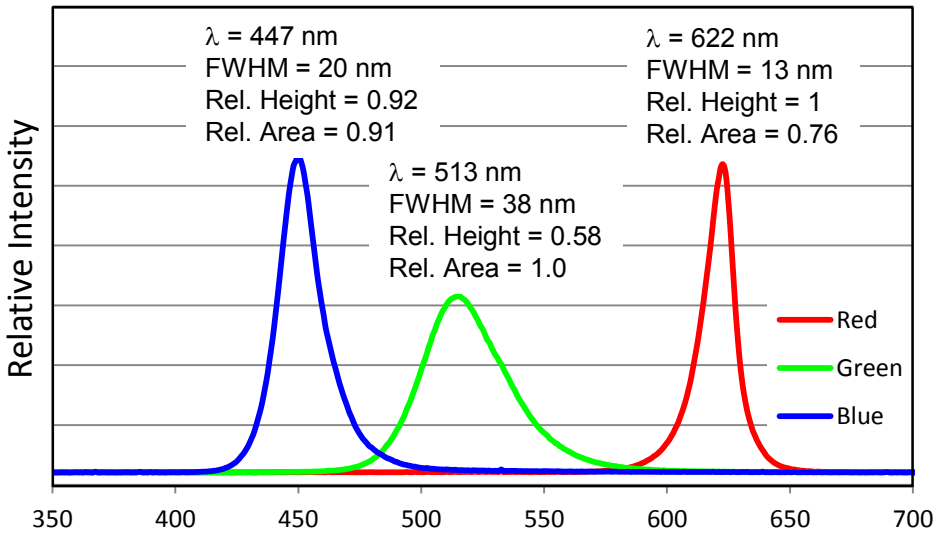

Figure 3.6 Emission profile of the illuminating red, green, and blue LEDs within the contact image sensor (CIS) used in the handheld scanner. Applied potential and illumination times were optimized to ensure that Red, Green, and Blue responses when scanning a uniform white sample were consistent and significantly under the saturation region of the photodiodes of the CIS.

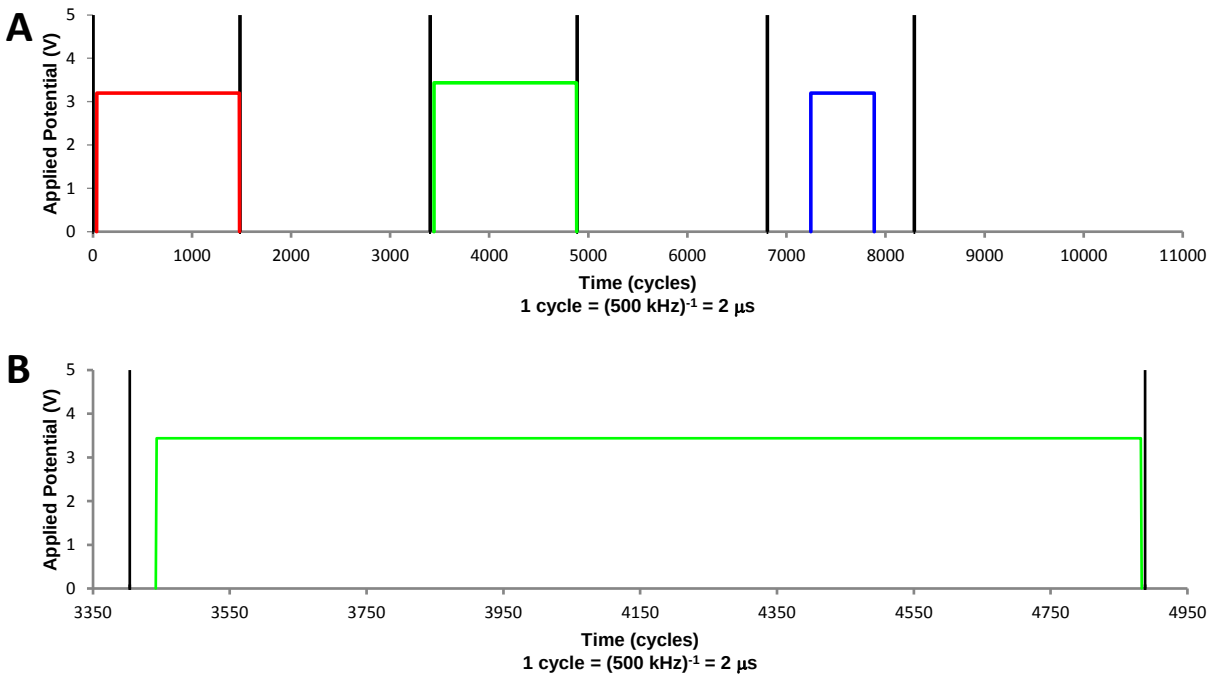

Figure 3.7 Illumination profile for a single scan of the CIS showing applied voltage (vertical) and time (horizontal). (A) Full profile over 10,212 cycles, i.e., one full scan of the RGB pixels, which consists of cycles of data collection during exposures to red LED illumination followed by a dummy cycle (without illumination) followed by green illumination, etc. The vertical black lines represent the beginning and end of the capture window of the photodiodes. (B) Closeup of the capture window bounding the green LED illumination. There are 1484 clock cycles in a capture window consisting of 38 processing cycles, 1440 active pixel cycles, and 6 overscan processing cycles; this scan period is used to fully clear the shift register and simultaneously expose the sensor elements to light. Light exposure is controlled through a combination of voltage and pulse-width modulation; red, green, and blue LEDs are kept on for 1440, 1440, and 640 cycles at 3.20 V, 3.44 V, and 3.20 V, respectively, and are centered around the center of the active scan period (i.e. starting at the 38th cycle relative to the start pulse for red and green LEDs, and the 438th cycle relative to the start pulse for the blue LED). Data is clocked out of the shift register at 1 pixel per cycle during a subsequent dummy scan period consisting of approximately 1920 cycles containing the aforementioned 38 inactive processing cycles, 1440 active pixel cycles, and 6 overscan

processing cycles combined with a variable number of cycles used to account for additional data processing. Note that LED on/off times are on the order of tens of nanoseconds, which is negligible compared to the 2 microsecond clock cycle.

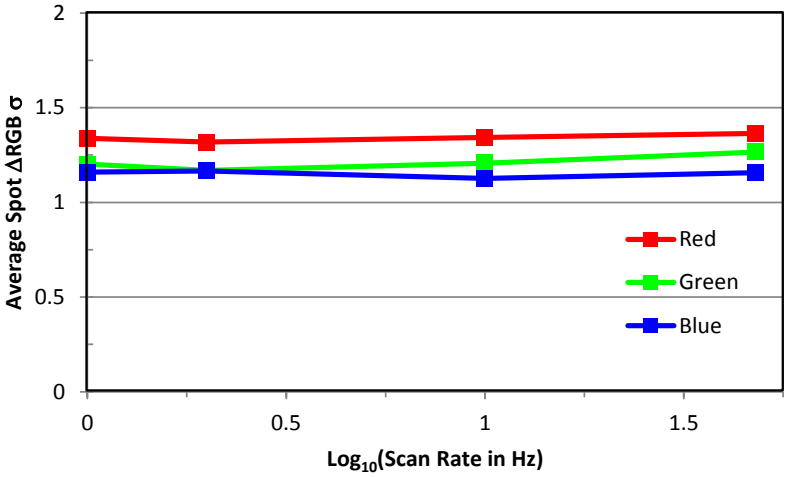

Figure 3.8 The effect of scan rate on output consistency of a 29-spot colorimetric sensor array. There is no significant change in observed noise as scan rates are varied from 1 Hz to 48 Hz.

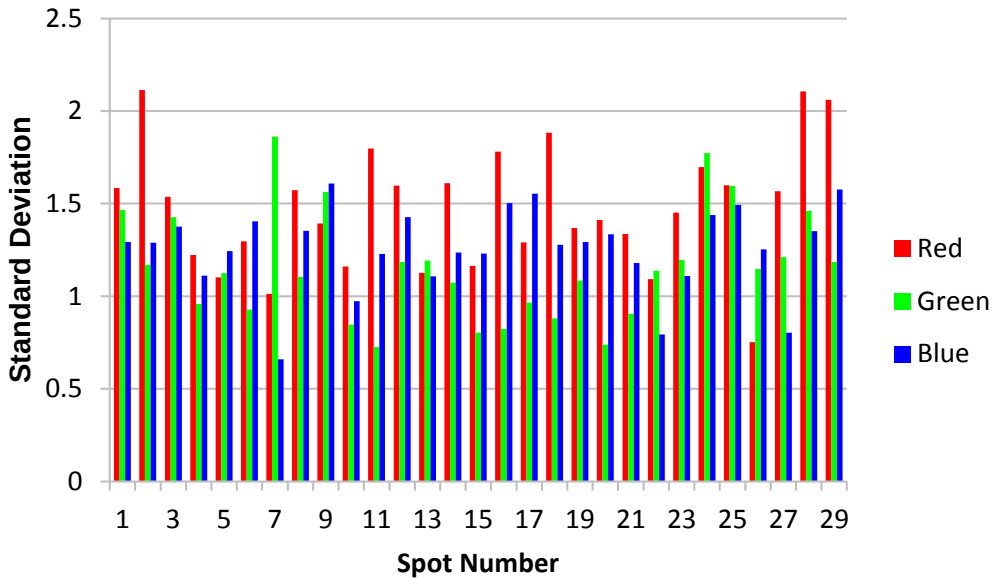

Figure 3.9 Observed noise profile of a typical 29-spot colorimetric sensor array. Spot diameter was fixed at 10 pixels. There was no correlation between observed noise and spot color (R^2 = [0.005, 0.093, 0.006] for [Red, Green, Blue]), nor was there a correlation between observed noise and spot location (R^2 = [0.018, 0.001, 0.002] for [Red, Green, Blue]).

Importantly, the current prototype reader suffers from intermittent overheating of the electronics (most likely overheating of the analog-digital converter by the CPU). When overheating does occur, the color difference maps will show artifacts in the color changes over broad regions of the CCIS, even between the sensor dye bars, as shown in Figure 3.10. Under most lab testing conditions, one does not usually tax the CPU sufficiently to cause significant heating. Under intensive testing conditions, however, continuous running of the handheld reader can lead to overheating in an idiosyncratic manner depending on rates of sample acquisition vs. wait times in between samples. We have a simple work-around to this problem: *after a sample acquisition, one should simply turn the reader off between acquiring samples and observe a 5 min waiting period before the next sample acquisition.* Longer term, this overheating problem can be easily addressed either by increasing the space and adding insulation

between the two electronics components or by increasing ventilation inside the currently sealed, non-vented case of the handheld.

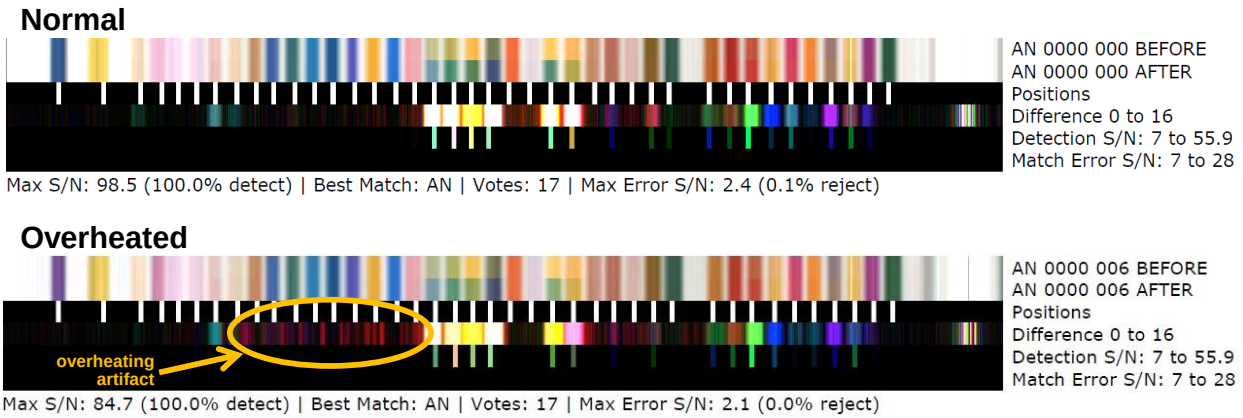

Figure 3.10 Artifacts created by overheating are shown and compared to a normal scan. When overheating occurs, the color difference maps will show artifacts in the color changes over broad regions of the CCIS, even between the sensor dye bars, These are taken from the Graphics Report pdf output from the PC GUI software.

3.3.4 Scan and processing rate comparison

Previous studies with colorimetric sensors use flatbed scanners[6,8,9,27-32,34] or digital cameras,[35-42] both of which capture a series of large, high-resolution two-dimensional images that are then analyzed using external software. The scan rates of each of these methods are primarily regulated by acquisition and data transfer speeds. In order to make a useful set of comparisons among available imaging devices, we examined an Epson V600 flatbed scanner, an iPhone 5s, a Canon EOS 5D Mark II DSLR camera, and the handheld reader (which uses a CMOS Sensor Inc. M116 CIS). The Epson V600 flatbed scanner has a moving scanning bar and transfers images directly to the connected computer, which limits its scan rate: 800 dpi images of a typical 2.5 cm x 2.5 cm array take approximately 45 seconds to acquire and transfer,

while higher-resolution images take even longer. DSLR cameras, on the other hand, are not limited by moving parts and have higher bandwidth data transfer methods available; a typical video mode using the DSLR has a collection rate of 30 Hz with a transfer rate of approximately 1 to 10 Hz during batch transfer, which means that 1 min of video data requires between 3 to 30 min to transfer the data from the camera to a computer for external processing. Smartphones such as the iPhone 5s operate similarly to DSLR cameras but also have onboard processing potential similar to the handheld reader, and data transfer times can thus be assumed to be zero; in-depth comparison would require access to specific onboard software (i.e., apps) dedicated to scanning similar chemical sensor arrays, so at present only hardware comparisons apply when considering use of a smartphone for array analysis. The handheld reader described here is capable of scan rates of 48 Hz with essentially real time processing (i.e., faster than time between subsequent scans) without affecting consistency, as shown in Figure 3.8.

Images collected with a flatbed scanner or camera are typically processed in batch using a manually calibrated spot-finder and can require additional steps (e.g., file conversion, extraction, or image cropping) which significantly increases processing time making real-time analysis impossible. Dedicated software could potentially eliminate these secondary steps, so comparison also requires looking at the fundamental nature of two-dimensional vs. one-dimensional images as they apply to colorimetric sensor arrays. During imaging, spot centers move relative to the imaging device and are not perfectly aligned relative to each other; determining the locations of these spots (i.e., spot-finding) is the primary bottleneck in data processing. The origin of this problem is two-fold: First, due to the realities of printing large numbers of arrays, sensor spot centers are not always perfectly aligned relative to each other. Second, when arrays are positioned for imaging, the spot locations are not aligned identically relative to the imaging device (i.e., pixel positions of sensor elements).

Data handling, and specifically spot-finding, with one-dimensional images collected by the handheld reader is relatively simple and fast compared to handling two-dimensional images: (1) the file size is

much smaller (e.g., 1440 pixels compared to 30x1440 or more pixels for the same linear array), (2) spot finding methods are much simpler for one-dimensional data than for two-dimensional data (i.e., there are no rotational or vertical degrees of freedom in one dimensional data)[2], and (3) the fraction of pixels relevant to image analysis is much greater in one-dimensional images (i.e., data efficiency is improved because pixels corresponding to non-sensor and interstitial areas are minimized).

Combining the improvements in data transfer and increased speed with one-dimensional spot-finding methods, image processing with the handheld device can be performed continuously in real time. With basic data collection, the primary bottleneck in the handheld device is actually the exposure time of the CIS itself: spot-finding (measured at ~6 ms) takes approximately half the time of a single scan cycle (measured at ~11 ms).

3.3.5 S/N comparison

Two-dimensional imaging methods use a number of pixels per sensor element that is proportional to the square of the chosen spot diameter; for the handheld reader with its linear CIS, the number of pixels is linearly proportional to the spot diameter. One might have expected that the much larger number of pixels per spot in 2D methods would translate to a lower calculated noise simply by virtue of signal averaging. Experimentally, however, this is not the case: as illustrated in Figure 3.11, the handheld reader shows lower average noise per spot than other methods for every tested spot size; a typical profile showing the noise of each spot is shown in Figure 3.9. The smallest improvement with the CIS is approximately five-fold (i.e., compared to the flatbed scanner with large spot size), and the largest improvement is more than 25-fold (i.e., compared to the smartphone with small spot size). The relative change in observed noise as the spot size increases (i.e., the trend as spot spot size varies) is similar among all four methods tested. It is also worth noting that the difference in observed noise per pixel

(rather than per spot) is even larger, as the 2-dimensional methods use more pixels per spot (i.e., ~πr^2 pixels in 2D methods vs ~2r pixels in the handheld device).

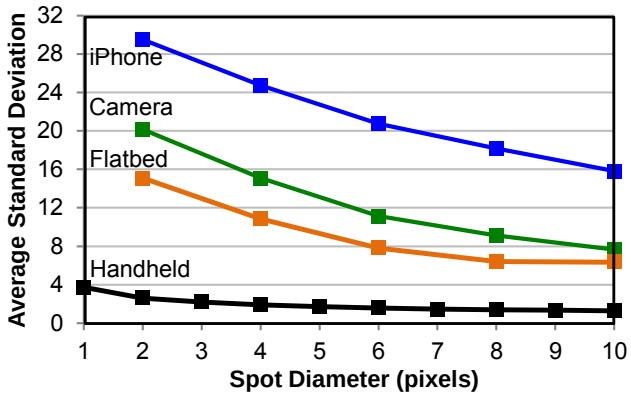

Figure 3.11 Typical noise observed in detected spots as a function of spot size in the handheld reader, flatbed scanner, DSLR camera, and smartphone camera; standard deviation shown is determined from 10 scans of an array with 29 spots. Note that each of these methods uses 12-bit color space (i.e., [0-4095]) and the dynamic range defined by the difference between fully white and fully black areas is approximately equal for each (i.e., ~2750).

Optical reading of arrays must also deal with the finite size of sensor spots. Printed spots have discontinuities at their edges: each sensor has some more or less uniform colored area at its center whose coloration eventually transitions (either gradually or abruptly) to a blank space between spot or to another overlapping spot. In the presence of physical jitter or vibration, there will be artifacts induced in color difference measurements at the edge of the spots. To maximize the response consistency for each spot, the most uniform area of each spot should be compared before and after exposure; i.e., avoid the edge regions. This minimizes the effect of physical jitter on the digital output. The usable spot radius is thus less than the apparent radius defined only by a printed spot's edge; this is analogous to capturing the top of a plateau and avoiding the cliff at the edge.

The sensitivity of each imaging technique to physical jitter can be measured by observing such edge region artifacts. If one measures the optical response across a spot, small changes in spot position (due to physical jitter) will result in significant apparent color changes at the spot edges, resulting in large standard deviations in color values measured near the edges, as seen in Figure 3.12. Dramatic increases in noise near the spot edges compared either to the spot center (located at 0 pixels) or to the areas between spots (located at -10 and +10 pixels) are observed in imaging with the flatbed scanner or the video camera. Images taken with an iPhone 5s camera show this edge effect to a lesser extent. Observed noise using the CIS is substantially decreased relative to these other methods and has no apparent correlation with relative position whatsoever (Figure 3.12B).

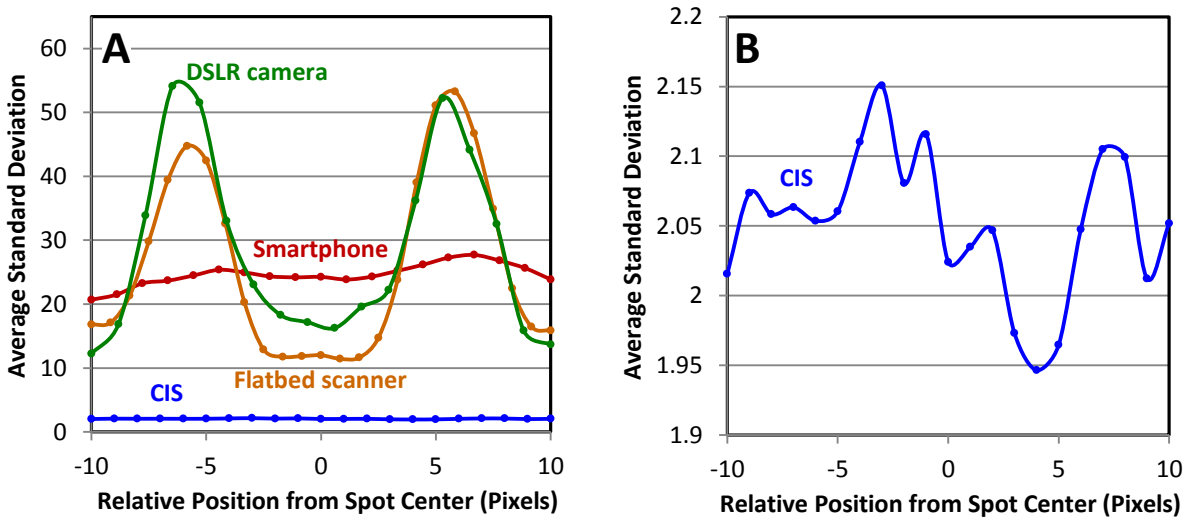

Figure 3.12 Reproducibility of spot imaging as a function of position across the spot, showing the appearance of edge effects. On the x-axis, 0 represents the spot center and ±10 represent the space between spots. (a) Comparison of the observed noise from four imaging devices vs. distance from the physical center of the dye spots, averaged over all 29 spots; (b) Greatly expanded scale for the standard deviation of the noise measured for imaging using the CIS; no edge artifacts are observed for the CIS. An

identical chemical sensor array was used for all scans; relative spot positions were normalized to the resolution of the CIS (600 ppi).

Edge artifacts of the sort seen in Figure 3.12A are explained by physical motion (i.e., jitter) between individual scans, which contributes significantly to the observed noise in imaging methods. In the case of a flatbed scanner, a moving scan bar controlled with servos introduces jitter in the location of the imaged pixels. In the case of the digital camera and the smartphone, the relatively long distance between the colorimetric sensor and the optical lens likely made the methods more susceptible to physical jitter caused by vibrations. With the necessary focal lengths for typical camera lenses, it is difficult to maintain absolute structural rigidity and eliminate relative motion. The smartphone focal length is one-third of the DSLR camera (10 vs. 30 cm), which contributes to the improvement in noise observed with the smartphone camera; additionally, the imaging software used in a smartphone has many automatic processing features built-in (importantly, including anti-shake software) and may have had an effect both in terms of the edge-center difference and overall measured noise. For the CIS, the substantial decrease in distance between the optical sensor element relative to spots (≈2 mm) and the absence of any moving components essentially eliminates the artifacts induced by jitter. Importantly for the CIS, adding physical vibration (e.g., turning on the gas micropump) did not have any effect on measured noise values.

3.3.6 Proof of concept: array analysis

To show the utility of the device, an array known to be sensitive to toxic industrial chemicals containing acid and base-treated pH indicators, porphyrins, and other chemoresponsive dyes (described in previous papers[8]) was exposed to a stream of NH_3 vapor at roughly its OSHA Permissible Exposure Limit (PEL) of 50 ppm. Digital output from the 12-bit ADC ranged from approximately 50 to 2800 (i.e.,

~2750 possible values, giving approximately 11 bits of color resolution), corresponding to 0% and 100% reflectance respectively. The maximum output from the CIS was adjusted by limiting the total light intensity so as to avoid loss of sensitivity due to overexposure; this is primarily a function of total reflectivity of the cartridge (specifically its internal flow channel), so adjustment of illumination intensity is a one-time calibration. Results of array exposure after 15 seconds are shown as Figure 3.13.

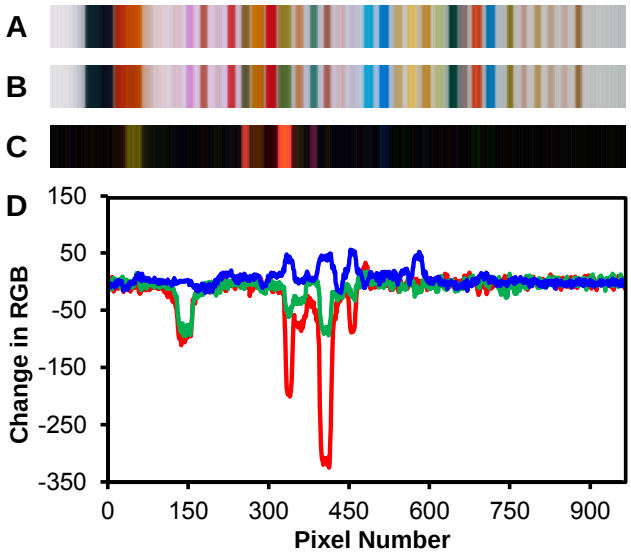

Figure 3.13 Differential array response to NH_3 at PEL concentration (50 ppm). (A) Image before exposure. (B) Image after 15 seconds exposure. (C) Difference image of A and B. (D) Graph of data used to construct C. Images are projected onto 8-bit RGB color space (i.e., [0-255]) for display; images A and B were normalized to a uniform white substrate, while difference image C was normalized to maximum and minimum difference values. Maximum signal/noise was approximately 280.

Spot locations were determined automatically by using a spot finding algorithm. As a test of this algorithm, a 45 spot array with intentionally added gaps and semi-overlapping spots was printed at 1.0 mm (approximately 23.6 pixel) spacings (Figure 3.14). Each spot had a full-width half-maximum of approximately 7 pixels, though this was intentionally made somewhat larger for several spots. To determine locations of spots vs. space between spots, a simple spot finding algorithm was used (cf. SI

for detailed description). This algorithm was tested with an array containing 45 spots and 3 interspersed gaps (i.e., blank areas not containing any sensor spots), as shown in Figure 3.14. In order to test the resilience of the algorithm, the print quality of this array is intentionally poor and contains irregular spacing and obvious overlap among some sensor elements. As shown in Figure 3.14, 44 of 45 printed spots were accurately located, and all 3 gaps were correctly identified; one spot (fifth from the left in Figure 3.14) was missed by the algorithm due to its color similarity and physical overlap with the adjacent spot (fourth from left).

With the CIS, the color data has only a single search dimension (i.e., it is a linear array), so locating spots is straightforward and requires computational time that scales linearly with the number of pixels in the array. In comparison, two-dimensional systems (e.g., camera images) have an additional search direction and increased area between spots, which require significantly more complex algorithms that demand computational time on the order of the square of the number of pixels (i.e., a factor of 10^2 to 10^3 increase in computation time for typical sensor arrays).[50]

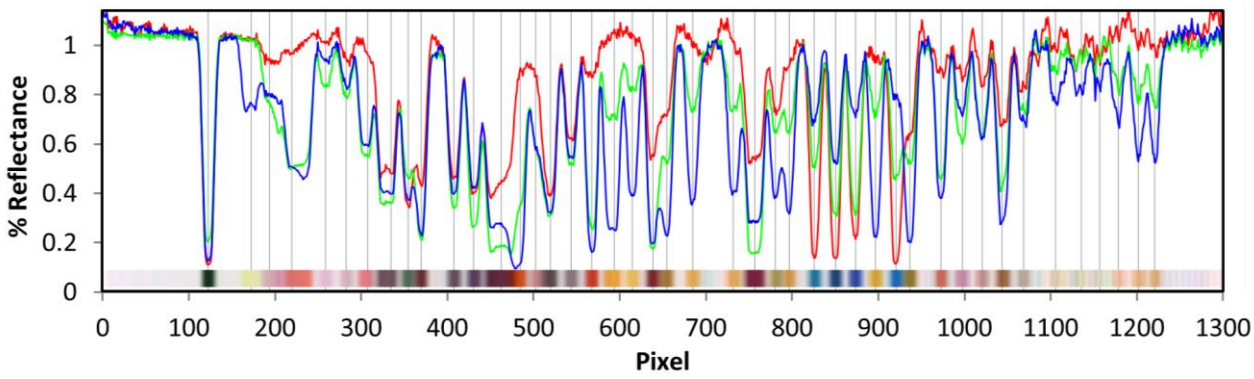

Figure 3.14 Results of spot-finding procedure applied to a problematic colorimetric sensor array. The print quality of this array was deliberately poor in order to test the resilience of the spot-finding algorithm; irregular spacing and overlap among sensor elements were intentional and are not present in typical sensor arrays (cf. Figure 3.2). Normalized RGB data is shown above an image of the array in red, green, and blue traces. Vertical gray lines correspond to spot centers and show accurate location of 44 of 45 spot locations and all three gaps.

3.3.7 Database processing and handling

Compared to low-dimensional sensor systems, high-dimensional sensor systems must involve a more sophisticated approach to statistics than that which chemists are often comfortable. The inherent problem with high dimensionality is that the analytical volume increases much more rapidly than the available data, so the datasets are often formally "sparse" compared to the total size of the parameter space. In addition, this "curse of dimensionality" creates difficulties for function approximation, model fitting, information extraction, as well as computation. Statistic methods for multidimensional data all share the common goals of displaying multidimensional data effectively, evaluating data sets, and predicting the identity of unidentified samples based on a known library.

There are a variety of statistical methods available to deal with high dimensional data well beyond the scope of this manual. We will give an overview here only one approach: support vector machine (SVM) analysis (other approaches are discussed in Chapter 1). In general, for chemometric data there are two distinct statistical approaches: clustering vs. classification. Cluster analysis essentially tells one what resembles what, e.g., how close the vectors representing data are to one another in a high dimensional space. Classification analysis, on the other hand, attempts to predict to which category (among a fixed number of known categories) any particular (new) datum belongs.

Statistical methods can be either *unbiased* (unsupervised, model-free)*,* where all cases are evaluated identically regardless of class identity, or *biased* (supervised)*,* in which case the evaluation algorithm is told of the class identities of individual cases. Unbiased methods, such as HCA, are typically used to evaluate a data set to provide a semi-quantitative idea of the quality of the data set and follow simple, straightforward algorithms. Biased methods such as SVM, on the other hand, can provide significantly more power and utility with a concomitant increase in complexity, but at the cost of demanding datasets for which one already knows the answers. Biased methods can be predictive, allowing for class assignment of new experimental cases by using a training set.

The classification method used in this project is a Support Vector Machine (SVM) using a linear kernel. It has similarities to Linear Discriminant Analysis (LDA), another very widely used method in pattern recognition. Like LDA, linear SVM finds a plane that best separates a single pair of classes (cf. Figure 3.15): an incoming sample is then classified as either "Class A" or "Class B" for each pair (a "one against one" method). One "vote" is collected for each pair in this way. The incoming sample is then classified as whichever class got the most votes. Unlike LDA, SVM does not require a large number of samples to maintain accuracy. This is because only a small number of points are picked from each class to generate a classifier. The method is not analytically solvable; generation of classifiers requires an initial guess followed by multiple rounds of iteration in order to find a specific classifier that maximizes separation between existing data and minimizes the chances that new data will be misclassified (how important these individual factors are) can be adjusted if necessary; this project uses the default parameters of the software library described below, which have been found to be optimal in most cases: http://www.csie.ntu.edu.tw/~cjlin/papers/guide/guide.pdf

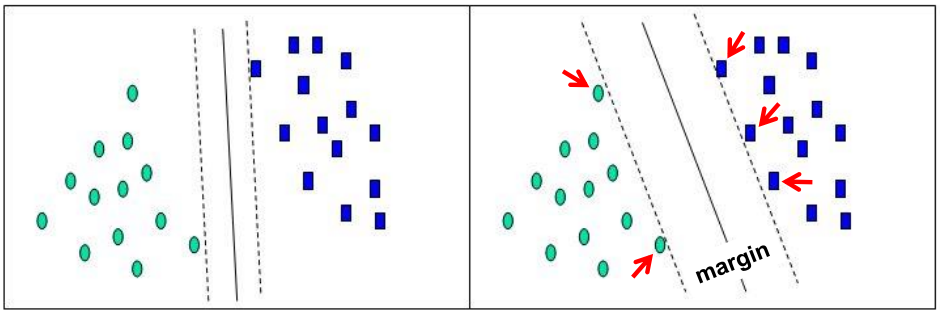

Figure 3.15 Two classes of data (green vs. blue) are present in this two dimensional example. SVM finds the best plane to divide the two sets (i.e., the rightmost image). The data points (which are vectors, in this case two-dimensional) that define the margins of the best separation are the “support vectors” (indicated by red arrows) and the algorithm that finds those is the support vector machine.

In order to do this, existing data points are identified as "support vectors" and assigned a weight that is proportional to how heavily they are used in the classifier; points near the border (the points that are most likely to be misidentified) are weighted most heavily, while points that are very far from the border are usually ignored completely. The key to the method is determining the identity of these points and their weights. There are multiple methods for doing this; the current industry standard uses algorithms developed by several computer scientists at the National Science Council of Taiwan in a software package known as LIBSVM http://www.csie.ntu.edu.tw/~cjlin/libsvm/. This package allows for flexibility to solve individual problems which are often much more complex than the data in this project. Because this project uses a linear kernel, the weighted points are collected into a single vector that is compared to each incoming sample (also a vector) using a dot product to generate a single "decision value" for each classifier; a decision value greater than zero indicates class A, while a decision value less than or equal to zero indicates class B.

Two other pieces of data are provided: first is the relationship between an incoming sample and the known-blank sample (the maximum signal-to-noise ratio as compared with each element of the blank data set). This allows for a "no detect" threshold, currently set to provide a 95% probability that any sample identified as outside the threshold will **not** actually be a blank (i.e. a maximum 5% rate of false positives; in general the rate of false positives is much less, generally below 1%). This uses a statistical distribution that varies based on the number of samples: the larger the numbers of samples, the narrower the detection threshold. The second piece of information is an identical relationship between the incoming sample and the top matches obtained via SVM (top 3 displayed on the handheld device, top 10 recorded for PC GUI software). Error is only described for sensor elements that are above the detection threshold. This provides a measure of how similar the incoming data is to the assigned classes that are already in the database (which may be especially useful in cases where the sample

analyte being collected is not previously in the database; it will be assigned an already existing class, but will also have a high error signal).

3.3.8 User software

There are two associated software packages that have been designed for the JawBreaker reader: a graphical user interface (GUI) run on a PC and the onboard software for the handheld reader operation untethered from a PC.

PC GUI Software. PC-Based Jawbreaker GUI Software does the following functions:

1. Downloads data from the handheld.
2. Generates databases. In the process, performs SVM classification on data set. This is similar to the SVM on the handheld - mathematically identical, but the steps taken use the whole dataset instead of the distilled version. This is necessary to generate a new distilled database.
3. Generates a no-detect threshold based on a t-distribution. This can be narrowed by collecting more blank samples.
4. Generates graphical reports based on downloaded data. In the process, performs SVM on data set. This is **identical** to the SVM on the handheld, as long as it's using the same database. It uses the distilled database.
5. Provides S/N and Error signal magnitude and probability based the aforementioned t-distribution.

The SVM classification methods that we are using are well developed in the pattern recognition community. The specifics of the SVM classifications are identical between the PC GUI and the Handheld software systems; the only difference is that the PC-Based GUI gives slightly more information (i.e.

probability estimates) because it has a more advanced math package. In both cases, the software follows the same logic chain, as follows:

1. Detect or no detect, based only on the previously collected library of blank/control samples. This answers the question of whether or not you can see anything at all.
2. If analyte is detected, uses SVM for classification based on loaded database. This answers the question of what pre-existing class of analyte the sample data most closely resembles.
3. Error signal of each identified class. This answers the question of how much you can trust the SVM classification and suggests the possibility of considering the new sample a new class of analyte.

Two screenshots of the PC GUI are provided in Figures 2.13 and 2.14 to illustrate its control options. Refer to sections 1.4-1.10 for detailed annotations. More sophisticated off-line statistical analysis (e.g., hierarchical cluster analysis, linear discriminant analysis, principal component analysis; cf. definitions in Table 3.1 above) of results using standard packages (we particularly like MVSP v. 3.1 or XLSTAT v. 2014 from KCS Corp., www.kovcomp.com) or other custom software (e.g., for more sophisticated support vector machine (SVM) analysis LIBSVM, http://www.csie.ntu.edu.tw/~cjlin/libsvm/ or SVMlight, www.svmlight.joachims.org) becomes possible once the reader responses are downloaded to a PC using the Report function of the GUI (Figures 3.16 and 3.17).

There are three types of reports that can be generated from the PC GUI software (excerpted output examples shown in Figure 3.18): (a) classification results, (b) graphical raw data, and (c) cross-validation, using the labeled buttons in the Reports section of the GUI opening page.

- '**Classification Results**' - A comma-separated table showing the top 10 classification results for each trial. This is given for each trial, even if the trial is found to be too low a response to be reliably assigned and is listed as 'Not detected'. (Section 1.7)
- **'Graphical Raw Data**' - An Adobe Acrobat PDF document showing the raw data graphically. This option also generates a table of the processed raw data. (Section 1.7)
- **'Cross-Validation**' – Using the SVM algorithms for classification, the cross-validation report is generated using a leave-one-out method: one at a time, each of the sample measurements is chosen to be left out from the classification database, the library is re-calculated, and then the chosen measurement is evaluated using the new library. (Section 1.9)

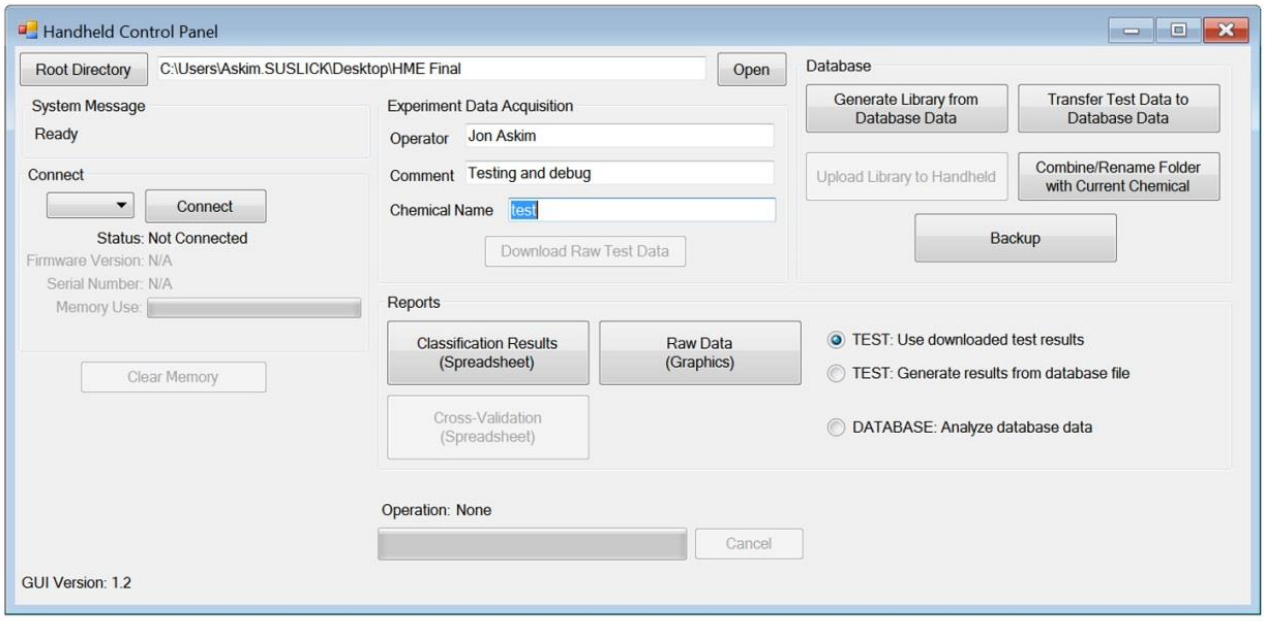

Figure 3.16 Opening screen image of the Jawbreaker_PC.exe graphics user interface.

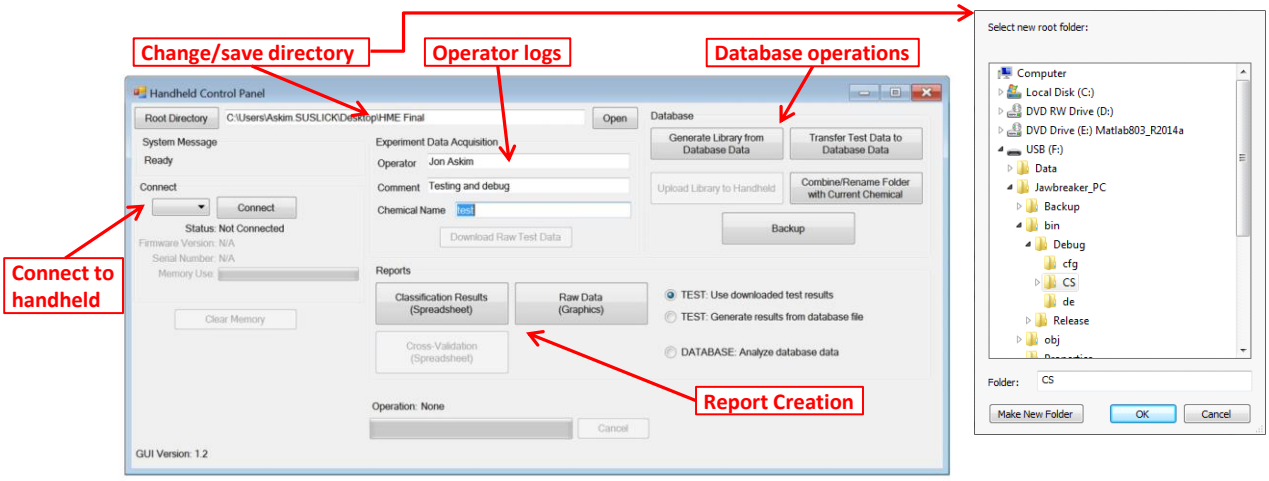

Figure 3.17 Annotated opening screen image of the Jawbreaker_PC.exe graphics user interface showing directory, handheld connection, data acquisition, library preparation, and report functions.

a.

Folder Name	Sample ID	Detected Yes/No	Detect Threshold S/N	Detect Threshold Pct	Detect S/N	Detect Pct	Match 1 Name	Match 1 Votes	Match 1 Error S/N	Match 1 Error Pct
AN	0JB2 000	Yes	4.213172	95	84.00447	100	AN	15	2.3808	0.035964

b.

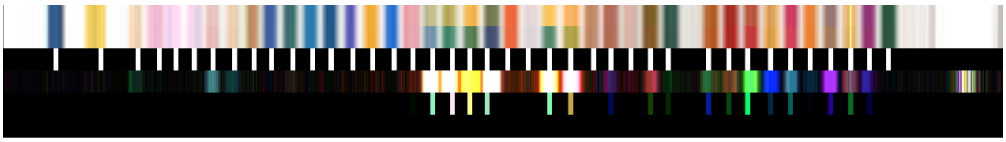

Max S/N: 98.5 (100.0% detect) | Best Match: AN | Votes: 17 | Max Error S/N: 2.4 (0.1% reject)

c.

Class Name	Count	Accuracy
!control	7	100.00%
AN	7	14.30%
ANFO	7	57.10%

Sample Folder	Rank 1 Name	Rank 1 Vote	Rank 2 Name	Rank 2 Vote
AN	ANFO	15	AN	14
AN	ANFO	15	AN	14
AN	ANFO	15	AN	14
AN	ANFO	15	AN	14
AN	ANFO	15	AN	14
AN	AN	15	ANFO	14
AN	ANFO	15	AN	14

Sample Folder	Rank 1 Name	Rank 1 Vote	Rank 2 Name	Rank 2 Vote
ANFO	AN	15	ANFO	14
ANFO	AN	15	ANFO	14
ANFO	ANFO	15	AN	14
ANFO	AN	15	ANFO	14
ANFO	ANFO	15	AN-NM	14
ANFO	ANFO	15	AN-NM	14
ANFO	ANFO	15	AN-NM	14

Figure 3.18 a) Excerpt from the Classification Results Report, showing only the first match from the library (remaining 9 matches would be in columns further to the right). **b)** An excerpt from the Raw Data Graphical Report output from the PC GUI Report. **c)** An excerpt from a cross-validation report. Match accuracy is the leftmost table. The right two tables show the first two closest matches (out of ten) for two sets of analytes, in this example, AN and ANFO.

Onboard software. The handheld reader has its own, separate software controlled by a two-button control panel (labelled “A” and “B”) on the front face of the handheld reader. There are three menus accessible on the handheld reader: **Main Menu**, **Diagnostic Menu**, and **Memory Management**; all

options proceed in A-B choices using the two-button controls. A flowchart of the entire menu tree on the handheld is presented in Figure 3.2.2. The classification methods are identical between the PC GUI and the handheld software systems. Online real-time SVM (support vector machine) classification software is built into the handheld and provides the three best matches from the pre-existing onboard library, in order of goodness of fit.

The handheld reader software does the following functions:

1. Collects and saves data.
2. Classifies incoming data and saves classification.
3. Provides S/N and Error signal magnitude.
4. Contains a *distilled* database - it contains enough information to perform SVM and related statistical tests, but not the entire database. (A distilled database contains one vector for each classifier. The full database would have upwards of 5 or more vectors for each classifier. The way the data is handled is identical.)

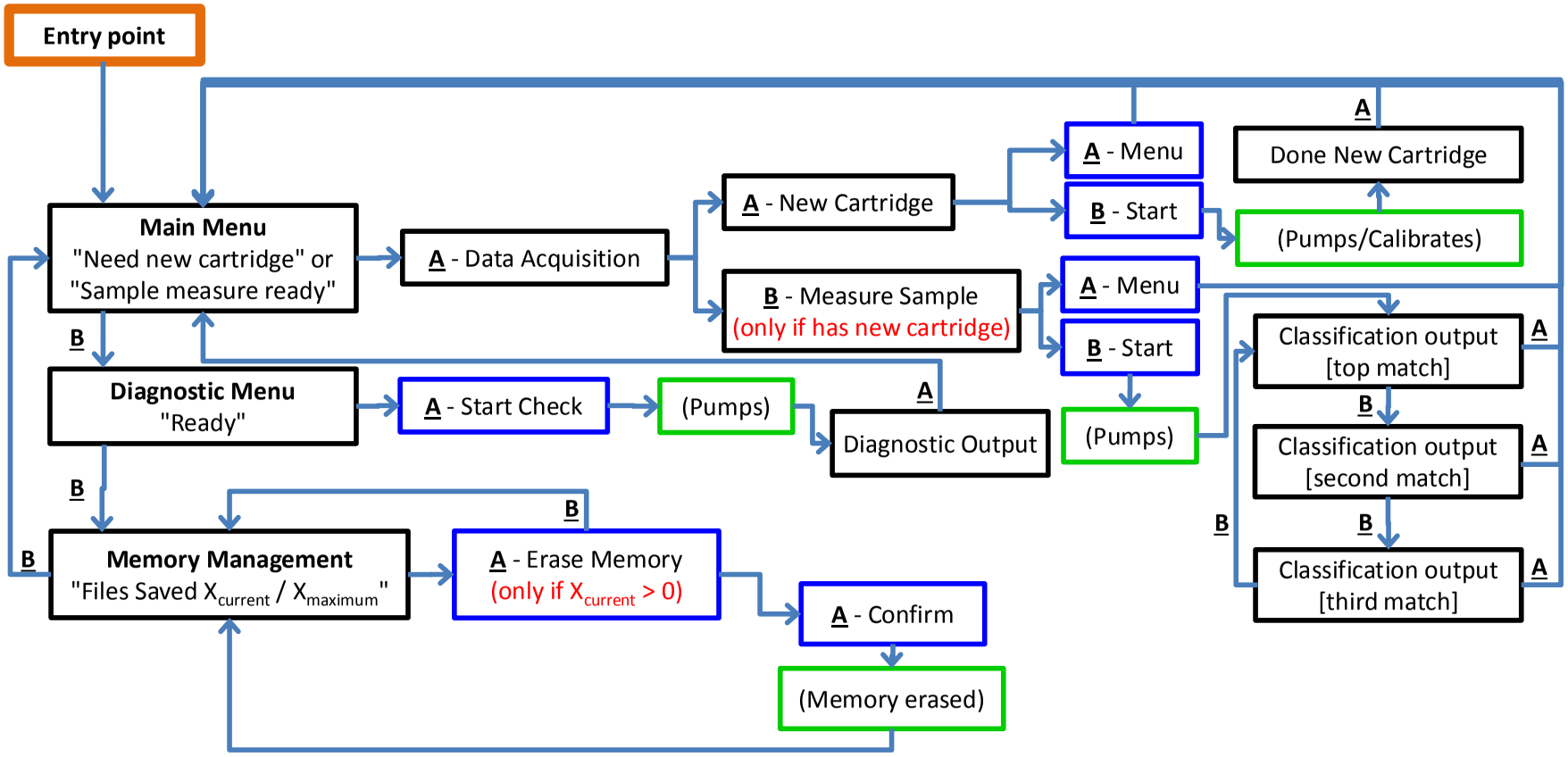

Figure 3.19 Handheld Software Flowchart

- **A** or **B** indicates a button press of A or B respectively on keypad: A B
- Unmarked arrows (i.e. arrows without an **A** or **B** label) indicate automatic advancement.
- **Black boxes** indicate a new display screen. **Orange box** is the main menu entry point.
- **Blue boxes** indicate menu options on the current screen. **Green boxes** indicate actions.
- **Red text** indicates that an option that will only appear under a certain condition.

3.4 Acknowledgments

This work was supported by the U.S. NSF (CHE-1152232) and the U.S. Dept. of Defense (JIEDDO/TSWG CB3614).

3.5 References

(1) Askim, J. R.; Mahmoudi, M.; Suslick, K. S. "Optical sensor arrays for chemical sensing: the optoelectronic nose" *Chem. Soc. Rev.* **2013**, *42*, 8649.

(2) McDonagh, C.; Burke, C. S.; MacCraith, B. D. "Optical Chemical Sensors" *Chemical Reviews* **2008**, *108*, 400.

(3) Stewart, S.; Ivy, M. A.; Anslyn, E. V. "The use of principal component analysis and discriminant analysis in differential sensing routines" *Chem. Soc. Rev.* **2014**, *43*, 70.

(4) Diehl, K. L.; Anslyn, E. V. "Array sensing using optical methods for detection of chemical and biological hazards" *Chem. Soc. Rev.* **2013**, *42*, 8596.

(5) Lu, Y. X. "Optical Chemical Sensor Array Based on Functional Nanomaterials" *Prog. Chem.* **2014**, *26*, 931.

(6) Lim, S. H.; Feng, L.; Kemling, J. W.; Musto, C. J.; Suslick, K. S. "An optoelectronic nose for the detection of toxic gases" *Nat. Chem.* **2009**, *1*, 562.

(7) Feng, L.; Musto, C. J.; Kemling, J. W.; Lim, S. H.; Suslick, K. S. "A colorimetric sensor array for identification of toxic gases below permissible exposure limits" *Chem. Comm.* **2010**, *46*, 2037.

(8) Feng, L.; Musto, C. J.; Kemling, J. W.; Lim, S. H.; Zhong, W.; Suslick, K. S. "Colorimetric sensor array for determination and identification of toxic industrial chemicals" *Anal. Chem.* **2010**, *82*, 9433.

(9) Lin, H.; Suslick, K. S. "A Colorimetric Sensor Array for Detection of Triacetone Triperoxide Vapor" *J. Am. Chem. Soc.* **2010**, *132*, 15519.

(10) Zhang, C.; Bailey, D. P.; Suslick, K. S. "Colorimetric sensor arrays for the analysis of beers: A feasibility study" *J. Agric. Food Chem.* **2006**, *54*, 4925.

(11) Zhang, C.; Suslick, K. S. "Colorimetric sensor array for soft drink analysis" *J. Agric. Food Chem.* **2007**, *55*, 237.

(12) Suslick, B. A.; Feng, L.; Suslick, K. S. "Discrimination of complex mixtures by a colorimetric sensor array: Coffee aromas" *Anal. Chem.* **2010**, *82*, 2067.

(13) Chen, Q. S.; Hui, Z.; Zhao, J. W.; Ouyang, Q. "Evaluation of chicken freshness using a low-cost colorimetric sensor array with AdaBoost-OLDA classification algorithm" *Lwt-Food Science and Technology* **2014**, *57*, 502.

(14) Huang, X. W.; Zou, X. B.; Shi, J. Y.; Guo, Y. N.; Zhao, J. W.; Zhang, J. C.; Hao, L. M. "Determination of pork spoilage by colorimetric gas sensor array based on natural pigments" *Food Chemistry* **2014**, *145*, 549.

(15) Li, H. H.; Chen, Q. S.; Zhao, J. W.; Ouyang, Q. "Non-destructive evaluation of pork freshness using a portable electronic nose (E-nose) based on a colorimetric sensor array" *Analytical Methods* **2014**, *6*, 6271.

(16) Li, J. J.; Song, C. X.; Hou, C. J.; Huo, D. Q.; Shen, C. H.; Luo, X. G.; Yang, M.; Fa, H. B. "Development of a Colorimetric Sensor Array for the Discrimination of Chinese Liquors Based on Selected Volatile Markers Determined by GC-MS" *J. Agric. Food Chem.* **2014**, *62*, 10422.

(17) Zaragoza, P.; Ros-Lis, J. V.; Vivancos, J. L.; Martinez-Manez, R. "Proof of concept of using chromogenic arrays as a tool to identify blue cheese varieties" *Food Chemistry* **2015**, *172*, 823.

(18) Shetty, V.; Zigler, C.; Robles, T. F.; Elashoff, D.; Yamaguchi, M. "Developmental validation of a point-of-care, salivary alpha-amylase biosensor" *Psychoneuroendocrinology* **2011**, *36*, 193.

(19) Martinez-Olmos, A.; Capel-Cuevas, S.; Lopez-Ruiz, N.; Palma, A. J.; de Orbe, I.; Capitan-Vallvey, L. F. "Sensor array-based optical portable instrument for determination of pH" *Sensors and Actuators B-Chemical* **2011**, *156*, 840.

(20) Carey, J. R.; Suslick, K. S.; Hulkower, K. I.; Imlay, J. A.; Imlay, K. R. C.; Ingison, C. K.; Ponder, J. B.; Sen, A.; Wittrig, A. E. "Rapid identification of bacteria with a disposable colorimetric sensing array" *J. Am. Chem. Soc.* **2011**, *133*, 7571.

(21) Lonsdale, C. L.; Taba, B.; Queralto, N.; Lukaszewski, R. A.; Martino, R. A.; Rhodes, P. A.; Lim, S. H. "The Use of Colorimetric Sensor Arrays to Discriminate between Pathogenic Bacteria" *Plos One* **2013**, *8*.

(22) Chen, Q. S.; Li, H. H.; Ouyang, Q.; Zhao, J. W. "Identification of spoilage bacteria using a simple colorimetric sensor array" *Sensors and Actuators B-Chemical* **2014**, *205*, 1.

(23) Zaragoza, P.; Fernandez-Segovia, I.; Fuentes, A.; Vivancos, J. L.; Ros-Lis, J. V.; Barat, J. M.; Martinez-Manez, R. "Monitorization of Atlantic salmon (Salmo salar) spoilage using an optoelectronic nose" *Sensors and Actuators B-Chemical* **2014**, *195*, 478.

(24) Ohta, J. *Smart CMOS Image Sensors and Applications*; CRC Press: Boca Raton, 2007.

(25) CMOS Sensor Inc. 300 - 600 DPI Contact Image Sensor. http://www.csensor.com/M116_CIS.htm (accessed 28 January, 2014).

(26) Schwarzer Precision. 100 EC-LC Eccentric Diaphragm Pumps. http://www.schwarzer.com/pages_en/produkt.php?id=191 (accessed 31 January 2014).

(27) Rakow, N. A.; Suslick, K. S. "A colorimetric sensor array for odour visualization" *Nature* **2000**, *406*, 710.

(28) Suslick, K. S. "An optoelectronic nose: "Seeing" smells by means of colorimetric sensor arrays" *MRS Bull.* **2004**, *29*, 720.

(29) Suslick, K. S.; Rakow, N. A.; Sen, A. "Colorimetric sensor arrays for molecular recognition" *Tetrahedron* **2004**, *60*, 11133.

(30) Janzen, M. C.; Ponder, J. B.; Bailey, D. P.; Ingison, C. K.; Suslick, K. S. "Colorimetric sensor arrays for volatile organic compounds" *Anal. Chem.* **2006**, *78*, 3591.

(31) Sen, A.; Albarella, J. D.; Carey, J. R.; Kim, P.; McNamara Iii, W. B. "Low-cost colorimetric sensor for the quantitative detection of gaseous hydrogen sulfide" *Sens. Actuator B* **2008**, *134*, 234.

(32) Lin, H.; Jang, M.; Suslick, K. S. "Preoxidation for colorimetric sensor array detection of VOCs" *J. Am. Chem. Soc.* **2011**, *133*, 16786.

(33) Kolthoff, I. M. *Acid-Base Indicators*; Macmillan: N.Y., 1937.

(34) Petersen, J.; Stangegaard, M.; Birgens, H.; Dufva, M. "Detection of mutations in the β-globin gene by colorimetric staining of DNA microarrays visualized by a flatbed scanner" *Anal. Biochem.* **2007**, *360*, 169.

(35) Walt, D. R. "Fiber Optic Array Biosensors" *BioTechniques* **2006**, *41*, 529.

(36) Steiner, M.-S.; Meier, R. J.; Duerkop, A.; Wolfbeis, O. S. "Chromogenic Sensing of Biogenic Amines Using a Chameleon Probe and the Red−Green−Blue Readout of Digital Camera Images" *Anal. Chem.* **2010**, *82*, 8402.

(37) García, A.; Erenas, M. M.; Marinetto, E. D.; Abad, C. A.; de Orbe-Paya, I.; Palma, A. J.; Capitán-Vallvey, L. F. "Mobile phone platform as portable chemical analyzer" *Sens. Actuator B* **2011**, *156*, 350.

(38) Lapresta-Fernandez, A.; Capitan-Vallvey, L. F. "Multi-ion detection by one-shot optical sensors using a colour digital photographic camera" *Analyst* **2011**, *136*, 3917.

(39) Lapresta-Fernández, A.; Capitán-Vallvey, L. F. "Environmental monitoring using a conventional photographic digital camera for multianalyte disposable optical sensors" *Anal. Chim. Acta* **2011**, *706*, 328.

(40) Dini, F.; Filippini, D.; Paolesse, R.; Lundström, I.; Di Natale, C. "Computer screen assisted digital photography" *Sens. Actuator B* **2013**, *179*, 46.

(41) Iqbal, Z.; Eriksson, M. "Classification and quantitative optical analysis of liquid and solid samples using a mobile phone as illumination source and detector" *Sens. Actuator B* **2013**, *185*, 354.

(42) Vallejos, S.; Munoz, A.; Ibeas, S.; Serna, F.; Garcia, F. C.; Garcia, J. M. "Solid sensory polymer substrates for the quantification of iron in blood, wine and water by a scalable RGB technique" *J. Mater. Chem. A* **2013**, *1*, 15435.

(43) Martinez, A. W.; Phillips, S. T.; Whitesides, G. M.; Carrilho, E. "Diagnostics for the Developing World: Microfluidic Paper-Based Analytical Devices" *Anal. Chem.* **2009**, *82*, 3.

(44) Iqbal, Z.; Bjorklund, R. B. "Colorimetric analysis of water and sand samples performed on a mobile phone" *Talanta* **2011**, *84*, 1118.

(45) Shen, L.; Hagen, J. A.; Papautsky, I. "Point-of-care colorimetric detection with a smartphone" *Lab on a Chip* **2012**, *12*, 4240.

(46) Oncescu, V.; O'Dell, D.; Erickson, D. "Smartphone based health accessory for colorimetric detection of biomarkers in sweat and saliva" *Lab on a Chip* **2013**, *13*, 3232.

(47) Wei, Q.; Nagi, R.; Sadeghi, K.; Feng, S.; Yan, E.; Ki, S. J.; Caire, R.; Tseng, D.; Ozcan, A. "Detection and Spatial Mapping of Mercury Contamination in Water Samples Using a Smart-Phone" *ACS Nano* **2014**, *8*, 1121.

(48) Ellerbee, A. K.; Phillips, S. T.; Siegel, A. C.; Mirica, K. A.; Martinez, A. W.; Striehl, P.; Jain, N.; Prentiss, M.; Whitesides, G. M. "Quantifying Colorimetric Assays in Paper-Based Microfluidic Devices by Measuring the Transmission of Light through Paper" *Anal. Chem.* **2009**, *81*, 8447.

(49) Lee, D.-S.; Jeon, B. G.; Ihm, C.; Park, J.-K.; Jung, M. Y. "A simple and smart telemedicine device for developing regions: a pocket-sized colorimetric reader" *Lab on a Chip* **2011**, *11*, 120.

(50) Flach, P. *Machine Learning: The Art and Science of Algorithms that Make Sense of Data*; Cambridge University Press, 2012.

Chapter 4: Optoelectronic nose for identification of explosives

This chapter taken in large part from the following reference:

Askim, J. R.; Li, Z.; Rankin, J. M.; LaGasse, M. K.; Suslick, K. S. "An Optoelectronic Nose for Identification of Explosives" *Manuscript in preparation* **2015**

4.1 Introduction

Detection and identification of explosive compounds has spawned intensive research in trace detection and rapid screening [1]. Situational requirements must be considered and optimized in order to provide appropriate detection methods; issues of sensitivity, selectivity, speed, analyte scope, environmental tolerance, device size and cost play into the balance between ideal and practical analysis. Single-target colorimetric tests and ion-mobility spectroscopy (IMS) are by far the most commonly-used techniques for explosives detection, as they can be very sensitive, selective, fast, small, and cost-effective [1-5]; these techniques, however, only function for a narrow range of analytes (e.g., individual colorimetric tests are highly specific, and IMS is fairly specific for nitro-organics). In comparison, methods that are useful for a broad range of analytes suffer from other limitations: gas chromatography/mass spectrometry, for example, is relatively slow, expensive, and non-portable [6], and traditional electronic nose technology, as another example, suffers from poor selectivity and environmental tolerance (e.g., changes in humidity) [7-9].

Gas-phase sensing using colorimetric sensor arrays offers an important alternative technique with broad analyte response, high sensitivity, and high selectivity [10-11]. These sensor arrays combine multiple cross-reactive colorimetric sensors that probe a wide range of analyte chemical properties [12-15], including Lewis and Brønsted acidity/basicity, molecular polarity, and redox properties. Colorimetric sensor arrays are cost-effective and have shown high environmental tolerance [10]. Imaging of the sensor ar-

rays has typically used digital cameras or flatbed scanners. Portable imaging methods (including both dedicated and cellphone-based systems) are also currently in development [16-23]. These colorimetric sensor array/imaging systems have been successfully used to differentiate among diverse families of analytes, ranging from toxic industrial chemicals [12,24-26], to various foods and beverages [27-34], to pathogenic bacteria and fungi [35-40]. While the application of optical methods for the detection of explosives has had significant success with fluorescent sensors [41-45], colorimetric sensor arrays for the identification of explosives still have significant room for improvement.

We report here the development of a new colorimetric sensor array and handheld reader for the identification of explosives and their components and describe several new classes of colorimetric sensors including cross-reactive metal-dye salts and other dyes designed to take advantage of the reactivity of carbonyl and nitro compounds. The resulting printed array had forty sensor elements mounted in a snap-together, disposable cartridge (shown in Figure 4.1) with a linear gas flow path. We have applied this array to the identification of sixteen analytes that include common explosives, home-made primary and secondary explosive mixtures, and non-explosive compounds characteristic of military-grade explosives [46-47]. Specifically, the analytes examined herein (with their abbreviations) are ammonium nitrate (farm grade, AN), ammonium nitrate/fuel oil (AN-FO), ammonium nitrate/nitromethane (AN-NM), cyclohexanone ($C_6H_{10}O$), cyclotrimethylenetrinitramine (RDX), 2,3-dimethyl-2,3-dinitrobutane (DMDNB), 2,4-dinitrotoluene (DNT), hydrogen peroxide (H_2O_2), hexamethylene triperoxide diamine (HMTD), nitromethane (NM), nitromethane/ethylene diamine (Picatinny Liquid Explosive, PLX), pentaerythritol tetranitrate (PETN), potassium chlorate/fuel oil ($KClO_3$-FO), potassium chlorate/sugar ($KClO_3$-S), and triacetone triperoxide (TATP).

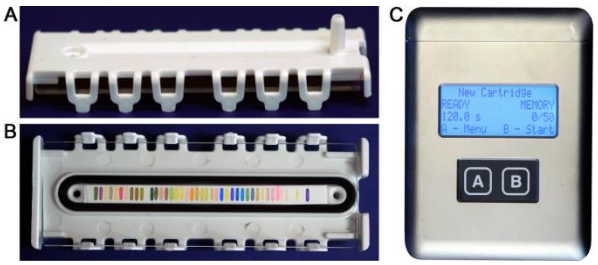

Figure 4.1 Linearized colorimetric sensor array and disposable cartridge. (A) Cartridge side view (7.9 x 2.8 x 1.0 cm). (B) Cartridge front view. (C) Handheld reader (12.8 x 9.5 x 4.0 cm).

4.2 Materials and methods

4.2.1 Array preparation

Colorimetric sensor arrays were printed on polypropylene substrates using a robotic pin printer; the procedure is described in previous works [25]. In this case, custom-designed rectangular pins were used instead of round pins, and 40 spots were printed at 1.2 mm center-center distance.

Polypropylene membranes (0.2 μm) were used as printing substrates for the array and were purchased from Sterlitech Corporation (Kent, WA, USA). All reagents were analytical-reagent grade, purchased from Sigma-Aldrich and used without further purification. Cartridges were custom injection-molded using low-volatility white polycarbonate (Dynamic Plastics, Chesterfield Twp, MI, USA), as shown in Figure 4.1 (a,b). Polypropylene substrates were adhered to cartridges using low-volatility 3M™ 465 Adhesive Transfer Tape (3M Co., St. Paul, Minnesota, USA). Colorimetric sensor arrays were printed on these substrates using procedures described previously[25]; in this case, custom-designed rectangular pins were used instead of round pins, and 40 spots were printed at 1.2 mm center-center distance; images of the pins used are shown in Figure 4.2. The chemoresponsive dyes used in each spot is described in Table 4.1 along with a color-coded legend indicating the intended purpose of each spot (i.e., expected chemical reactivity).

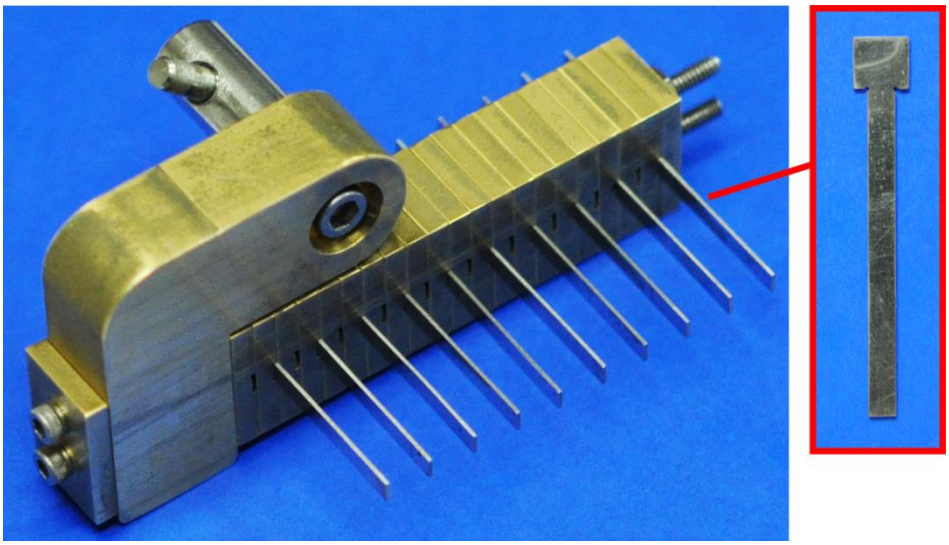

Figure 4.2 Pin holder for rectangular pins used to print linear colorimetric sensor arrays (left) and close-up view of a rectangular pin (right).

Table 4.1 Array composition (top) and category legend (bottom). TsOH = p-toluenesulfonic acid (1M in 2-methoxyethanol); TBAH = tetrabutylammonium hydroxide (40% in H_2O); DNPH = 2,4-dinitrophenylhydrazine.

#	Name	#	Name
1	$FeCl_2$ + Nile Red + TsOH	21	$HgCl_2$ + Bromophenol Blue
2	a-Naphthyl Red + TsOH	22	$LiNO_3$ + Bromocresol Green
3	Tetraiodophenolsulfonephthalein + TsOH	23	$AgNO_3$ + Bromocresol Green
4	Pyrocatechol Violet + TsOH	24	$Pb(OAc)_2$ + Disperse Red
5	Bromocresol Green + TsOH	25	Bromophenol Blue + TBAH
6	Methyl Red + TsOH	26	Methyl Red + TBAH
7	Bromocresol Purple + TsOH	27	Chlorophenol Red + TBAH
8	DNPH + Pararosaniline + TsOH	28	Nitrazine Yellow + TBAH
9	DNPH + Pararosaniline + TsOH	29	Bromothymol Blue + TBAH
10	DNPH + Pararosaniline + TsOH	30	Thymol Blue + TBAH
11	$FeCl_2$ + Nile Red	31	m-Cresol Purple + TBAH
12	ZnTPP	32	N,N'-diphenyl-1,4-diphenyldiamine + TBAH
13	ZnTMP	33	tolidine + TBAH
14	CoTMP	34	o-dianisidine + TBAH
15	CdTPP	35	Nile Red
16	Bromophenol Red	36	Nile Red
17	Bromophenol Blue	37	Merocyanine 540
18	Nile Red	38	1-ethyl-4-(2-hydroxystyryl)pyridinium iodide
19	Acridine Orange Base	39	TBAH
20	$Zn(NO_3)_2$ + Bromophenol Blue	40	Methylene Blue

What	How	Why
DNPH spot	Brady reaction	Ketones and Aldehydes
Locator spot	None, though spot may have other reactivity	Slide edge
Metal salts	Metal complexation	Ligands
pH indicators	pH and Lewis acidity/basicity	Acidic/Basic compounds
Porphyrins	Ligation, Lewis acidity/basicity	Ligands
Redox-sensitive dyes	Fenton chemistry / other oxidation	Redox compounds
Solvatochromic dyes	Solvatochromism	Solvents
Strong base	Meisenheimer adduct formation	Nitroaromatics

4.2.2 Analyte samples

All reagents were purchased from Sigma and used without purification except as follows: generic farm-grade/commercial-grade ammonium nitrate (AN) was purchased from Fredrich Electronics (Boonville, MO). RDX and PETN were supplied by Los Alamos National Labs (Los Alamos, NM). HMTD and TATP was synthesized as described in ref [48]. HMTD was synthesized as described in ref [49] at 1/50 scale. Fuel oil was purchased as diesel fuel from a local gas station. Powdered sugar was purchased from a local market. Detailed composition of all analytes, in addition to a control, are described in Table 4.2. The experimental setup using the handheld imaging device is shown in Figure 4.4.

Table 4.2 Composition of all explosive analytes and related compounds.

Name	Component(s)
control	Ambient lab air (approx. 15% rel. humidity at 24°C)
AN	Ammonium Nitrate, farm grade (FG)
AN-FO	94.48 wt% Ammonium Nitrate, FG + 5.52 wt% Fuel Oil (diesel)
AN-NM	66.30 wt% Ammonium Nitrate, FG + 33.70 wt% Nitromethane
$C_6H_{10}O$	Cyclohexanone
DMDNB	2,3-Dimethyl-2,3-dinitrobutane
DNT	2,4-Dinitrotoluene
H_2O_2	Hydrogen Peroxide (30% in H_2O)
HMTD	Hexamethylene Triperoxide Diamine
NM	Nitromethane
PC-S, $KClO_3$-S	74.12 wt% Potassium Chlorate + 25.88 wt% Powdered Sugar
PC-FO, $KClO_3$-FO	89.73 wt% Potassium Chlorate + 10.27 wt% Fuel Oil
PETN	Pentaerythritol Tetranitrate
PLX	95.00 wt% Nitromethane + 5 wt% Ethylene Diamine
RDX	Cyclotrimethylenetrinitramine
TATP	Triacetone Triperoxide

4.2.3 Array response

Using the onboard micropump, arrays were initially exposed to control media (ambient lab air, ~30% relative humidity at 24°C) for 2 minutes and scanned as a 'before exposure' image. Arrays were then exposed to analyte head space by pumping from sample vials using a short Teflon feed tube (3.8 cm) for 2 minutes and scanned as an 'after exposure' image. Analyte response was calculated by calculating the difference between the measured red, green, and blue (RGB) values before and after exposure (e.g., R_{after} - R_{before}). Seven independent samples were measured for each analyte.

Difference maps (for visualization) were constructed by taking the absolute value and scaling a relevant color range (indicated on each difference map) to the 8-bit color scale (i.e., 0-255). For S/N measurements, signal and noise were calculated for each dimension using all trials in the control data set (i.e., each of red, green, and blue values for each sensor element; total of 120 dimensions for an array with 40 sensor elements); signal for each dimension was defined as the difference between each

analyte trial measurement and the control average (e.g., $R_{analyte\text{-}n}$ - $R_{control\text{-}avg}$) and noise was defined as the standard deviation in the control data set (e.g., $\sigma_R^2 = \Sigma_n(R_{control\text{-}n} - R_{control\text{-}avg})^2/(N\text{-}1)$).

4.2.4 ^{1}H-NMR spectra of DMDNB and PETN

^{1}H-NMR spectra of DMDNB (2,3-dimethyl-2,3-dinitrobutane) and PETN (pentaerythritol tetranitrate) were collected with a Varian 500 MHz NMR spectrometer with a narrow-bore coil (Varian Inc, Palo Alto, CA, USA). The limit of detection of this method was defined as the point at which peaks could no longer be resolved from baseline noise (i.e., 3*100 mol % / $\sigma_{baseline}$).

4.2.5 Attempts to detect $KClO_3$ mixture volatile species

Control samples and samples of $KClO_3$ and $KClO_3$+Sugar were analyzed using solid-phase micro-extraction (SPME) and iodometry ($KClO_3$+Fuel Oil was deliberately avoided due to the large amounts of volatile hydrocarbons expected). For SPME, a PDMS/DVB fiber (Supelco, Bellefonte, PA) was exposed to headgas of the samples in 2 mL vials fitted with teflon septa for 60 seconds. Fibers were analyzed with an Agilent 7890A GC at an injector temperature of 200°C. SPME desorption time was 2 min onto a Restek TRX-5 SILMS capillary GC column. Carrier gas was helium (1 mL/min); initial oven temperature was maintained at 100°C for 2 min and increased by 7.5°C/min for 20 min (total run time 22 min). No peaks were discernible from the baseline. We interpret this as the failure to detect any volatile organic species, which are primarily expected to be oxidation products.

For iodometry, headspace was sampled from 7 mL vials identically to experimental trials using the handheld reader, except that an impinger was inserted between the sample vial and the colorimetric sensor array and gas was collected for 1 hour. The impinger contained 50 mL of 2 wt% KI in deionized water and was fitted with a stainless steel gas dispersion frit in order to maximize bubble surface area. Following collection, 1 mL of liquid from the impinger was added to 100 μL of starch indicator solution (1

mg/mL in H_2O), acidified with 20 μL of 1M TsOH, stirred, and allowed to sit for 10 minutes. $KClO_3$ samples showed no color change. We interpret this as the failure to detect oxidizing species (e.g., ClO, ClO_2, Cl_2, etc).

4.2.6 Sampling protocol

Samples were prepared by weighing 100 mg of each analyte into 7 mL scintillation vials; fuel-oxidizer mixtures were prepared based on a 1:1 stoichiometric ratio. TATP and HMTD instead used 20 mg samples in order to reduce risks during synthesis and storage. All sample vials were sealed with air-tight Teflon-lined caps and equilibrated for 12 h before testing, which permits complete saturation of the head volume of the vial. *Safety note: screw-type caps should not be used for explosive materials - particles caught in the threading potentially can explode when caps are screwed down.*

The limits of detection (LODs) for this sampling protocol were estimated for AN, NM, and DNT samples (representing highly responsive, moderately responsive, and weakly responsive analytes respectively) using sample masses ranging from 0.5-100 mg; calculated LODs were as follows: AN (0.13 mg), NM (0.52 mg), DNT (1.8 mg). Limits of detection were calculated as follows. Response values for a control sample were collected in septuplicate. Response values were also collected in triplicate trials at several different sample masses: AN: 0.5 mg, 1 mg, 2 mg, 5 mg, 10 mg, 20 mg; NM: 2 mg, 5 mg, 10 mg, 20 mg, 50 mg; DNT: 5 mg, 10 mg, 20 mg, 50 mg. A single-point LOD was then calculated for each dimension using $LOD_{single} = 3 * StDev_{control} / (Response_{Avg\ Trial} - Response_{Avg\ Control})$. Plotting LOD_{single} vs. sample mass, second-order least-squares interpolation gave polynomials of the form $Ax^2 + Bx + C$ with the following R^2 values: AN (0.999158), NM (0.990908), DNT (0.997853). These 2nd order polynomials were then solved for y = x, corresponding to the position where the calculated LOD was equal to the sample mass. Note that single-point LOD estimates calculated using the lowest tested sample mass (AN: 0.5 mg, NM: 2 mg, DNT: 5 mg) were only 30-40% higher than values calculated using quadratic fitting.

4.2.7 Database analysis and classification

Hierarchical cluster analysis (HCA) was performed using using Ward's method (i.e., total Euclidean distance variance minimization) with Matlab software (MathWorks Inc, Natick, MA, USA). Principal component analysis (PCA) was performed using MVSP software (Kovach Computing Services, Pentraeth, Isle of Anglesey, UK). Support vector machine (SVM) analysis was performed using custom software making use of LIBSVM, an open source SVM library, using a linear kernel with default parameters [50].

4.3 Results and discussion

4.3.1 Handheld reader details

The portable reader used in this work uses a compact color line imager (contact image sensor, or CIS) combined with a linear chemoresponsive dye array. CIS operation is shown schematically in ref [51]. The reader itself is shown in Figure 4.3 and specifications are provided in Table 4.3. As indicated, the analyte gas flow path is directly from the sample container into the cartridge over the sensor array and out through a diaphragm micropump (Schwarzer SP100-ECLC), which minimizes the possibility of cross-contamination. Illumination levels for the red, green, and blue (RGB) LEDs were controlled using a combination of applied voltage and pulse-width modulation. Raw data was normalized using a calibration created from a one-time measurement of a 0% reflectance standard (i.e., the sensor array with all LEDs turned off) and a 100% reflectance standard (i.e., a blank array without any sensor dye elements printed on it).

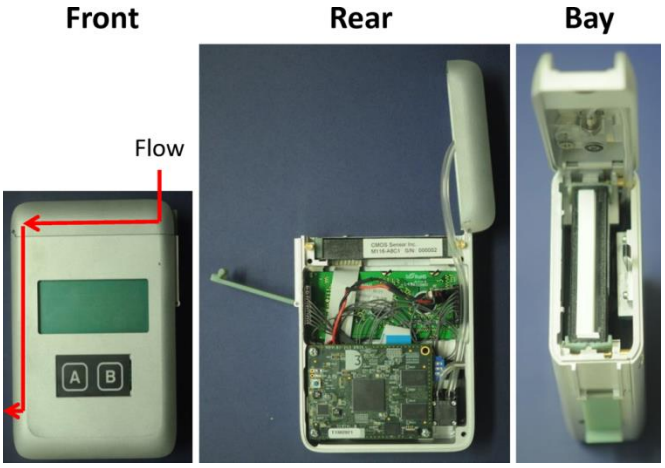

Figure 4.3 Photographs of the handheld reader including front, rear, and cartridge bay views. Dimensions are 12.5 cm tall by 9.5 cm wide by 4.0 cm thick. The rear panel and 9 V battery were removed in order to provide a better view of the internal electronics and diaphragm micropump (located in rear image, lower right).

Table 4.3 Relevant component parameters of the handheld reader.

Scanner Size	12.8 cm x 9.5 cm x 4.0 cm
Scanner Weight	460 g + battery + cartridge
Cartridge Size	7.9 cm x 2.8 cm x 1.0 cm
Cartridge Weight	11 g
Battery Weight	48 g
Static Pressure	550 mbar typical
Pump Rate	580 cm^3/min typical
Current Draw	~400 mA
Battery Charge	1200 mAh typical
Samples/Battery	100 typical

4.3.2 Colorimetric sensor array

Colorimetric sensor arrays make use of multiple cross-reactive dyes in order to give analyte specificity [10-11]. Such arrays are robotically printed and disposable [10,25]. In order to develop a colorimetric

sensor array for explosive analytes, several dyes previously found to be broadly cross-reactive (i.e., in discriminating among toxic chemicals [12,24-25], oxidants [26], and common organic solvents [52]) were optimized; these included acid and base-treated pH indicators, Lewis acids, redox-sensitive dyes and chromogens, and solvatochromic dyes formulated with immobilization matrices for printing (Table 4.1). In addition, several chromogenic species were added to the array to target specific analytes important to the identification of explosives, as discussed below.

Hydrogen peroxide. The array sensor elements responsible for the detection of H_2O_2 are based on Fenton's reagent [53] and on well-established redox indicators [26]. Acidified ferrous chloride was combined with an empirically-optimized dye (Nile Red, a very intense, neutral, solvatochromic and pH-responsive dye with a highly conjugated structure) in a printable plasticized medium. When exposed to H_2O_2 vapor, the green-blue sensor spot turns yellow-brown as the dye is oxidized by radicals produced catalytically by reaction with Fe^{2+}/Fe^{3+}.

Cyclohexanone. Acidified 2,4-dinitrophenylhydrazine (DNPH), also known as Brady's reagent [6], was combined with an empirically-optimized dye (Pararosaniline, a cationic triphenylmethane dye). When exposed to ketones such as cyclohexanone, the red-orange sensor spot turns yellow-brown. There is evidence suggesting that this mixture forms the DNPH analog of Schiff's reagent [54]; of the several pH indicators tested, only triphenylmethane dyes (e.g. methyl violet, crystal violet, pararosaniline, etc.) showed any reaction and the color of these dyes changed significantly upon addition of the DNPH reagent, which suggests the specific involvement of reactions between DNPH and the dyes.

Nitro-organics. Two strategies were employed for the detection of nitro-organic compounds. First, the use of tetrabutylammonium hydroxide was incorporated into the array for the formation of Meisenheimer complexes with nitroaromatic compounds (2,4-dinitrotoluene) [55]; under the sampling conditions and concentrations use, however, this approach proved to be of limited effectiveness. Second, a family of chemoresponsive metal cation dye anion salts were created *in situ* by reaction of the

acidic form of dyes and the metal chloride or nitrate salts. A large number of alkali and transition metal ions were screened, and Ag^{+}, Li^{2+}, Hg^{2+}, and Zn^{2+} were found to be the most responsive. Screening of pH indicator dyes revealed bromocresol green (pH range ~3.8-5.4) and bromophenol blue (pH range ~3.0-4.6) to be effective. Further investigation of these salts and the origin of their colorimetric response is ongoing.

4.3.3 Array response

Analytes were tested using a field-appropriate sampling protocol; milligram-scale samples (100 mg for most analytes, 20 mg for HMTD and TATP) were stored in small glass vials and the headspace was sampled through a short Teflon tube while open to the ambient environment (Figure 4.4). The data was collected in septuplicate trials for each analyte and consisted of red, green, and blue (RGB) values measured for each of 40 printed sensor elements in the array before and after exposure using an optical line imager (12-bit contact image sensor, CIS). The resulting 120-dimensional difference vectors had values ranging from -100% to +100% reflectance change. Graphical representations of the average signal/noise vectors (i.e., scaled color difference maps) for each analyte class are shown in Figure 4.5. These difference maps demonstrate a broad range of response patterns, which are discernable even by eye. Among analytes of similar chemical composition, the array responses are similar, but still differentiable. One example showing a graphical form of subtraction on raw images is shown as Figure 4.6; note that this was figure was generated by subtracting the numeric values and constructing a bitmap for visualization. Average difference maps for each analyte class and the control are shown in Figure 4.7. As shown, the array responses vary considerably across the range of tested analytes.

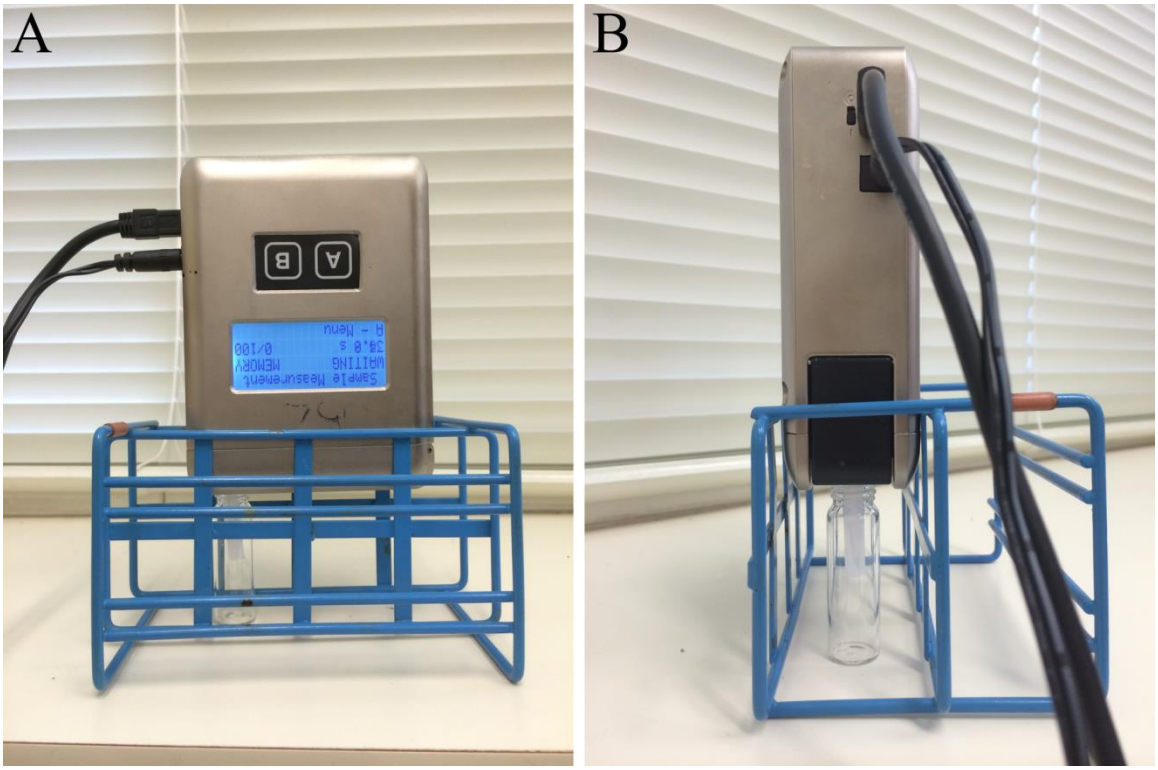

Figure 4.4 Image of sampling procedure. The handheld device was held in a metal rack with a tube inserted into a glass vial containing the analyte, shown from the (A) front, and (B) side. The array cartridge is attached to a short feed tube (3.8 cm). Prior to analyte headspace sampling, the array is equilibrated to the ambient background atmosphere for 2 minutes. The feed tube is then inserted into a 7 mL glass vial for headspace sampling, and measurements were collected after 2 minutes of exposure to sample headspace at a flow rate of approximately 580 cm^3/minute (sccm).

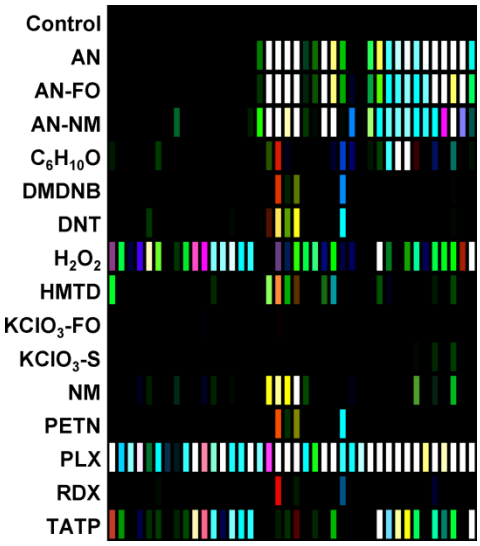

Figure 4.5 Difference maps of the 40-element colorimetric sensor array showing signal-to-noise of 16 explosives, related analytes, and the control. S/N ratios of 3-10 were scaled for display on an 8-bit RGB color scale (i.e., 0-255). The average response of all analytes except for $KClO_3$-Sugar and $KClO_3$-Fuel Oil are obviously detectable.

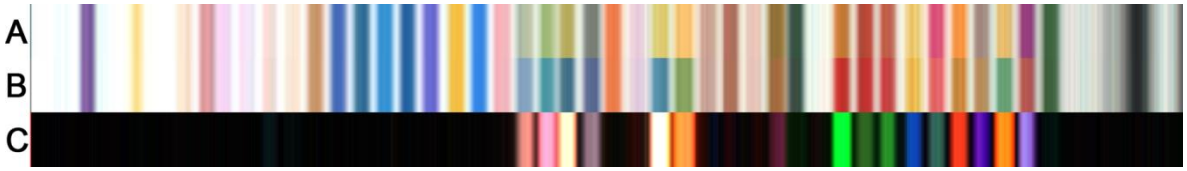

Figure 4.6 Raw sensor images collected before (A) and after (B) exposure to AN head gas, and a scaled difference map (C, RGB color range 0-16 scaled to 0-255).

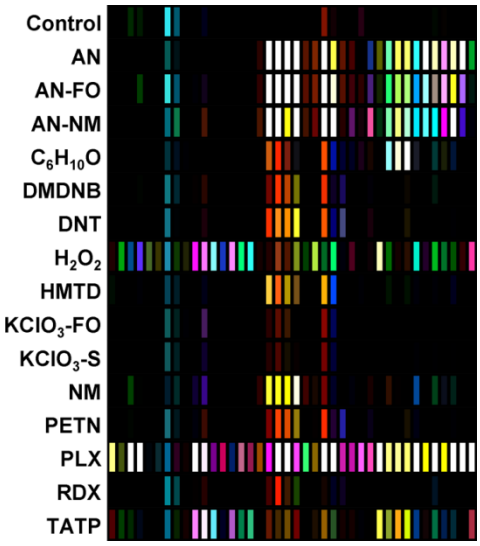

Figure 4.7 Average sensor response vectors of 15 explosives and related compounds. Normalized reflectance values were scaled so that the relevant response range (i.e., 0.39% to 3.9% of maximum reflectance) is displayed on an 8-bit RGB color scale (i.e., 0-255).

4.3.4 Database evaluation

Hierarchical cluster analysis (HCA) was used to give a preliminary evaluation of the acquired database and the relative similarities among the data collected. HCA is an unsupervised evaluation technique that groups array response data in the full 120-dimensional vector space (i.e., color difference changes in red, green, and blue for each of the 40 sensor elements on the colorimetric sensor array); starting with single data points, clusters are formed hierarchically by connecting the centroids of unconnected clusters or data points (in this case using Ward's method, which minimizes the total within-cluster variance). The resulting dendrogram shows connectivity (indicates which clusters are most similar to each other), and inter-cluster distance (describes the magnitude of similarity). The HCA dendrogram for the response of these common explosives is shown as Figure 4.8. The method shows obvious discrimination among 11 of the 16 analytes (including the control). Confusions of clustering were observed among the group containing the weakly-responding potassium chlorate mixtures ($KClO_3$-Fuel Oil

and $KClO_3$-Sugar) and separately among the group containing nitroalkyls and nitroamines (PETN, RDX, and DMDNB).

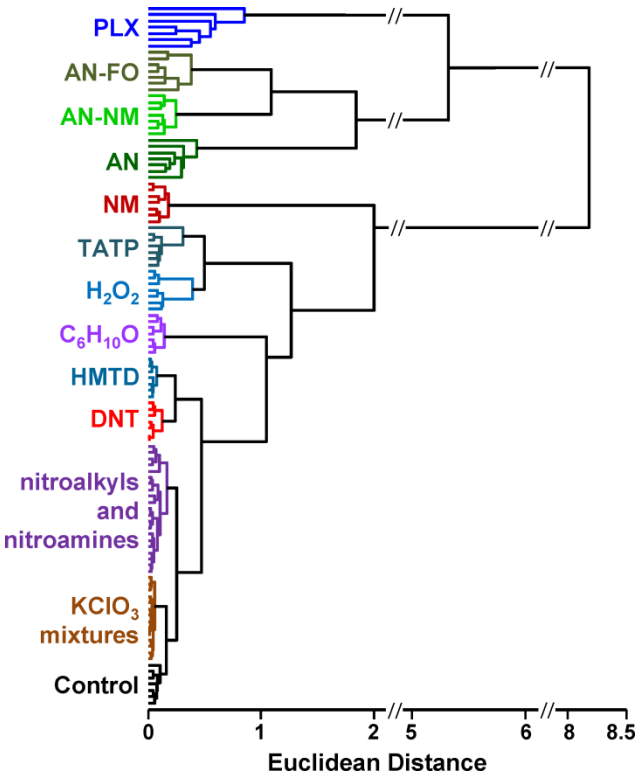

Figure 4.8 Hierarchical cluster analysis (HCA) of the normalized difference vectors (i.e., changes in reflectance) for 16 explosives, related analytes, and the control; 112 trials in total. All species were clearly differentiable except among members of two groups: KClO3 mixtures (KClO3-Sugar and KClO3-Fuel Oil) and nitroalkyls/nitroamines (DMDNB, PETN, and RDX).

In addition to HCA, principal component analysis (PCA) [56-59] was employed to provide an estimation of the dimensionality of the data acquired with the colorimetric sensor array, which is itself a measure of the dimensionality of the chemical reactivity space probed by the sensor array. PCA is an unsupervised statistical approach that generates a set of orthogonal vectors (i.e., principal components) using a linear combination of array response vectors to maximize the amount of variance in each principal

component. A scree plot of the normalized data is given in Figure 4.9. A total of 10 dimensions were required to capture 90% of the total variance and 16 dimensions for 95% of the total variance; this strongly suggests that the colorimetric sensor array is probing a very broad range of chemical reactivities, as intended. The high dimensionality of this sensor array is in stark contrast to traditional electronic nose sensor arrays in which only 1 or 2 dimensions are required to reach 95% of the total variance (in these cases, the sensor array is probing only a very limited range of chemical properties, e.g., hydrophobicity).

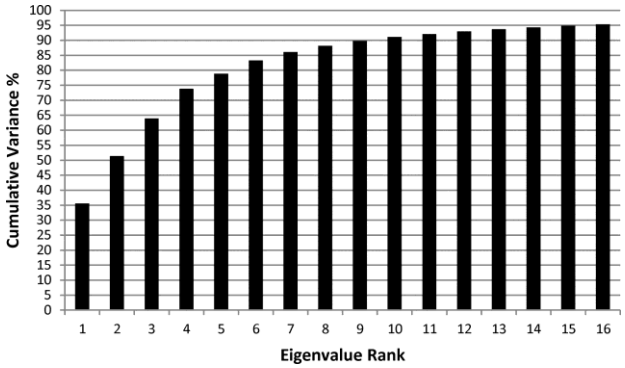

Figure 4.9 Scree plot of the principal component analysis for 15 explosives and related compounds. 10 dimensions were required to account for 90% of the total variance and 16 dimensions for 95% of the total variance, which strongly suggests that the colorimetric sensor array probes a broad range of chemical reactivity.

The high dimensionality of the colorimetric sensor arrays also makes PCA unsuitable for use in discrimination among analyte species: too little of the variance is captured in two or three dimensions to avoid overlap of analyte classes, and in fact, PCA score plots show significant overlap among classes even among samples that show obvious qualitative differences in response (Figure 4.10). In order to demonstrate how this translates into discrimination ability (or lack thereof) and compare this sensor array to other works using PCA for analysis, the first four principal components were plotted as shown in Figure 4.20. Upon cursory examination, it is obvious that PCA using the first two dimensions provides

adequate discrimination for some analytes (e.g., AN, AN-NM, AN-FO, NM, etc) but shows essentially no discrimination for others (e.g., both nitroalkanes, both chlorate-containing analytes, and HMTD all appear to be inseperable using the first two dimensions). Extending this to the third and fourth dimensions, additional analytes are able to be discriminated (TATP, H_2O_2, cyclohexanone, etc) but there is still significant overlap among many analytes.

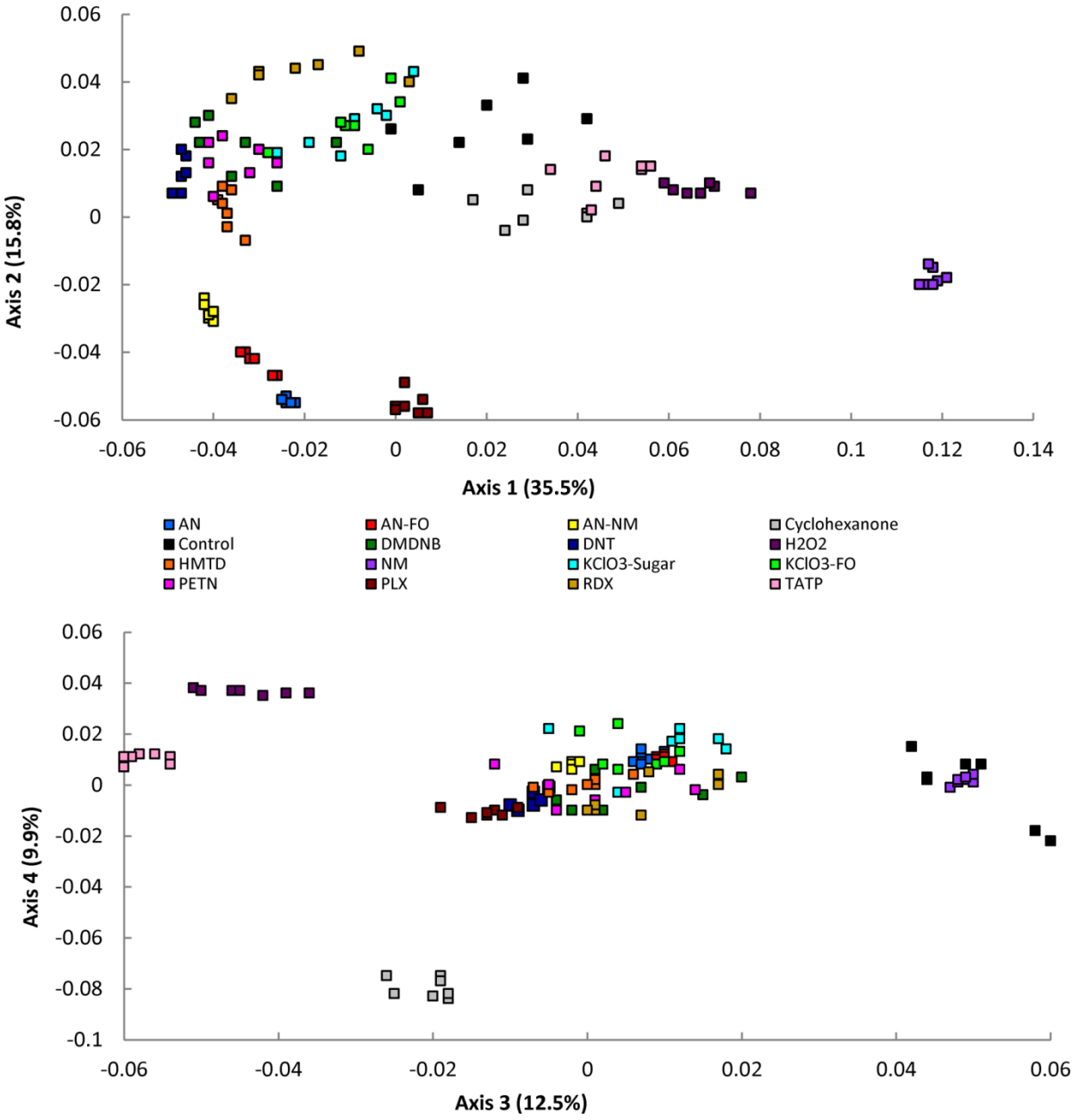

Figure 4.10 PCA score plots showing the first four principal component axes. The first four components show essentially no discrimination among several analyte classes (e.g., nitroalkanes, chlorate-containing species, HMTD).

4.3.5 Classification using Support Vector Machines (SVM)

PCA and HCA are unsupervised analysis tools for an existing data set, and they are inherently not well suited for predictive (i.e., classification) use. They provide no direct method for classification of unknown data. For example, if one were to use PCA for classification of unknown data, a decision method must be implemented using a set of criteria. In datasets where PCA plots do provide good discrimination in 1 or 2 dimensions [11], one can do a simple supervised pairwise comparison by manually drawing a line connecting the two clusters and setting the decision value somewhere in the middle; unknown data is then projected onto that line and compared to the decision value (note that this is identical to separation using a dividing plane). Using this method, PCA is essentially a form of optimization for the decision boundaries. PCA, however, does not optimize differentiation among analyte classes—instead it simply minimizes the number of dimensions needed to describe the shape of the dataset.

There are other methods of optimizing decision boundaries in higher dimensional space that do not require projection onto a one or two dimensional space (as in PCA). Specifically, here we make use of a common machine learning tool, support vector machine (SVM) analysis. Unlike unsupervised methods such as PCA, HCA, or other clustering methods, SVM is a predictive method that is designed to classify incoming data that is not part of the training database. SVM classification is based on pairwise class prediction and focuses on the data most likely to be misclassified (i.e., data near the decision boundary for any given class pair, the so-called support vectors) to create decision boundaries that best separate the data for any given pair of classes in high dimensional space. The result of each pairwise comparison gives a vote that is used to determine the final classification [60]. SVM optimization factors have been fully developed and incorporated into LIBSVM, an open-source SVM library [50].

Compared to PCA, SVM is better optimized for discrimination of multidimensional data: PCA describes the shape of the entire data set, while SVM maximizes discrimination ability. Implementation of SVM requires multiple rounds of iteration and optimization parameters. In this work, class data was

found to be roughly normally distributed and no data transformation was necessary (i.e., a linear kernel was used). Default SVM parameters were found to be quite well-optimized for the colorimetric sensor array database; this is not surprising, since HCA results already showed a high level of separation using a Euclidean distance clustering method. Classifiers took the form of a decision hyperplane based on a 120-dimensional vector (i.e., optimized linear combinations of ΔRGB values of the sensor array) combined with a scalar decision value.

Classification accuracy. Classification accuracy of the SVM method was estimated using cross-validation which split the database and created classifiers based on training and evaluation data sets. Cross-validation results using a leave-one-out permutation method are shown in Table 4.4. Interestingly, the two $KClO_3$ mixtures (KClO3-Sugar and KClO3-Fuel Oil) and nitroalkanes (DMDNB and PETN) were non-separable within their respective groupings, but the method showed no other misclassifications.

Table 4.4 Support vector machine (SVM) classification results (i.e., leave-one-out cross-validations of 112 permutations) of 16 common explosives, related compounds, and the control. The Accuracy column shown for each analyte represents the percentage of correctly identified analytes among 7 independent trials. Similarly, the Misidentifications column indicates which incorrect classifications were supplied by the algorithm.

Analyte	Accuracy	Misidentifications
control	100% (7/7)	
AN	100% (7/7)	
AN-NM	100% (7/7)	
AN-FO	100% (7/7)	
$C_6H_{10}O$	100% (7/7)	
DNT	100% (7/7)	
H2O2	100% (7/7)	
HMTD	100% (7/7)	
NM	100% (7/7)	
PLX	100% (7/7)	
RDX	100% (7/7)	
TATP	100% (7/7)	
KClO3-Sugar	86% (6/7)	KClO3-FO (1/7)
KClO3-FO	57% (4/7)	KClO3-Sugar (3/7)
DMDNB	0% (0/7)	PETN (7/7)
PETN	14% (1/7)	DMDNB (6/7)

In the case of the $KClO_3$ mixtures, both analytes have very low response but all individual trials were distinguishable from the control group. Neither $KClO_3$ nor sucrose or corn starch (the primary additive in commercial sugar) are sufficiently volatile to provide a strong response and the sensor array is known to be insensitive to hydrocarbons [61]; confusions among the chlorate analytes are therefore unsurprising. We are not confident in the colorimetric sensor array's ability to detect these species: the maximum signal in all $KClO_3$ mixture samples barely exceeds estimated detection requirements (maximum S/N ~9, estimated detection limit requires S/N ~8-9) and no volatile reactants were detected using headspace analysis with either solid phase microextraction or iodometry. The origin of any apparent detection of $KClO_3$ mixtures and discrimination from control samples remains an open question.

Since DMDNB and PETN were unable to be distinguished from each other, it was suspected that the PETN sample may contain significant amounts of DMDNB (which is commonly used as a taggant for PETN and other explosives). The absence of any detectable DMDNB peak in the PETN spectrum (Figure 4.21) indicates that the amount of DMDNB present in the PETN sample is less than the detection limit of the method, which was estimated to be approximately 0.02 mol %. This detection limit is slightly below the concentration expected for a standard taggant (~ 0.04 mol %) [9,62-63]. Based on this, it is unlikely that the response of both analytes is due to the same compound, since that compound would have to be very volatile as well as highly reactive due to its low concentration. The similarity in array response is then likely due to the similar chemical reactivity of the two analytes; the array cannot distinguish between these two nitroalkyl species.

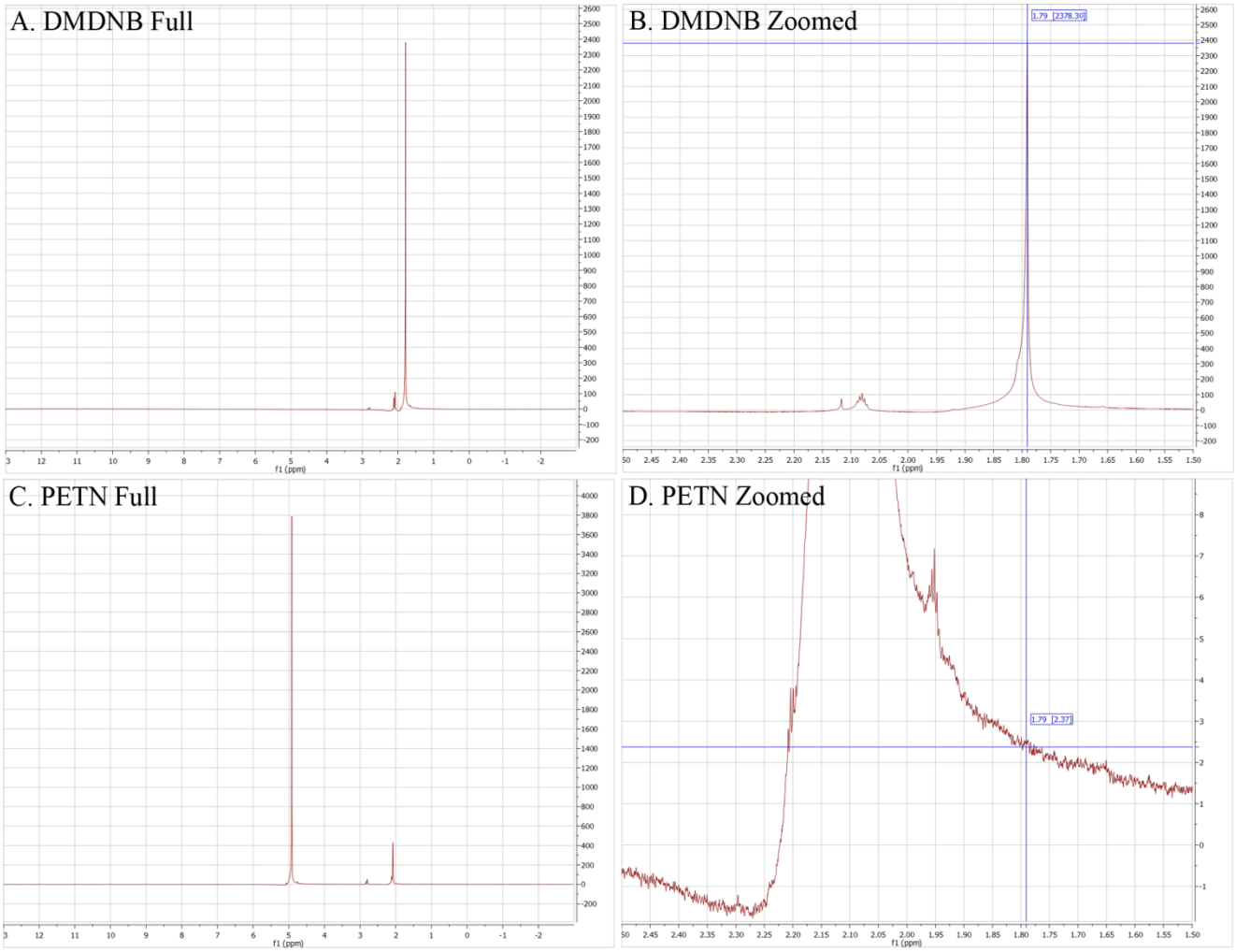

Figure 4.11 ^{1}H-NMR spectra of DMDNB and PETN showing both a full range and zoomed in on the primary DMDNB peak at 1.79 ppm.

Such grouping does not diminish the utility of the method: $KClO_3$ is the relevant component in its explosive mixtures (it will react with essentially any oxidizable material), and both DMDNB and PETN are similar nitro-organics; also, DMDNB is commonly used as a volatile taggant for explosives containing the less-volatile PETN and RDX at a recommended concentration of 0.05 wt% [9,62-63]. Confusions were only observed within each of these groups. If one re-analyzes all the data with 14 classes (i.e., including groupings of chlorate mixtures and nitroalkanes), SVM accuracy is raised to 100%. In comparison to HCA, SVM was able to perform classification of new data and could completely differentiate RDX (a nitroamine) from DMDNB and PETN (nitroalkanes).

4.4 Conclusion

A colorimetric sensor array was developed for classification of common explosives and related compounds representing a broad range of relevant species and chemical reactivity. The array incorporates pH indicators, metal-dye salts, redox-sensitive chromogenic compounds, solvatochromic dyes, and other reactive chromogenic mixtures designed to take advantage of the unique reactivity of carbonyl and nitro compounds; ultimately, this results in a highly cross-reactive sensor array capable of probing a very large range of chemical reactivities. Experiments were performed with a specially-designed handheld system making use of a linear color contact image sensor; the handheld unit provided automated classification without operator input. Based on cross-validation results, support vector machine analysis was able to discriminate 16 separate analytes into 14 groups with an estimated acccuracy approaching 100%. This method has significant implications in portable explosives identification and may prove to be a useful supplement to other current technologies.

4.5 Acknowledgments

The authors thank Ray Martino, Sung Lim, and Richard Huang of iSense, LLC / Metabolomx for helpful discussions. We also thank Dana Dlott of the University of Illinois for providing explosives samples and Will Bassett of the University of Illinois for assistance with explosives synthesis and handling. This work was supported by the U.S. NSF (CHE-1152232) and the U.S. Dept. of Defense (JIEDDO/TSWG CB3614).

4.6 References

(1) Beveridge, A. *Forensic Investigation of Explosions, Second Edition*; CRC Press, 2011.
(2) Germain, M. E.; Knapp, M. J. *Chem. Soc. Rev.* **2009**, *38*, 2543.
(3) Buryakov, I. A. *J Anal Chem* **2011**, *66*, 674.
(4) Mäkinen, M.; Nousiainen, M.; Sillanpää, M. *Mass Spectrometry Reviews* **2011**, *30*, 940.
(5) Caygill, J. S.; Davis, F.; Higson, S. P. J. *Talanta* **2012**, *88*, 14.
(6) Poole, C. F. *Gas Chromatography*; Elsevier Science: Oxford, UK, 2012.
(7) Stitzel, S. E.; Aernecke, M. J.; Walt, D. R. *Annu. Rev. Biomed. Eng.* **2011**, *13*, 1.
(8) Röck, F.; Barsan, N.; Weimar, U. *Chem. Rev.* **2008**, *108*, 705.
(9) Nakamoto, T.; Ishida, H. *Chem. Rev.* **2008**, *108*, 680.

(10) Askim, J. R.; Mahmoudi, M.; Suslick, K. S. *Chem. Soc. Rev.* **2013**, *42*, 8649.

(11) Diehl, K. L.; Anslyn, E. V. *Chem. Soc. Rev.* **2013**, *42*, 8596.

(12) Lim, S. H.; Feng, L.; Kemling, J. W.; Musto, C. J.; Suslick, K. S. *Nat. Chem.* **2009**, *1*, 562.

(13) Janzen, M. C.; Ponder, J. B.; Bailey, D. P.; Ingison, C. K.; Suslick, K. S. *Anal. Chem.* **2006**, *78*, 3591.

(14) Suslick, K. S. *MRS Bull.* **2004**, *29*, 720.

(15) Rakow, N. A.; Suslick, K. S. *Nature* **2000**, *406*, 710.

(16) García, A.; Erenas, M. M.; Marinetto, E. D.; Abad, C. A.; de Orbe-Paya, I.; Palma, A. J.; Capitán-Vallvey, L. F. *Sens. Actuator B* **2011**, *156*, 350.

(17) Iqbal, Z.; Bjorklund, R. B. *Talanta* **2011**, *84*, 1118.

(18) Iqbal, Z.; Eriksson, M. *Sens. Actuator B* **2013**, *185*, 354.

(19) Oncescu, V.; O'Dell, D.; Erickson, D. *Lab on a Chip* **2013**, *13*, 3232.

(20) Salles, M. O.; Salles, G. N.; Meloni, W. R.; de Araujo, T. R. L. C.; Paixão *Anal. Methods* **2014**, *6*, 2047.

(21) Shen, L.; Hagen, J. A.; Papautsky, I. *Lab on a Chip* **2012**, *12*, 4240.

(22) Vallejos, S.; Munoz, A.; Ibeas, S.; Serna, F.; Garcia, F. C.; Garcia, J. M. *J. Mater. Chem. A* **2013**, *1*, 15435.

(23) Wei, Q.; Nagi, R.; Sadeghi, K.; Feng, S.; Yan, E.; Ki, S. J.; Caire, R.; Tseng, D.; Ozcan, A. *ACS Nano* **2014**, *8*, 1121.

(24) Feng, L.; Musto, C. J.; Kemling, J. W.; Lim, S. H.; Suslick, K. S. *Chem. Comm.* **2010**, *46*, 2037.

(25) Feng, L.; Musto, C. J.; Kemling, J. W.; Lim, S. H.; Zhong, W.; Suslick, K. S. *Anal. Chem.* **2010**, *82*, 9433.

(26) Lin, H.; Suslick, K. S. *J. Am. Chem. Soc.* **2010**, *132*, 15519.

(27) Zhang, C.; Bailey, D. P.; Suslick, K. S. *J. Agric. Food Chem.* **2006**, *54*, 4925.

(28) Zhang, C.; Suslick, K. S. *J. Agric. Food Chem.* **2007**, *55*, 237.

(29) Suslick, B. A.; Feng, L.; Suslick, K. S. *Anal. Chem.* **2010**, *82*, 2067.

(30) Chen, Q. S.; Hui, Z.; Zhao, J. W.; Ouyang, Q. *Lwt-Food Science and Technology* **2014**, *57*, 502.

(31) Huang, X. W.; Zou, X. B.; Shi, J. Y.; Guo, Y. N.; Zhao, J. W.; Zhang, J. C.; Hao, L. M. *Food Chemistry* **2014**, *145*, 549.

(32) Li, H. H.; Chen, Q. S.; Zhao, J. W.; Ouyang, Q. *Anal. Methods* **2014**, *6*, 6271.

(33) Li, J. J.; Song, C. X.; Hou, C. J.; Huo, D. Q.; Shen, C. H.; Luo, X. G.; Yang, M.; Fa, H. B. *J. Agric. Food Chem.* **2014**, *62*, 10422.

(34) Zaragoza, P.; Ros-Lis, J. V.; Vivancos, J. L.; Martinez-Manez, R. *Food Chemistry* **2015**, *172*, 823.

(35) Rangin, M.; Basu, A. *J. Am. Chem. Soc.* **2004**, *126*, 5038.

(36) Phillips, R. L.; Miranda, O. R.; You, C.-C.; Rotello, V. M.; Bunz, U. H. F. *Angew. Chem. Int. Ed.* **2008**, *47*, 2590.

(37) Carey, J. R.; Suslick, K. S.; Hulkower, K. I.; Imlay, J. A.; Imlay, K. R. C.; Ingison, C. K.; Ponder, J. B.; Sen, A.; Wittrig, A. E. *J. Am. Chem. Soc.* **2011**, *133*, 7571.

(38) Lonsdale, C. L.; Taba, B.; Queralto, N.; Lukaszewski, R. A.; Martino, R. A.; Rhodes, P. A.; Lim, S. H. *Plos One* **2013**, *8*.

(39) Chen, Q. S.; Li, H. H.; Ouyang, Q.; Zhao, J. W. *Sensors and Actuators B-Chemical* **2014**, *205*, 1.

(40) Zaragoza, P.; Fernandez-Segovia, I.; Fuentes, A.; Vivancos, J. L.; Ros-Lis, J. V.; Barat, J. M.; Martinez-Manez, R. *Sensors and Actuators B-Chemical* **2014**, *195*, 478.

(41) Yang, J.-S.; Swager, T. M. *J. Am. Chem. Soc.* **1998**, *120*, 11864.

(42) Yang, J.-S.; Swager, T. M. *J. Am. Chem. Soc.* **1998**, *120*, 5321.

(43) McQuade, D. T.; Pullen, A. E.; Swager, T. M. *Chem. Rev.* **2000**, *100*, 2537.

(44) Thomas, S. W.; Joly, G. D.; Swager, T. M. *Chem. Rev.* **2007**, *107*, 1339.

(45) Rochat, S.; Swager, T. M. *ACS Appl. Mater. Interfaces* **2013**, *5*, 4488.

(46) Lee, D.-S.; Jeon, B. G.; Ihm, C.; Park, J.-K.; Jung, M. Y. *Lab on a Chip* **2011**, *11*, 120.

(47) McDonagh, C.; Burke, C. S.; MacCraith, B. D. *Chem. Rev.* **2008**, *108*, 400.

(48) Peterson, G. R.; Bassett, W. P.; Weeks, B. L.; Hope-Weeks, L. J. *Cryst. Growth Des.* **2013**, *13*, 2307.

(49) Wierzbicki, A.; Salter, E. A.; Cioffi, E. A.; Stevens, E. D. *J. Phys. Chem. A* **2001**, *105*, 8763.

(50) Chang, C.-C.; Lin, C.-J. *ACM Trans. Intell. Syst. Technol.* **2011**, *2*, 1.

(51) CMOS Sensor Inc. 300 - 600 DPI Contact Image Sensor. http://www.csensor.com/M116_CIS.htm (accessed 28 January, 2014).

(52) Rankin, J. M.; Zhang, Q.; LaGasse, M. K.; Zhang, Y.; Askim, J. R.; Suslick, K. S. *Analyst* **2015**.

(53) Fenton, H. J. H. *J. Chem. Soc. Trans.* **1894**, *65*, 899.

(54) Robins, J. H.; Abrams, G. D.; Pincock, J. A. *Can. J. Chem.* **1980**, *58*, 339.

(55) Crampton, M. *Adv. Phys. Org. Chem.* **1969**, *7*, 211.

(56) Hair, J. F.; Black, B.; Babin, B.; Anderson, R. E.; Tatham, R. L. *Multivariate Data Analysis, 6th Edition*; Prentice Hall: New York, 2005.

(57) Janata, J. *Principles of Chemical Sensors, 2nd Edition*; Springer: New York, 2009.

(58) Johnson, R. A.; Wichern, D. W. *Applied Multivariate Statistical Analysis, 6th Edition*; Prentice Hall: New York, 2007.

(59) Stewart, S.; Ivy, M. A.; Anslyn, E. V. *Chem. Soc. Rev.* **2014**, *43*, 70.

(60) Flach, P. *Machine Learning: The Art and Science of Algorithms that Make Sense of Data*; Cambridge University Press, 2012.

(61) Lin, H.; Jang, M.; Suslick, K. S. *J. Am. Chem. Soc.* **2011**, *133*, 16786.

(62) *Convention of the Marking of Plastic Explosives for the Purpose of Detection*; International Civil Aviation Organization: Montreal, Canada, 1991.

(63) *Public Law 104–132: Antiterrorism and Effective Death Penalty Act of 1996*; US Government: Washington, DC, 1996.

Appendix: Device programming

Onboard software

Prerequisite software for development:

- Texas Instruments Code Creator Studio 5.4 (editor for Windows); http://processors.wiki.ti.com/index.php/Download_CCS
- Texas Instruments TMS320DM6437 bios 5.41.10.36 (bios library); http://software-dl.ti.com/dsps/dsps_public_sw/sdo_sb/targetcontent/dspbios/index.html
- ActivePerl 5.8.8 (2nd stage compiler); http://www.activestate.com/activeperl
- Texas Instruments C6000 code generation tools 7.3.5 (1st stage compiler); http://processors.wiki.ti.com/index.php/TI_Development_Tools_Information
- D3 Electronics Mercury library for TMS320DM6437 (code library); provided in digital appendix

Code Creator Studio uses a customized version of C that includes such concepts as 'far externs', which are not commonly supported in other compilers; as such, it would be very difficult to compile this software using another studio/compiler.

The primary contribution to the onboard device software fell into three categories: user interface, file operations, and statistics processing. It is worth noting that the TMS320DM6437 uses a multi-threaded processor and each processor can be assigned a "task" that it works on roughly independently of other active threads. Communication between these threads uses a standard semaphore method using a mailbox and wait statements; improper implementation of the semaphore was the primary cause of many errors including scan failure and general poor performance. Scan failure was affected by semaphore timing due to an extremely poor choice by D3 Engineering to control part of the scanner

with a microcontroller (i.e., independent of the CPU) and part with the CPU; as such, it is very easy to cause desynchronization between the microcontroller and CPU because the microcontroller continues to run while the CPU is in a wait cycle.

The user interface of the handheld device is a simple menu that steps through the three primary functions of the device (collecting/processing scans, memory management, and a status display). Each of these functions is relatively straightforward and will not be discussed in-depth.

File operations consisted of creating the file format and manipulating the onboard NAND flash memory in order to allow proper saving of data. The file format is documented well in the source code and will not be discussed. Manipulating the NAND flash memory was necessary due to a bug in D3 Electronics code: their built-in command to save data to the NAND flash memory would fail due to an incorrectly-written evaluation/test step following the write to the flash memory. The process of writing to NAND flash memory is fairly convoluted: first, a memory block must be write-unprotected, then erased, then written, then write-protected. Memory blocks cannot be subdivided, meaning that the data in each memory block must be saved first so that no data is lost. The file-save algorithm used by D3 electronics was very slow; it is suspected that it was performing multiple redundant operations, such as saving memory blocks which did not need to be altered. The file save procedure was sped up and made significantly more reliable by carefully writing only those blocks that required alteration. In addition, a specifically-sized memory area was dedicated to save files in order to more-easily calculate which memory blocks were in use.

Statistics processing primarily involved implementation of evaluation algorithms taken from SVM.NET. Importantly, linear classifiers can be collected into a single vector; evaluation of new data involves trivial data transformations (the dot product of each classifier with the incoming data vector). The relative magnitude (i.e., positive or negative) provides a vote for one class or another; collection of these votes

then gives the predicted class of the incoming data. The most difficult challenge of this was implementing vector mathematics in C language; due to thread memory limitations (i.e., only so much memory can be allocated for any particular subroutine), each intermediate vector in the mathematics required careful allocation in order to maintain data integrity.

PC GUI software

Prerequisite software for development:

- SVM.NET (LIBSVM code library for .net, i.e., C# language); http://www.matthewajohnson.org/software/svm.html
- PdfSharp for .net (pdf creation library); http://www.pdfsharp.net
- Microsoft Visual Studio 2013 (editor and compiler for Windows); http://www.visualstudio.com/

Source code for the PC GUI software is provided in the digital appendix in the 'PC GUI software' folder. The software was written in C#.

The PC GUI software was written as a major overhaul to PC GUI software originally provided by D3 Engineering. As such, every aspect of the software was altered or newly created. The major components worth discussing are the implementation of statistical handling, report output, and communication protocols.

Statistical handling was done through a minor modification of SVM.NET, which is a C# port of LIBSVM (a well-known SVM library). Normally, classifiers in SVM require implementation of a kernel function with each support vector (i.e., weighted data point in the training set); there can be anywhere from three to tens of support vectors depending on the complexity and ambiguity of data. With a linear classifier, however, these support vectors can be pooled together into a single vector that is suitable for export to

the handheld device. Other than that, statistical handling was performed using basic functions in the library API in order to appropriately classify incoming data via a voting mechanism, as described above for the onboard software.

Report output used a combination of basic text output (via a comma separated value table) and generation of Adobe Acrobat (pdf) documents using the PdfSharp library API. While this API is extraordinarily slow and is a bottleneck in performance, it is the difficulty of working with pdf documents through Adobe's proprietary libraries that causes this bottleneck rather than the PdfSharp library itself. Report output was done by inserting graphics and text; graphics were created by directly generating bitmap files by manipulating their binary representations.

Communication protocols were modified from those used by the original implementation of the D3 Engineering PC GUI. Specifically, the original implentation would abort immediately upon being commanded to do so; this resulted in many problems where the software did not stop "gracefully" and cause freezes and lockups. By altering the communication protocol such that the PC GUI and handheld device would communicate their attempts to abort and subsequently drain the data buffer harmlessly, this problem was eliminated completely. Additionally, new commands were added to facilitate saving and loading of new software and new chemical libraries.